TÉCNICO LISBOA

# Radiation reaction in magnetized black holes

**João Rebelo Sieiro dos Santos**

Thesis to obtain the Master of Science Degree in

**Engineering Physics**

Supervisors: Prof. Vítor Manuel dos Santos Cardoso
Prof. José António Maciel Natário

## Examination Committee

Chairperson: Profª. Ana Maria Vergueiro Monteiro Cidade Mourão
Supervisor: Prof. José António Maciel Natário
Members of the Committee: Prof. Richard Pires Brito

**October 2023**

*I dedicate this work to Zé David.*

# Acknowledgments

I must start by expressing my gratitude to my supervisors Vítor Cardoso and José Natário. Learning about physics, and more importantly, about what it means to be a researcher in the field from talented and prolific researchers like yourselves is something I will carry with me for the rest of my life. So I thank you for what you taught me, for being patient and always making me feel comfortable, and with that firing up my aspiration to become a researcher myself.

To all the researchers at GRIT I crossed with over the last two years, for allowing me to take part in the group meetings where I learned so much. I am very grateful to all of you.

To Hugo Terças and Pedro Cosme, for providing me with my first research experience in a stimulating yet warm and welcoming environment. The time with you was instrumental in setting stone on my ambition to become a researcher in physics.

I must also thank my friends and colleagues, Bernardo Barbosa, Carolina Figueiredo, Diogo Ribeiro, Carolina Paiva, Filipa Valente, Luís Dias, José Cruz, Thomas Gaehtgens, and Tomás Lopes, who were with me throughout my journey in physics. What I learned and laughed with you is priceless, and without your support getting here would have been a lot more difficult, you all are a part of this work. In that regard, a special word is reserved for Sérgio Carrôlo; you will certainly become a great scientist, just like you are a great friend. You helped me get through a lot, thank you for everything.

The completion of this thesis is a feat that, for me, goes beyond producing science, which by itself is saying a lot. It is also the product of 24 years of personal development, both on a personal and an academic level; for that reason, and since it is the first time I have the formal opportunity to express my gratitude, I apologize to the reader if I extend this section a bit further.

To my mother, Helena, for being my example that through hard work, moral clarity, passion, and an element of luck anything can be achieved; the person I am today I owe to you more than anyone. To my dad, Paulo Jorge, for his unwavering support and for doing everything in his power to stay close when he was very far away. To Filipe, for treating me like his own son and letting me call him a father. To Anya, for always hearing me talk about physics. To my siblings, Sofia, Zé, Carolina, Sasha and Taya, and sibbling in law, Rita, for the unconditional joy and love. To Beatriz for sharing this passion with me. And finally, to my grandparents, Bia, Tina, David and João, for the inspiration they all are to me.

I also want to leave a special word to my chosen family: I could never name everyone, but specially to António, Bibs, Daniela, Francisco, Jade, Martim, Rita and Rodrigo. You have been by my side through it all and are also a very big part of the person I am today. All the laughs, and relaxing moments, but also the hard conversations, I am very grateful to have you all in my life.

Last but definitely not least, to my girlfriend, Inês, who has brightened up the past year of my life and has been by my side everyday as I was writing this work. You inspire me to outcome my shortcomings, and sharing thoughts about physics with you has made me love it even more than I already did. Thank you for believing in me even when I find it most difficult to do so.

We acknowledge financial support provided under the European Union's H2020 ERC Advanced Grant "Black holes: gravitational engines of discovery" grant agreement no. Gravitas–101052587. Views and opinions expressed are however those of the author only and do not necessarily reflect those of the European Union or the European Research Council. Neither the European Union nor the granting authority can be held responsible for them. We acknowledge support from the Villum Investigator program supported by the VILLUM Foundation (grant no. VIL37766) and the DNRF Chair program (grant no. DNRF162) by the Danish National Research Foundation.

This project has received funding from the European Union's Horizon 2020 research and innovation programme under the Marie Sklodowska-Curie grant agreement No 101007855 and No 101131233.

## Resumo

Nesta tese, estudamos a reação à radiação eletromagnética de partículas carregadas em movimento circular em torno de um buraco negro de Schwarzschild imerso num campo magnético assintoticamente uniforme. As órbitas circulares neste sistema podem ser caracterizadas como estando na configuração positiva ou negativa. Se incluirmos a radiação, a equação de movimento é a equação de DeWitt-Brehme, que inclui um termo de cauda complexo; há resultados na literatura que afirmam que esse termo pode ser negligenciado.

Assim, neste trabalho realizamos uma análise do limite Newtoniano que mostra que a cauda não pode ser negligenciada nesse limite, a menos que toda a radiação seja ignorada, ou a curvatura em si seja negligenciável.

Também estudamos a reação à radiação no regime de campo forte, usando teoria de perturbações de buracos negros. Encontramos expressões para o fluxo de energia no horizonte e no infinito usando métodos analíticos (limitados a movimentos lentos e a modos de baixa frequência) e métodos numéricos, que produziram resultados compatíveis. Também descobrimos que, para órbitas na configuração positiva, o aumento do raio orbital leva a que a razão entre o fluxo de energia no horizonte e em infinito se aproxime de um valor constante para o modo dipolar, enquanto que tende para infinito para os multipólos de ordem superior. Finalmente, em relação ao termo de cauda na equação de DeWitt-Brehme, o caso de campo forte apenas reforça que ele não pode ser negligenciado no estudo da reação de radiação na solução de Schwarzschild em qualquer cenário não trivial.



**Palavras-chave:** Radiação; Buracos negros magnetizados.

## Abstract

In this thesis, we study the electromagnetic radiation reaction of charged particles in circular motion around a Schwarzschild black hole immersed in an asymptotically uniform magnetic field. Without considering radiation, circular orbits in this system are restricted to the equatorial plane and can be characterized as being in a plus or minus configuration. If we include radiation, the equation of motion is the DeWitt-Brehme equation, which includes a complicated tail term; there are results in the literature claiming this term can be neglected.

We perform an analysis of the Newtonian limit that shows the tail cannot be neglected in this limit, unless all radiation is ignored or curvature itself is negligible.

We also study radiation reaction in the strong field regime, using BH perturbation theory. We find expressions for the energy flux on the horizon and at infinity using analytical methods (restricted to slow motion and low frequency modes) and numerical methods, and the two produced compatible results. We also find that, for plus configuration orbits, increasing the orbital radius leads to the ratio between the energy flux on the horizon and at infinity going to a constant for the dipole mode, and to infinity for the higher order multipoles. Finally, regarding the tail term in the DeWitt–Brehme equation, the strong field case only strengthens the previous claim that it cannot be neglected in the study of radiation reaction in the Schwarzschild spacetime in all non-trivial scenarios.



**Keywords:** Radiation; Magnetized black holes.

# Contents

# List of Tables

# List of Figures

# Nomenclature

### Geometry symbols

$\nabla_\mu$ Covariant derivative.

$\delta^\mu_\nu$ Identity operator.

$g_{\mu\nu}$ Metric tensor.

### Greek symbols

$\omega_c$ Cyclotron frequency.

$\omega_K$ Keplerian frequency.

$\Omega_0$ Angular frequency of particle in circular orbit as seen by stationary observers at infinity.

$\Omega_{\text{MC}}$ Asymptotic angular frequency of minus configuration orbits.

$\Omega_{\text{PC}}$ Asymptotic angular frequency of plus configuration orbits.

### Roman symbols

$A_\mu$ Electromagnetic 4-potential.

$F_{\mu\nu}$ Electromagnetic field strength tensor.

$E$ Killing energy.

$\mathcal{E}$ Killing energy per unit mass.

$L$ Killing angular momentum along $\hat{z}$.

$\mathcal{L}$ Killing angular momentum along $\hat{z}$ per unit mass.

$v_0$ 3-Velocity as seen by stationary observers at infinity

### Subscripts and superscripts

$t, x, y, z$ Cartesian coordinate indices.

$t, r, \theta, \phi$ Spherical coordinate indices.

# Acronyms

**BH** Black hole.

**EM** Electromagnetic.

**GLF** Generalized Larmor formula.

**GR** General Relativity.

**ISCO** Innermost stable circular orbit.

**MC** Minus configuration.

**PC** Plus configuration.

**RHS** Right-hand side.

**RLF** Relativistic Larmor formula.

# Chapter 1

# Introduction

In the broadest sense, Physics is about striving to understand the fundamental workings of our Universe. It must be said that since the birth of the scientific method and Galileo's works on mechanics, we as a species have taken great steps toward that goal. In particular, quantum field theory and the Standard Model of particle physics describe, with outstanding accuracy, three of the four fundamental interactions in the Universe. It only leaves out gravity, which was elegantly described in 1915, through General Relativity (GR) [1]. Einstein's brilliant idea was to use the framework of Riemannian geometry to express gravity as a manifestation of the curvature of space and time in the presence of energy and momentum. Since then, for over 100 years, GR has described all known observations with remarkable accuracy, and with the detection of gravitational waves at LIGO in 2015 [2, 3] we entered a new age of gravitational wave astrophysics, allowing for more and more precise tests of GR.

Together, the Standard Model and GR provide a good description of the fundamental nature of the Universe. However, at very high energies, of the order of the Planck scale, the two theories are incompatible, and a fully quantum theory of gravity has to emerge. This is one of the most exciting open questions in modern physics, but we will not try to answer it in this thesis; instead, we will just use it as justification to state that we are still very far from having a complete understanding of how the 4 fundamental forces of nature interact with each other, and that, moreover, GR is most likely an effective theory in the low energy limit of a quantum theory of gravity which is valid at Planck scale energies. This last claim can be supported by one of the most exciting predictions of GR: the existence of black holes (BH) [4, 5]. These are solutions of the Einstein field equations describing the most compact objects in the cosmos: the gravitational field surrounding them is so strong that beyond the surface of no escape – the event horizon – nothing, not even light, can escape. Beyond the event horizon, everything is falling towards the central singularity, a "place" where curvature and energy density are infinite. Singularities are present in many physical theories, but only as a result of ill-posed or incomplete problems (e.g. the Coulomb field in electromagnetism or renormalization in quantum field theory); however, in GR, the theorems of Hawking and Penrose [6–8] show that the existence of singularities is an intrinsic property of the theory. At the singularity, energies reach the Planck scale, and so a quantum theory is most likely needed. As Hawking once said, *"(..) the theory probably breaks down, but only when quantum*

*gravitational effects become important."*.

All of this is to say that GR is most likely not the ultimate theory of gravity, and it is important to keep putting it to the test of experiment, by exploring the inherent phenomenology. Perhaps one day we will be able to improve upon this centenary theory, developed by arguably the most brilliant mind in the history of science. And what better place to do so than by looking at BHs, not only because of the extreme dynamics they can power, but also because of the new burst of gravitational wave detections? On that topic, the gravitational field around BHs is so strong that it can accelerate particles to velocities very close to the speed of light. They are therefore good particle accelerators, and can efficiently convert gravitational energy to electromagnetic (EM) radiation [9]. Rotating Kerr BHs [10] are also prone to energy extraction mechanisms, whereby their rotational energy can be converted to kinetic energy of particles or occupation number of fields [11–14].

This makes energy extraction from rotating BHs a particularly appealing explanation for the production of high-energy cosmic rays with energies exceding $10^{20}$ eV [15–18] or for other violent astrophysical phenomena. Understanding the origin of such extremely high-energy processes may even allow us to probe a little bit further into the structure of the elusive compact objects. However, mechanisms for energy extraction, relying on rotation alone (either via the original Penrose process or variants thereof) are not efficient enough to explain the origin of cosmic rays or extremely energetic phenomena [19–24].

Alternatives to the above simple scenario include the addition of external magnetic fields, which can increase the efficiency of energy extraction via Penrose-like mechanisms [25–34]. Accretion disks can support magnetic fields, and there is ample evidence that these are ubiquitous around stellar-mass and supermassive BHs [35–38], with typical intensities of $10^4 - 10^8$ Gauss. It is a standard result of classical electrodynamics that an accelerated charged particle experiences a radiation reaction force as a result of radiating EM waves [39–42]. In flat space, the energy carried by the EM field is always positive, so the particle loses energy as a result of the radiation reaction force. However, if the particle is moving inside the ergoregion of a BH, where negative energy states are allowed, we could, in principle, find that the particle gains energy as a result of the radiation reaction force. This was precisely the idea presented in Ref. [29] for the radiative Penrose process, where the authors take a charged particle moving in the field of a Kerr BH, also assuming the presence of a magnetic field which could enhance the efficiency of the energy extraction.

In order to study this phenomenon, it is of the utmost importance to have a good understanding of the motion of radiating charged particles around BHs surrounded by magnetic fields. To do so, one must start by understanding the motion without the inclusion of radiation, first for non-rotating Schwarzschild BHs [43–49], and only afterward for rotating Kerr BHs [50, 51]. The next step is to include radiation reaction in the equations of motion for the Schwarzschild case, which was attempted for the simplest case of an asymptotically uniform magnetic field surrounding the BH in Refs. [52, 53]; however, those works reported a seemingly unphysical "orbit widening", which appeared to us a clear violation of energy conservation. Indeed, we ultimately called these results into question in our published paper [54].

Thus, the aim of this work is to perform a consistent analysis of the motion of radiating charged particles around magnetized Schwarzschild BHs, with a view to studying the Kerr case and the asso-

ciated energy extraction mechanisms. Including radiation reaction leads to the complicated non-linear DeWitt-Brehme equation of motion [55–59], which in turn makes the problem of solving for the general motion of a point charge highly non-trivial; therefore we focused on the simplest case of circular orbits and asymptotically uniform magnetic fields. The external magnetic fields are always treated as fixed test fields, meaning they do not influence the geometry of spacetime and they are not perturbed by the particle motion nor by its EM radiation field [50, 60]. Regarding the radiation reaction force, its treatment in curved space is a very complicated subject and has been the topic of intense research [61]. The DeWitt-Brehme equation can be solved analytically in the Newtonian limit [62, 63]. Still, for the strong field case, the problem is more challenging, especially because of the non-local tail term, as it involves the complicated task of directly calculating the retarded Green's function [64]. Alternatively, when we are studying a small object around a BH, the more popular approach is using BH perturbation theory. In the case of Schwarzschild spacetime, the odd and even parity gravitational perturbations are governed by the Regge-Wheeler [65] and Zerilli [66] equations, respectively. The perturbations of rotating Kerr BHs are described by the Teukolsky equation [67, 68], which governs perturbations of both scalar, spinor, vector and tensor nature. If one takes the limit where the BH is not spinning (i.e. a Schwarzschild BH), one finds the Bardeen-Press equation [69], which was shown to be equivalent to the Regge-Wheeler and Zerilli equations by Chandrasekhar [70]. Using the BH perturbation formalism, it is possible to calculate the radiation field of the particle, see how much energy is escaping to infinity and being absorbed by the BH [71], and with that obtain an estimate for the radiation reaction force. This was done to study particle orbits in a large number of works [20, 72–86], some of which by D. V. Gal'tsov and collaborators even included the presence of an external magnetic field [87–90].

With all of this in mind, we will start by discussing some of the background needed for our work in Chapter 2. There, we will start by looking into cyclotron motion and radiation reaction in flat space; then we move on to a characterization of the circular orbits around magnetized Schwarzschild BHs, starting with the unmagnetized case and including a discussion of the magnetic field configuration as well as the validity of the test field approximation; finally, we give an introduction of the topic of radiation reaction in curved space. Next, in Chapter 3, we make use of the Newtonian limit to show how some of the previous results on the subject of radiating charged particles around magnetized Schwarzschild BHs give an incorrect picture of the problem. We then give an overview of the Teukolsky equation, its solutions describing EM waves around Schwarzschild BHs, and how those can be used to determine energy fluxes at infinity and on the horizon in Chapter 4. This is ultimately used to find analytical and numerical results which we present in Chapters 5 and 6, respectively, where the analytical results are obtained in the low-frequency and slow-motion approximation. We give a final discussion and concluding remarks in Chapter 7.

We use a system of units with $G = c = 1$, and use Gaussian units for electromagnetism, meaning that we have $4\pi\varepsilon_0 = 1$ and $\mu_0 = 4\pi$. The metric signature is $(-,+,+,+)$, Greek indices run from 0 to 3, and boldface quantities are three-vectors.

# Chapter 2

# Background

## 2.1 Charged particle motion in a uniform magnetic field in flat space

We begin by looking at the case of a single test particle of mass $m$ and charge $q$ moving under the influence of a uniform magnetic field in flat space. In this section, we follow the standard book by Jackson [42].

### 2.1.1 Motion without radiation reaction

We start by considering the motion of the charged particle without including radiation reaction so that the only force present is the Lorentz force. Thus, using Cartesian coordinates $\{t, x, y, z\}$, the equation of motion is

$$\frac{du^\mu}{d\tau} = \frac{q}{m} F^\mu{}_\nu u^\nu \,, \tag{2.1}$$

where $u^\mu(\tau)$ is the 4-velocity, $\tau$ is the proper time, and $F_{\mu\nu}$ is the EM field tensor. By introducing the 4-potential $A_\mu$, Maxwell's equations in vacuum can be written as

$$F_{\mu\nu} = \partial_\mu A_\nu - \partial_\nu A_\mu \,, \quad \partial_\mu F^\mu_\nu = 0 \,. \tag{2.2}$$

For a uniform magnetic field along the z direction, $\boldsymbol{B} = B_0 \hat{z}$, where $B_0$ can be positive or negative, we have that the EM field tensor and the 4-potential are given, respectively, by

$$F_{xy} = -F_{yx} = B_0 \tag{2.3}$$

and

$$A_x = -\frac{B_0}{2} y, \quad A_y = \frac{B_0}{2} x \,, \tag{2.4}$$

with all other components set equal to zero. This can very easily be verified to satisfy Maxwell's equations in vacuum Eq. (2.2).

Replacing the EM field in the equation of motion we get

$$\frac{du^x}{d\tau} = \omega_c u^y \,, \qquad \frac{du^y}{d\tau} = -\omega_c u^x \,, \qquad \frac{du^z}{d\tau} = \frac{du^t}{d\tau} = 0 \,, \tag{2.5}$$

where we introduced the cyclotron frequency of the particle

$$\omega_c \equiv \frac{qB_0}{m} \,. \tag{2.6}$$

This frequency can be negative if $q$ and $B_0$ have opposite signs. This system of differential equations is very easy to solve, yielding circular motion in the $xy$ plane and uniform motion along the $\hat{z}$ direction. Without loss of generality, we can shift the origin and rotate the spatial axes so that we have

$$x(\tau) = r_0 \cos\left(\omega_{\mathsf{c}}\tau\right) \,, \qquad y(\tau) = -r_0 \sin\left(\omega_{\mathsf{c}}\tau\right) \,, \qquad z(\tau) = u^z\tau \,, \quad \text{and} \quad t(\tau) = u^t\tau \,, \tag{2.7}$$

where $u^z$ and $u^t$ are constants, and $r_0$ is the radius of the orbit. Finally, we boost the frame so we have $u^z = 0$, and are left with just circular motion in the equatorial plane.

Minkowski spacetime has 10 different Killing vector fields (see Appendix A), but for the purposes of our work we only make use of

$$X^\mu = \delta^\mu_t \qquad \text{and} \qquad Y^\mu = \delta^\mu_\phi \,, \tag{2.8}$$

which are associated with the conservation laws for energy and angular momentum along the $\hat{z}$ direction, respectively. According to Appendix. A, these conserved quantities are given by

$$E = -m\left(u_\mu + \frac{q}{m}A_\mu\right)\delta^\mu_t = \frac{m}{\sqrt{1-v_0^2}} \tag{2.9}$$

and

$$L = m\left(u_\mu + \frac{q}{m}A_\mu\right)\delta^\mu_\phi = -\frac{1}{2}m\, r_0^2\omega_{\mathsf{c}} \,, \tag{2.10}$$

where $v_0$ is the velocity as measured by stationary observers,

$$v_0 \equiv r_0\Omega_0 \,, \tag{2.11}$$

and $\Omega_0$ is the angular velocity measured by the same observers,

$$\Omega_0 = -\frac{\omega_{\mathsf{c}}}{\sqrt{1+(r_0\omega_{\mathsf{c}})^2}} \equiv \Omega_{\mathsf{MC}} \,. \tag{2.12}$$

The notation $\Omega_{\mathsf{MC}}$ will be explained further ahead. In the flat space case, all circular orbits with $r_0 > 0$ are stable, and by looking at Eqs. (2.9), (2.11) and (2.12), we can see that the energy of the orbit grows with the radius. This means that if the particle loses energy by radiation we expect it to fall to the center of the trajectory. We will look into this in the next subsection.

### 2.1.2 Motion with radiation reaction

If we include electromagnetic radiation reaction, the equation of motion of the particle becomes

$$\frac{du^\mu}{d\tau} = \frac{q}{m} F^\mu{}_\nu u^\nu + \frac{2q^2}{3m}\left(\frac{d^2u^\mu}{d\tau^2} + u^\mu u_\nu \frac{d^2u^\nu}{d\tau^2}\right), \tag{2.13}$$

where the term proportional to $q$ is the usual Lorentz force and the one proportional to $q^2$ is the radiation reaction force, also known as the Abraham-Lorentz-Dirac force, which we derive in Appendix B. This is a third-order differential equation, famously plagued with runaway solutions. For more than 100 years, possible solutions to this problem have been discussed; today, it is believed that its root lies in the consideration point particles, which are fundamentally unphysical both from the point of view of quantum mechanics and GR [1]. Indeed, if the limit of point particles is taken consistently, we should perform an order reduction of the Abraham-Lorentz-Dirac term by taking [92]

$$\frac{d^2u^\mu}{d\tau^2} = \frac{d}{d\tau}\left(\frac{q}{m} F^\mu{}_\nu u^\nu\right). \tag{2.14}$$

This order reduction procedure dates back to the late 1940s [93]. Initially, it was seen as a mere approximation [92, 94–96] but it has become more and more established as the correct description of radiation reaction in flat space. In the end, the equation of motion becomes

$$\frac{du^\mu}{d\tau} = \frac{q}{m} F^\mu{}_\nu u^\nu + \frac{2q^3}{3m^2}\left(\nabla_\alpha F^{\mu\nu} u^\alpha u_\nu\right) + \frac{2q^3}{3m^2}\left(\frac{q}{m}\left(F^{\mu\nu}F_{\nu\rho} + F^{\nu\alpha}F_{\alpha\rho}u_\nu u^\mu\right)u^\rho\right). \tag{2.15}$$

Looking at the individual coordinates separately and replacing the EM field in Eq. (2.3) we find

$$\frac{du^x}{d\tau} = \omega_c u^y - \frac{2q^2}{3m}\omega_c^2\left(1+u_\perp^2\right)u^x, \tag{2.16}$$

$$\frac{du^y}{d\tau} = -\omega_c u^x - \frac{2q^2}{3m}\omega_c^2\left(1+u_\perp^2\right)u^y, \tag{2.17}$$

$$\frac{du^z}{d\tau} = -\frac{2q^2}{3m}\omega_c^2 u_\perp^2 u^z, \tag{2.18}$$

$$\frac{du^t}{d\tau} = -\frac{2q^2}{3m}\omega_c^2 u_\perp^2 u^t, \tag{2.19}$$

where $u_\perp^2 = u_x^2 + u_y^2$ is the squared velocity in the $xy$ plane. Although $u^z$ is not constant, $v_z = u^z/u^t$, the speed seen by a stationary observer, is constant:

$$\frac{d}{d\tau}\left(\frac{u^z}{u^t}\right) = \frac{1}{u^t}\frac{du^z}{d\tau} - \frac{u^z}{(u^t)^2}\frac{du^t}{d\tau} = 0\,, \tag{2.20}$$

which means that again we can boost to a frame where the particle is moving only in the $xy$ plane (because radiation only affects that component of the motion).

The quantities defined in Eqs. (2.9) and (2.10) are no longer conserved and we can use Eq. (2.19), to study the rate of energy change of the particle. We find that after some algebra we recover the relativistic

[1] In quantum mechanics we can see this from the perspective of the Heisenberg uncertainty principle. In GR, to put it simply, an infinitely dense object would always collapse to a BH with a finite radius. A more general study of the pathologies of point particles in GR can be found in Ref. [91].

Larmor formula (RLF)

$$\frac{dE}{dt} = -\frac{2}{3} q^2 \gamma^4 (r_0 \Omega_0^2)^2 \,, \tag{2.21}$$

where $\gamma = 1/\sqrt{1 - v_0^2}$ is the Lorentz factor. When we take the Newtonian limit $\gamma \to 1$, we recover the usual Larmor power formula

$$\frac{dE}{dt} = -\frac{2}{3} q^2 (r_0 \Omega_0^2)^2 \,. \tag{2.22}$$

Both the relativistic and non-relativistic Larmor formulas are derived in Appendix B. As for the rate of change of angular momentum along the $\hat{z}$ direction, we get

$$\frac{dL}{dt} = \frac{1}{\Omega_0} \frac{dE}{dt} \,. \tag{2.23}$$

If we translate the rate of energy change and the rate of angular momentum change into the rate of change of the radius of the orbit, $r_0$, we find that the two results are compatible with the particle remaining in a circular orbit.

We found that our result for the angular momentum (Eq. (2.10)) is in disagreement with the result presented in Eq.(13) of Ref. [53].

## 2.2 The Schwarzschild solution

Throughout this work, we will be almost always looking at the Schwarzschild solution of the Einstein field equations. This solution was found by Karl Schwarzschild in 1916 [4] and it describes a one-parameter family of static, spherically symmetric, and asymptotically flat vacuum BH spacetimes. According to Birkhofff's theorem [97], a vacuum spherically symmetric solution is necessarily static and asymptotically flat, and the Schwarzschild solution is the only non-trivial case. This means that any spherically symmetric astrophysical body is described by the Schwarzschild metric in the exterior region (outside the surface of the body) [98].

We mainly follow Wald [99] for the characterization of the solution. Using standard Schwarzschild coordinates $\{t, r, \theta, \phi\}$, this solution is described by the line element

$$ds^2 = -f(r) dt^2 + f(r)^{-1} dr^2 + r^2 d\theta^2 + r^2 \sin^2\theta \, d\phi^2 \,, \tag{2.24}$$

$$f(r) = 1 - \frac{2M}{r} \,, \tag{2.25}$$

where $M$ is the BH mass. The Schwarzschild solution admits four Killing vector fields (see Appendix A): one corresponding to the stationarity of the metric (invariance under time translations) and three corresponding to its spherical symmetry (invariance under rotations). In the coordinate system we are using, only two of these are evident: the generator of time translations and the generator of rotations about $\hat{z}$; their definition in these coordinates coincides with the flat space definition given in Eq. (2.8):

$$X^\mu = \delta^\mu_t \qquad \text{and} \qquad Y^\mu = \delta^\mu_\phi \,. \tag{2.26}$$

### 2.2.1 Timelike circular geodesics

Now take a particle of rest mass $m$ in free fall under the action of the gravitational field of a Schwarzschild BH. The particle's equation of motion is just the geodesic equation

$$\frac{Du^\mu}{d\tau} = 0\,, \tag{2.27}$$

where $u^\mu(\tau)$ is the 4-velocity, $\tau$ is the proper time and $D/d\tau \equiv u^\mu \nabla_\mu$ is the covariant derivative along the velocity of the particle. The proper time is just the affine parameter along the trajectory of the particle for which

$$g_{\mu\nu} u^\mu(\tau) u^\nu(\tau) = -1\,. \tag{2.28}$$

We can use the Killing vector fields we defined above to construct two different conserved quantities (see Appendix A):

$$E = -m\, u_\mu X^\mu = m\, f(r) u^t\,, \tag{2.29}$$

$$L = m\, u_\mu Y^\mu = m\, r^2 \sin(\theta) u^\phi\,. \tag{2.30}$$

These correspond, respectively, to the energy and angular momentum along $\hat{z}$, as measured by a stationary observer at infinity.

Because of the spherical symmetry of the spacetime, there must be two other independent Killing vector fields, associated with the conservation of the two other components of the angular momentum. Since we will not need them for our analysis, we will not dwell on this topic, and will instead focus on the equations of motion for a particle in the equatorial plane.

For a trajectory in the equatorial plane ($\theta = \pi/2\,,\ u^\theta = 0$), the equations of motion for a free-falling particle are obtained from Eq. (2.27) and take the form

$$\frac{du^t}{d\tau} = -\frac{2M}{r^2 f}\,, \tag{2.31}$$

$$\frac{du^r}{d\tau} = -\frac{M}{r^2} f (u^t)^2 + \frac{M}{r^2 f}(u^r)^2 + r f (u^\phi)^2\,, \tag{2.32}$$

$$\frac{du^\phi}{d\tau} = -\frac{2}{r} u^r u^\phi\,. \tag{2.33}$$

Note that the equation for $u^\theta$ in the equatorial plane is just $du^\theta/d\tau = 0$, so it is compatible with the orbit remaining in the equatorial plane. Now suppose that the particle is following a circular orbit of radius $r_0$. In that case, the equations for $u^t$ and $u^\phi$ above become trivial, and the circular orbit condition is taken from Eqs. (2.28) and (2.32), yielding

$$\Omega_0 \equiv \frac{u^\phi}{u^t} = \frac{d\phi}{dt} = \sqrt{\frac{M}{r_0^3}} \equiv \omega_{\mathsf{K}}\,, \tag{2.34}$$

$$u^t = \left(1 - \frac{2M}{r_0} - v_0^2\right)^{-1/2}\,, \tag{2.35}$$

where $\omega_{\mathsf{K}}$ is the Keplerian angular frequency, $\Omega_0$ is the angular velocity as seen by a stationary observer at infinity, and $v_0$ is the 3-velocity as seen by the same family of observers (see Eq. (2.11)).

The remaining question is the stability of circular orbits under small perturbations. In Sec. 2.2.3 we go over how this is done for the case of a uniformly magnetized Schwarzschild BH, of which the unmagnetized case is obtained by taking the cyclotron frequency to zero ($\omega_c = 0$). When that is done, one finds that the innermost stable circular orbit (ISCO) for an unmagnetized Schwarzschild BH is $r_{\mathsf{ISCO}} = 6M$. It is also easy to show from Eqs. (2.29) and (2.35) that the energy of a stable orbit increases with the radius; this means that if the particle loses energy by radiation, it will ultimately fall into the BH.

### 2.2.2 Asymptotically uniform magnetic field

In this subsection, we follow Ref. [100] to show how a solution to Maxwell's equations can be constructed from a Killing vector field in a vacuum spacetime. This will allow us to describe a Schwarzschild BH in an asymptotically uniform magnetic field.

The EM fields are always treated as test fields, meaning they don't influence the geometry of spacetime, which will continue to be a vacuum solution of the Einstein field equations, namely the Schwarzschild solution. This places a bound on the strength of the magnetic field, $B_0$, as the energy of the EM field must always be negligible when compared to the energy of the BH. Consider a cylinder of height $\sim 2M$ and radius $R$; it contains EM energy $\sim \pi M R^2 B_0^2/\mu_0$, where $\mu_0$ is the vacuum permeability. This energy must be small when compared with the energy of the BH that is sourcing the gravitational field, that is, its mass $M$. Taking $R \sim 2M$ we find the bound originally obtained in Ref. [60],

$$\left(\frac{B_0}{1\,\mathsf{Gauss}}\right) \ll 2.4 \times 10^{19} \left(\frac{M_\odot}{M}\right) , \tag{2.36}$$

where $M_\odot$ is the mass of the sun. It must be noted that this bound is for the magnetic field near the BH, where the curvature is large; for large distances, $r \gg M$, the approximation will always break down. We are far more interested in understanding, for a given value of $B_0$, what is the value of $R$ up to which we can use the test field approximation. Indeed we can restate the condition above as a function of the radius, yielding

$$\left(\frac{R}{GM/c^2}\right) \ll 4.7 \times 10^{19} \left(\frac{1\,\mathsf{Gauss}}{B_0}\right) \left(\frac{M_\odot}{M}\right) . \tag{2.37}$$

This gives us plenty of room to study circular orbits within the test field approximation, especially given that the typical values of magnetic fields around BHs are in the $10^4 G$ – $10^8 G$ range [35–38].

Moving on to the actual calculation of the EM field, the covariant formulation of Maxwell's equations in vacuum is obtained by replacing the ordinary derivatives in Eq. (2.2) with covariant derivatives:

$$F_{\mu\nu} = \nabla_\mu A_\nu - \nabla_\nu A_\mu, \qquad \nabla_\nu F^{\mu\nu} = 0. \tag{2.38}$$

If the spacetime being considered contains a Killing vector field $\xi^\mu$ (see Appendix A), we can systemati-

cally use it to obtain a solution to these equations by taking $A = \xi$:

$$F_{\mu\nu} = \nabla_\mu \xi_\nu - \nabla_\nu \xi_\mu = -2\nabla_\nu \xi_\mu \,, \tag{2.39}$$

which, when replaced, in Eq. (2.38), yields

$$\nabla_\nu F^{\mu\nu} = -2g^{\nu\rho}\nabla_\nu \nabla_\rho \xi^\mu = 2R_{\rho\alpha}{}^{\rho\mu}\xi^\alpha = 0, \tag{2.40}$$

where we use the definition of the Riemann tensor, the Killing equation, the first Bianchi identity, and the fact that we are studying a vacuum spacetime so $R_{\mu\nu} = 0$.

This procedure can be tested in Minkowski space, and we find that while the translation Killing vector fields generate no EM field, rotations generate uniform magnetic fields, and boosts generate uniform electric fields. Using Cartesian coordinates $\left\{x^0, x^1, x^2, x^3\right\} = \{t, x, y, z\}$, we find:

Translations $\rightarrow$ No field,

$$\xi_\mu = \delta^\alpha_\mu \Rightarrow F_{\mu\nu} = 0 \,, \tag{2.41}$$

Rotations $\rightarrow$ Uniform B-field,

$$\xi_\mu = x^i \delta^j_\mu - x^j \delta^i_\mu \Rightarrow F_{\mu\nu} = 2\left(\delta^j_\mu \delta^i_\nu - \delta^i_\mu \delta^j_\nu\right), i \neq j \,, \tag{2.42}$$

Boosts $\rightarrow$ Uniform E-field,

$$\xi_\mu = x^i \delta^0_\mu - x^0 \delta^i_\mu \Rightarrow F_{\mu\nu} = 2\left(\delta^0_\mu \delta^i_\nu - \delta^i_\mu \delta^0_\nu\right) \,. \tag{2.43}$$

In this work, we are interested in surrounding a Schwarzschild BH with an asymptotically uniform magnetic field. Thus, since the Schwarzschild solution is asymptotically flat, we can take inspiration from the result for Minkowski spacetime and guess that the desired EM field can be constructed from the Killing vector fields $X^\mu$ and $Y^\mu$ (see Eq. (2.8)), that is

$$F^{(X)}_{\mu\nu} = -2\nabla_\nu X_\mu \,, \tag{2.44}$$

$$F^{(Y)}_{\mu\nu} = -2\nabla_\nu Y_\mu \,, \tag{2.45}$$

which can easily be seen to satisfy

$$\mathcal{L}_{X,Y} F^{(X)}_{\mu\nu} = \mathcal{L}_{X,Y} F^{(Y)}_{\mu\nu} = 0 \,. \tag{2.46}$$

This allows us to conclude that the test fields being generated are both stationary and axisymmetric. Furthermore, as the spacetime is asymptotically flat, $F^{(X)}$ must generate an EM field that vanishes asymptotically ($X$ is the generator of $t$-translations in Minkowski) while $F^{(Y)}$ must approach a uniform magnetic field asymptotically ($Y$ is the generator of rotations around $\hat{z}$ in Minkowski). In Ref. [100], the author studies the EM field around rotating Kerr BHs which are also stationary and axisymmetric vacuum solutions of the Einstein field equations. Here we just present that analysis in Schwarzschild spacetime. With that in mind, the properties of the EM fields in Eq. (2.45) are:

- $F^{(X)}$ - *stationary, axisymmetric test field which vanishes asymptotically, has no magnetic monopole moment and has electric charge* $Q^{(X)} = -2M$.

- $F^{(Y)}$ - *stationary, axisymmetric test field which asymptotically approaches a uniform magnetic field along the* $\hat{z}$ *direction and has no magnetic monopole moment and no electric charge.*

At this point, we need to invoke the following theorem [101]:

***Theorem****: Let* $F$ *be a Maxwell test field on a stationary, axisymmetric, vacuum BH spacetime. Suppose* $F$ *satisfies:*

1. $F$ *is stationary and axisymmetric.*

2. $F$ *is non-singular in the exterior region and the BH event horizon.*

3. $F$ *vanishes asymptotically at large distances from the BH.*

4. $F$ *has no charge or magnetic monopole moment.*

*Then* $F = 0$.

We now have all the tools to discuss what sort of EM field arises when a Schwarzschild BH is placed in an initially uniform magnetic field of strength $B_0$ along the $\hat{z}$ direction. On physical grounds only, the following can be said about the resulting field $F$:

1. $F$ must be stationary and axisymmetric.

2. $F$ must be non-singular in the exterior region and the BH event horizon.

3. $F$ must asymptotically approach a uniform magnetic field of strength $B_0$ parallel to the $\hat{z}$ direction.

4. The net charge of the BH must be zero.

Given these conditions, we start by noting that if a solution is found, then it is unique, since if two EM fields $F$ and $F'$ satisfy the above conditions then $F - F'$ satisfies the conditions for the theorem above, and hence $F = F'$. Indeed it is easy to see that the EM field

$$F_{\mu\nu} = \frac{B_0}{2} F^{(Y)}_{\mu\nu} = -B_0 \, \nabla_\nu Y_\mu \,, \tag{2.47}$$

satisfies all the conditions listed above. Thus it corresponds to the EM field that is generated around a Schwarzschild BH which is placed in an initially uniform magnetic field. This EM field corresponds to the vector potential

$$A_\mu = \frac{B_0}{2} Y_\mu = \frac{B_0}{2} r^2 \sin^2\theta \delta^\phi_\mu. \tag{2.48}$$

### 2.2.3 Non-geodesic motion in the presence of a magnetic field

Before discussing the radiation reaction force in curved spacetime, we want to study the dynamics of charged particles in magnetized Schwarzschild BHs without radiation reaction. The topic of particle motion in magnetized BH spacetimes has been the focus of much research in the past and present [43–47, 50, 60].

#### Equations of motion

To obtain the equations of motion, we will use the Hamiltonian formalism and follow Ref. [46]. We start by writing the Lagrangian for a free particle

$$\mathcal{L}_{\text{FP}} = \frac{1}{2}\, m\, g_{\alpha\beta} u^{\alpha} u^{\beta}\,, \tag{2.49}$$

where $g_{\mu\nu}$ is the Schwarzschild metric, given in Eq. (2.24), $u^{\mu}$ is the 4-velocity of the particle and $m$ is its mass. For a free particle, the canonical 4-momentum, $\pi_{\mu}$, coincides with the kinematic momentum, $p_{\mu}$ and is defined as

$$p_{\mu} = \pi_{\mu} = \frac{\partial L_{\text{FP}}}{\partial u^{\mu}} = m u_{\mu}\,. \tag{2.50}$$

By performing a Legendre transformation we obtain the free particle's Hamiltonian

$$H_{\text{FP}} = \pi_{\alpha} u^{\alpha} - L_{\text{FP}} = \frac{1}{2m} g^{\alpha\beta} \pi_{\alpha} \pi_{\beta}. \tag{2.51}$$

Since adding a constant to the Hamiltonian does not change the resulting equations of motion, and multiplying it by a constant only rescales the time parameter, we choose to rewrite the Hamiltonian as

$$H_{\text{FP}} = \frac{1}{2} g^{\alpha\beta} \pi_{\alpha} \pi_{\beta} + \frac{1}{2} m^2, \tag{2.52}$$

so we always have $H = 0$. This rescaling implies that we must also transform the Hamilton equations, which now read

$$m \frac{dx_{\mu}}{d\tau} = \frac{\partial H}{\partial \pi^{\mu}}, \quad m \frac{d\pi_{\mu}}{d\tau} = -\frac{\partial H}{\partial x^{\mu}}\,. \tag{2.53}$$

If we replace the free particle Hamiltonian, we recover the conservation laws for the energy, $E = p_t = \pi_t$, and angular momentum along $\hat{z}$, $L = p_{\phi} = \pi_{\phi}$, of free-falling particles we had obtained in Eqs. (2.29) and (2.30).

Introducing an EM interaction is easy because the particle is minimally coupled to the EM field. Thus, even though the kinematic momentum is defined in the same way, we must redefine the canonical momentum as $\pi_{\mu} = p_{\mu} + qA_{\mu}$, finally yielding the Hamiltonian

$$H_{\text{EM}}\left(\pi^{\mu}, x^{\mu}\right) = \frac{1}{2} g^{\alpha\beta} \left(\pi_{\alpha} - qA_{\alpha}\right) \left(\pi_{\beta} - qA_{\beta}\right) + \frac{1}{2} m^2. \tag{2.54}$$

The redefinition we did of the canonical momentum to include EM interactions was precisely the trans-

formation we performed in Appendix A to obtain the conservation laws associated with Killing vectors in the presence of EM fields.

This was to be expected, as if the spacetime possesses a symmetry (i.e. a Killing vector), and the 4-potential also shares the same symmetry (i.e. it commutes with the Killing vector), then, in the appropriate coordinates, the Hamiltonian will be cyclic in the position variable associated with this symmetry, and so the conjugate momentum associated to it will be conserved.

Returning to the problem at hand, if we substitute the expression (2.48) for the 4-potential in the Hamiltonian we obtain the Hamiltonian for a charged particle moving around a Schwarzschild BH immersed in an asymptotically uniform magnetic field:

$$H_{\text{MS}}\left(\pi^{\mu}, x^{\mu}\right) = \frac{1}{2} f(r) \pi_r^2 + \frac{1}{2r^2} \pi_\theta^2 - \frac{1}{2} \frac{m^2}{f(r)} \left(\mathcal{E}^2 - V_{\text{eff}}\left(r, \theta; \mathcal{L}, \omega_c\right)\right) , \tag{2.55}$$

where we recall $\omega_c$ is the cyclotron frequency which can be negative (see Eq. (2.6)). We also define $\mathcal{E}$ and $\mathcal{L}$, the energy and angular momentum along $\hat{z}$ per unit mass,

$$\begin{aligned} \mathcal{E} &= \frac{E}{m} = -\frac{\pi_t}{m} = f(r) u^t, \\ \mathcal{L} &= \frac{L}{m} = \frac{\pi_\phi}{m} = r^2 \sin^2\theta \left(u^\phi + \frac{\omega_c}{2}\right), \end{aligned} \tag{2.56}$$

(both conserved quantities, as a result of the Hamiltonian not depending on $t$ or $\phi$, that is, of the Schwarzschild metric and the 4-potential being stationary and axisymmetric), and the effective potential is given by

$$V_{\text{eff}} = f(r) \left[1 + \left(\frac{\mathcal{L}}{r \sin\theta} - r \sin\theta \, \frac{\omega_c}{2}\right)^2\right] . \tag{2.57}$$

It is clear from Eq. (2.55) that we must generally have $\mathcal{E}^2 \geq V_{\text{eff}}$, so the effective potential governs the region of phase space accessible to the particle.

### Circular orbits

Looking back at Eq. (2.55), it is clear that circular orbits in the equatorial plane can only ever exist if

$$\mathcal{E}^2 = V_{\text{eff}}. \tag{2.58}$$

This condition however does not tell us anything about the characteristics of the orbit itself, it is just a statement of the normalization of the 4-velocity. To get more information, we obtain the equations of motion for the system from the Hamilton equations (2.53). To study circular orbits, we don't need the full equations of motion: we can just consider small perturbations around a circular orbit,

$$x^{\mu} = \left(t(\tau), r_0 + \varepsilon^r(\tau), \theta_0 + \varepsilon^\theta(\tau), \phi(\tau)\right) , \tag{2.59}$$

where $r_0$ and $\theta_0$ are constants and $\epsilon^r \ll r_0$ and $\epsilon^\theta \ll \theta_0$ are small perturbations from circular orbit motion. The equation of motion for $r$ results in

$$\ddot{\varepsilon}^r = -\frac{1}{2}\left(\partial_r V_{\text{eff}}(r_0,\theta_0) + \partial_r^2 V_{\text{eff}}(r_0,\theta_0)\varepsilon^r\right) + \mathcal{O}(\varepsilon^2). \tag{2.60}$$

The equation for $\theta$ results in a similar expression:

$$\ddot{\varepsilon}^\theta = -\frac{1}{2}\frac{1}{r^2 f(r)}\left(\partial_\theta V_{\text{eff}}(r_0,\theta_0) + \partial_\theta^2 V_{\text{eff}}(r_0,\theta_0)\varepsilon^\theta\right) + \mathcal{O}(\varepsilon^2). \tag{2.61}$$

The takeaway from these equations is that for the circular orbit to even exist we must ensure that

$$\partial_r V_{\text{eff}}(r_0,\theta_0) = \partial_\theta V_{\text{eff}}(r_0,\theta_0) = 0\,, \tag{2.62}$$

for otherwise, the particle drifts away from circular motion even without an initial perturbation. The condition $\partial_\theta V_{\text{eff}}(r_0,\theta_0) = 0$ implies $\theta_0 = \pi/2$, so all circular orbits lie in the equatorial plane. The other condition yields

$$\mathcal{L}^2(r_0 - 3M) + M\mathcal{L}\,\omega_c r_0^2 - \omega_c^2 r_0^4(r-M)/4 - M r_0^2 = 0\,. \tag{2.63}$$

This means that if we want to find a circular orbit of radius $r_0$ then the particle must have one of two specific angular momenta, the two roots of the polynomial above:

$$\mathcal{L}_\mp = \frac{-M\omega_c r_0^2 \mp r_0 F(r_0)}{2\,(r_0 - 3M)}\,, \quad F(r) = \sqrt{\omega_c^2 r^2 (r-2M)^2 + 4M(r-3M)}. \tag{2.64}$$

Given the symmetry of the effective potential, which is invariant under the transformation $(\mathcal{L},\omega_c) \to (-\mathcal{L},-\omega_c)$, it is important to distinguish between two fundamentally different types of circular motion that may arise in this system and which exhibit the same symmetry: *minus configuration* (MC), where $\mathcal{L} > 0$ and $\omega_c < 0$; this configuration exists in flat space as the Lorentz force is attractive in this case; *plus configuration* (PC), where $\mathcal{L} > 0$ and $\omega_c > 0$; this configuration does not exist in flat space, as the Lorentz force is repulsive in this case. We show schematic representations of the two configurations in Figure 2.1.

We choose to always show positive angular frequencies and angular momenta so the sign of the cyclotron frequency is what distinguishes minus ($\omega_c < 0$) and plus ($\omega_c > 0$) configuration orbits. In that regard, in Eq. (2.64) we only need the solution with the "+" sign: the solution with the "-" sign refers to the orbits obtained when we take $(\mathcal{L},\omega_c) \to (-\mathcal{L},-\omega_c)$. With that in mind, the angular frequency, as seen by a stationary observer at infinity (that is, $d\phi/dt$), is

$$\Omega_0 = \left[\frac{1}{2 + 2r_0^2\omega_c^2}\left(2\omega_K^2 + \omega_c^2\,(1 - 2M/r_0) - \omega_c\sqrt{\omega_c^2\,(1-2M/r_0)^2 + 4\omega_K^2\,(1-3M/r_0)}\right)\right]^{1/2}, \tag{2.65}$$

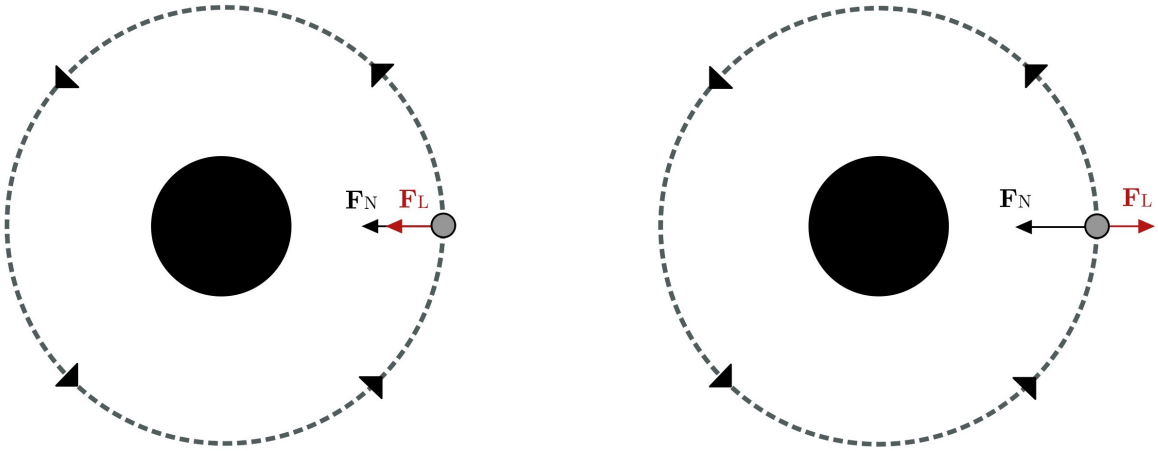


(a) Minus configuration (MC): $\omega_c < 0$.

(b) Plus configuration (PC): $\omega_c > 0$.

Figure 2.1: Schematic representation of the two configurations of circular orbits discussed in this thesis. They lie in the equatorial plane of a Schwarzschild BH immersed by an asymptotically uniform magnetic field along $\hat{z}$. The charged particle (grey dot) is assumed to orbit the BH (black disk) anticlockwise; The cyclotron frequency is $\omega_c = qB_0/m$, where $B_0$ is the magnetic field strength at infinity, $q$ is the charge of the particle, and $m$ is its mass. The configurations are invariant under inversion of the direction of the orbit and of the sign of $\omega_c$. We also include a Newtonian interpretation of the difference between the two configurations: $\boldsymbol{F}_\mathrm{N}$ and $\boldsymbol{F}_\mathrm{L}$ represent the gravitational and Lorentz forces respectively, with the latter being attractive (resp. repulsive) in MC (resp. PC) orbits.

where we recall that the typical frequencies of the problem are the Keplerian and cyclotron frequencies,

$$\omega_\mathrm{K} = \sqrt{\frac{M}{r_0^3}} \quad \text{and} \quad \omega_\mathrm{c} = \frac{qB_0}{m}\,. \tag{2.66}$$

These two timescales determine the relative importance of the two competing forces in the system: the gravitational and the Lorentz force. The gravitational force is stronger closer to the BH, and associated with the frequency $\omega_\mathrm{K}$. Conversely, since the magnetic field being considered is uniform, the Lorentz force does not depend explicitly on $r_0$, and neither does its associated frequency $\omega_\mathrm{c}$. Thus, we expect gravitational effects to dominate closer to the BH, while magnetic effects ought to become more relevant further away from the BH[2]. If that is the case, for what value of $r_0$ can we tell these two regimes apart, that is, what do we mean by close/far from the BH? The natural answer is to find for which value of $r_0$ the absolute values of the two frequencies coincide. This yields a critical radius

$$r_c = \left(\frac{M}{\omega_c^2}\right)^{1/3}\,. \tag{2.67}$$

[2]We must be careful not to say that magnetic effects dominate far away from the BH. While that is true for MC orbits, which do approach cyclotron motion in flat spacetime (see Sec. 2.1) for sufficiently far away orbits, the same is not true for PC orbits, because of the repulsive nature of the Lorentz force.

Now what happens if we take limits of Eq. (2.65) with respect to this value? We find

$$\begin{aligned} \Omega_0 &\xrightarrow[r_0 \ll r_c]{\text{MC}} \omega_{\text{K}}\,, \qquad \Omega_0 \xrightarrow[r_0 \gg r_c]{\text{MC}} \Omega_{\text{MC}}\,, \\ \Omega_0 &\xrightarrow[r_0 \ll r_c]{\text{PC}} \omega_{\text{K}}\,, \qquad \Omega_0 \xrightarrow[r_0 \gg r_c]{\text{PC}} \Omega_{\text{PC}}\,. \end{aligned} \tag{2.68}$$

In the limit $r_0 \ll r_c$ we find that the Keplerian frequency is recovered, as in this limit we have dominance of the gravitational effects. This goes for both PC and MC orbits, as they do not differ in this limit. For MC orbits, in the limit $r_0 \gg r_c$ we get cyclotron motion with the same angular frequency as in flat space Eq. (2.12),

$$\Omega_{\text{MC}} = -\frac{\omega_{\text{c}}}{\sqrt{1+(r_0\omega_{\text{c}})^2}}\,. \tag{2.69}$$

The velocity as seen by a stationary observer at infinity ($v_0 = r_0\Omega_0$) of particles traveling with orbital frequency $\Omega_{\text{MC}}$ approaches the speed of light for $r_0 \to \infty$. For PC orbits, the asymptotic frequency in the limit $r_0 \gg r_c$ doesn't yield any familiar result, as this type of orbit doesn't exist in flat space; instead, we find that the orbital frequency asymptotically approaches

$$\Omega_{\text{PC}} = \frac{\omega_{\text{K}}^2}{\omega_{\text{c}}} = \frac{M}{r_0^3\,\omega_c}\,. \tag{2.70}$$

Having established the limits of Eq. (2.65), we now turn to the study of the stability of circular orbits. If (2.62) is satisfied, then (2.60) and(2.61) reduce to harmonic oscillator equations with frequencies

$$\omega_r^2 = \frac{\partial_r^2 V_{\text{eff}}(r_0,\theta_0)}{2} = \frac{(r_0-2M)^2(3\mathcal{L}_+^2 + r_0^4\omega_c^2/4) - 2Mr_0(\mathcal{L}_+ - r_0^2\omega_c/2)^2 - 2Mr_0^3}{(r_0-2M)r_0^5}\,, \tag{2.71}$$

$$\omega_\theta^2 = \frac{\partial_\theta^2 V_{\text{eff}}(r_0,\theta_0)}{2\,r_0^2 f(r_0)} = \frac{\mathcal{L}_+^2}{r_0^4} - \frac{\omega_c^2}{4} = u^\phi\left(u^\phi + \omega_c\right)\,. \tag{2.72}$$

Note that $\mathcal{L}_+$ is the specific angular momentum at the circular orbit (see Eq. (2.64)). When we are at a minimum of the potential, these frequencies are real and the circular orbit is stable under perturbations. Conversely, if either frequency is not real, the orbit is unstable and, when perturbed, the particle will drift away from circular motion.

Thus we must study the sign of the RHS of Eqs. (2.71) and (2.72). We can easily see that angular perturbations are always stable in both PC and MC orbits: for PC orbits $u^\phi$ and $\omega_c$ have the same sign, and so the problem is trivial; for MC orbits, gravitational and magnetic effects work together to speed up the particle, so it only makes sense that $u^\phi > |\omega_c|$, as $u^\phi = |\omega_c|$ in flat space (see Eq. (2.7)).

Regarding radial perturbations, the RHS of Eq. (2.71) is positive for $r_0 \to \infty$, so all orbits are stable up to the innermost stable circular orbit (ISCO). We calculated the location of the ISCO (see Fig. 2.2) and found that for PC orbits increasing the absolute value of the cyclotron frequency allows for the ISCO to be pulled in arbitrarily close to the BH horizon $r_0^{\text{ISCO}}/M \to 2$; for MC orbits, we find the radius of the ISCO approaches

$$r_0^{\text{ISCO}}/M \to \frac{5+\sqrt{13}}{2} \approx 4.30\,, \tag{2.73}$$

hence corroborating and further extending the results in Refs. [43, 47, 60].

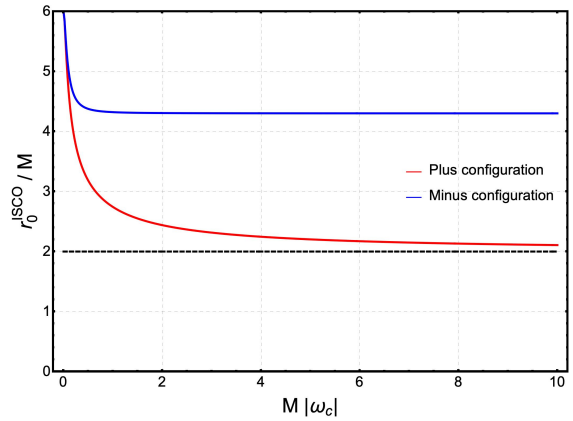


Figure 2.2: Radius of the innermost stable circular orbit of a charged particle around a Schwarzschild BH of mass $M$ in an asymptotically uniform magnetic field as a function of $|\omega_c|$. The red and blue curves correspond to PC and MC orbits, respectively. The black dashed line indicates the position of the event horizon of the BH.

The question we ask next is: what is the velocity of the particles traveling at the ISCO? This can be answered easily once we know the value of the ISCO, and we present results concerning the velocity as seen by a stationary observer at infinity in Fig. 2.3a. We find that for PC orbits the velocity becomes smaller as the EH is approached, which is a direct result of the repulsive nature of the Lorentz force. For MC orbits, the velocity tends to the constant value

$$v_0^{\rm ISCO} \to \frac{\sqrt{6+\left(3+\sqrt{13}\right)}}{5+\sqrt{13}} \approx 0.732\,, \tag{2.74}$$

as the particle approaches the barrier at $r_0^{\rm ISCO}$.

The reason why particles in the ISCO of MC orbits cannot get any closer to the EH is that in order for this to happen the stationary observers at the orbit of the particle would see it traveling faster than the speed of the light. Gravitational redshift hides this effect from stationary observers at infinity, but if we plot the velocity seen by local stationary observers at the ISCO ($v_L = v_0/\sqrt{f}$) we obtain the results in Fig. 2.3b. Indeed, stationary observers at the ISCO see particles in the MC approaching the speed of light; perhaps more surprisingly, they see particles in the PC approaching half the speed of light.

To get a better understanding of the structure of circular orbits, we also looked at the velocity profiles as seen by stationary observers at infinity for MC and PC orbits (Fig. 2.4). In these plots, we compare the results obtained with Eq. (2.65) with the limits given in Eq. (2.68), while also showing the value of $r_c$ (see Eq. (2.67)). We find that, in general, the results recover what was expected from the discussion given after Eq. (2.65).

In particular, for MC orbits the velocity profile changes from monotonically decreasing ($\omega_c = 0$), to non-monotonic ($M|\omega_c| = 10^{-3}$) and then monotonically increasing ($M|\omega_c| = 10^{-1}$). This change in monotonicity happens because the inclusion of a magnetic field makes asymptotic orbits in the MC relativistic. As for PC orbits, we find that the velocity profile is always monotonically decreasing, so that increasing $\omega_c$ simply causes the velocity to decay more rapidly towards asymptotically stationary orbits.

Regarding the comparison with the limiting formulas, we find that in the $\omega_c = 0$ case, the “Keplerian”

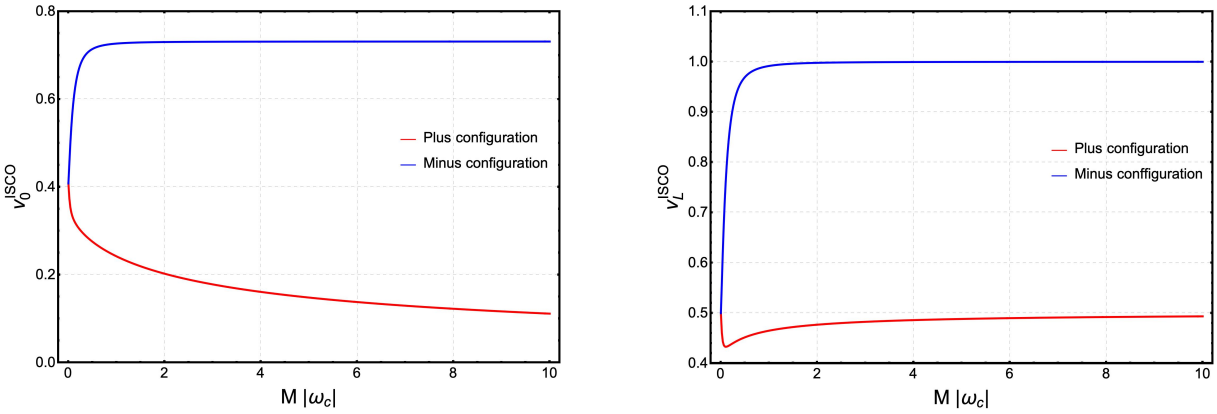


(a) Stationary observers at infinity.

(b) Stationary observers at the ISCO.

Figure 2.3: Orbital velocity of particles at the ISCO, as seen by two families of observers, as a function of $|\omega_c|$. The red and blue curves correspond to PC and MC orbits, respectively.

result is exactly recovered, as expected. For $M|\omega_c| = 10^{-3}$ the Keplerian curve gives a good approximation close to the BH; as $r_0 = r_c$ is approached, the "Keplerian" curve starts to diverge from the velocity profile, which is when we start to see the "magnetic" curve become a better approximation for $v_0$; for $r_0 \gg r_c$ the "magnetic" curve is good approximation. For $M|\omega_c| = 10^{-1}$ we don't see the Keplerian result ever being a good approximation, because now $r_c$ is very close to the EH; instead we see the "magnetic" curve becoming closer and closer to the actual velocity profile.

## 2.3 Radiation reaction force in curved space

### 2.3.1 The DeWitt – Brehme equation of motion

The generalization to curved space of the dynamics of a radiating charged particle of mass $m$ and charge $q$ in the presence of an EM field was obtained in [55, 56] (see also the review article [59]), and reads

$$\frac{Du^\mu}{d\tau} = \frac{q}{m} F^\mu{}_\nu u^\nu + \frac{2q^2}{3m}\left(\frac{D^2u^\mu}{d\tau^2} + u^\mu u_\nu \frac{D^2u^\nu}{d\tau^2}\right) + \frac{q^2}{3m}\left(R^\mu{}_\nu u^\nu + R^\nu{}_\alpha u_\nu u^\alpha u^\mu\right) + \frac{2q^2}{m} f^{\mu\nu}_{\text{tail}} u_\nu \,, \tag{2.75}$$

where $u^\mu(\tau)$ is the particle's four-velocity, $\tau$ is the proper time, $F_{\mu\nu} = \partial_\mu A_\nu - \partial_\nu A_\mu$ is the Faraday tensor with EM four-potential $A_\mu$, and $R_{\mu\nu}$ is the Ricci tensor (identically zero for vacuum spacetimes). The first two terms on the RHS of Eq. (2.75) were already present in flat space (see Eq. (2.13)), and correspond, respectively, to the Lorentz and Abraham-Lorentz-Dirac forces. The last two terms are curved spacetime effects: one coupling to the Ricci curvature tensor and another corresponding to the tail term, given by

$$f^{\mu\nu}_{\text{tail}} = \int_{-\infty}^{\tau^-} \nabla^{[\mu} G^{\nu]}{}_{\lambda'}\left(z(\tau), z(\tau')\right) u^{\lambda'} d\tau' \,, \tag{2.76}$$

where square brackets denote anti-symmetrization, $z(\tau)$ is the world line of the particle, $G^\nu{}_{\lambda'}(x, x')$ is the retarded Green's function for the vector wave equation in curved space, and the integral is taken

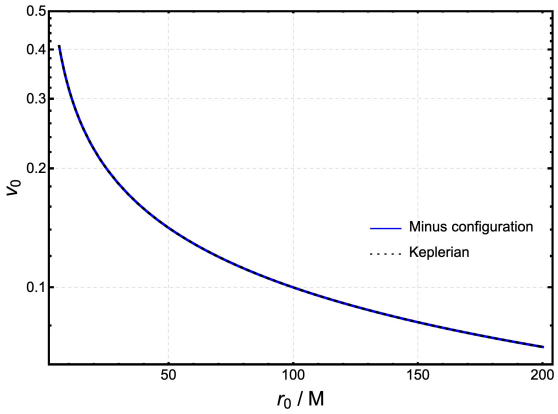


(a) MC orbits with $\omega_c = 0$.

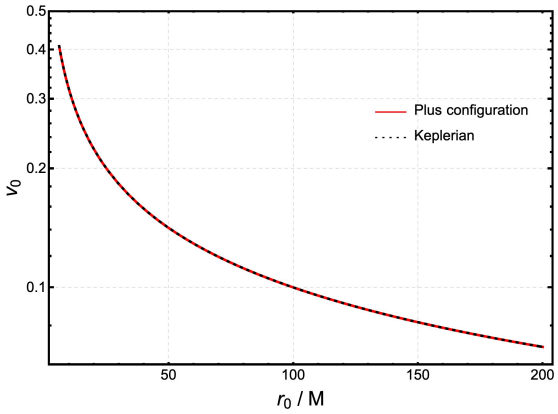


(b) PC orbits with $\omega_c = 0$.

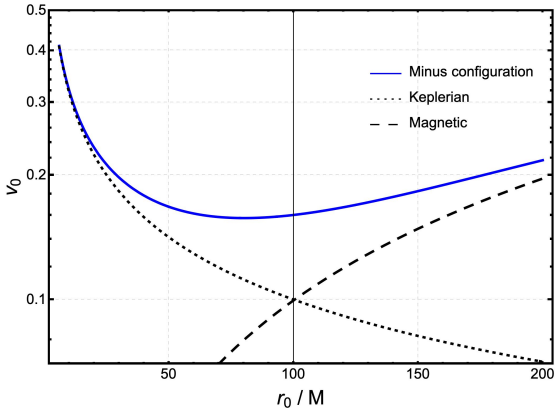


(c) MC orbits with $M\omega_c = -10^{-3}$.

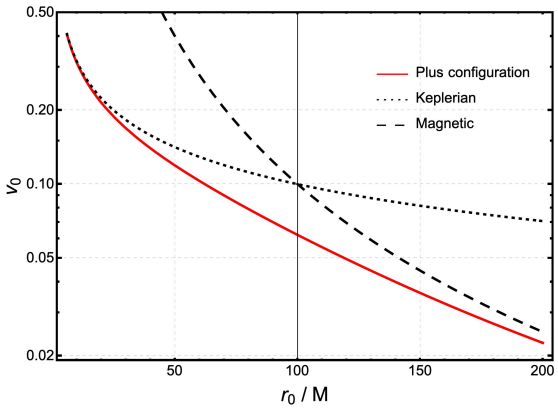


(d) PC orbits with $M\omega_c = 10^{-3}$.

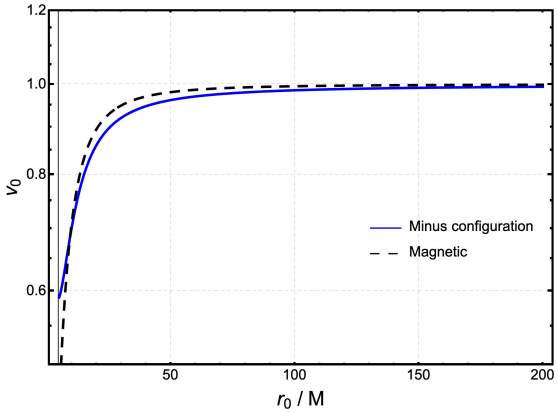


(e) MC orbits with $M\omega_c = -10^{-1}$.

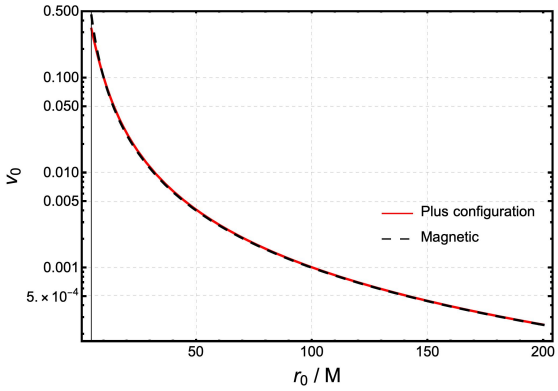


(f) PC orbits with $M\omega_c = 10^{-1}$.

Figure 2.4: Velocity profiles, as seen by a stationary observer at infinity, of circular orbits with radius $r_0$ for different values of $\omega_c$. *Left column* – MC orbits. *Right column* – PC orbits. The blue and red curves correspond to the velocity profiles for MC and PC orbits, respectively; the "Keplerian" curves (black dashed) are obtained by taking $\Omega_0 = \omega_K$; the "Magnetic" (black dotted) curves are obtained by taking $\Omega_0 = \Omega_{\rm MC}$ in MC orbits and $\Omega_0 = \Omega_{\rm PC}$ in PC orbits. Finally, the black solid thin vertical line indicates the position of the critical radius $r_c/M = \infty,\ 100,\ 4.64$, for the top, center, and bottom cases, respectively. The "Keplerian" result is recovered for $r_0 \ll r_c$ and the "Magnetic" result is recovered for $r_0 \gg r_c$.

over the entire history of the particle. For a modern derivation of Eqs. (2.75) and (2.76) see the review by Poisson [59].

Equation (2.75) is a third order equation for the position of the particle, and so it has several unwanted

features, such as the existence of runaway solutions. This issue is solved by performing an order reduction of the equation, identical to what we did in flat space to obtain Eq. (2.15). The idea is to make the substitution

$$\frac{D^2 u^\mu}{d\tau^2} \to \frac{q}{m}\frac{D}{d\tau}\left(F^\mu{}_\nu u^\nu\right) . \tag{2.77}$$

The validity of this approximation in flat space has been widely studied [92–96], and some analysis has also been done in the curved space case [59, 102]. Replacing Eq. (2.77) in Eq. (2.75) leads to the reduced equation of motion, which in vacuum spacetimes ($R_{\mu\nu} = 0$) takes the form

$$\frac{Du^\mu}{d\tau} = \frac{q}{m}F^\mu{}_\nu u^\nu + \frac{2q^3}{3m^2}\left(\nabla_\alpha F^\mu{}_\nu u^\alpha u^\nu\right) + \frac{2q^3}{3m^2}\left(\frac{q}{m}\left(F^{\mu\nu}F_{\nu\rho} + F^{\nu\alpha}F_{\alpha\rho}u_\nu u^\mu\right)u^\rho\right) + \frac{2q^2}{m}f^{\mu\nu}_{\text{tail}}u_\nu . \tag{2.78}$$

Here, the only new term when compared to the reduced Abraham-Lorentz-Dirac equation in flat space (Eq. (2.13)) is the tail term. This non-local term happens to be very complicated, both from a numerical and from an analytical point of view, due to the integral over the entire history of the particle. With that in mind, it would make the study of the dynamics of charged particles way simpler if we could exclude the tail term (Eq. (2.76)) from our analysis.

### 2.3.2 Motion without the tail term

We will now assume the tail term can be neglected and see what sort of dynamics arise in that case. This is precisely what was done in Ref. [53] [3] , where the tail term is neglected based on an estimate for this force taken from the works by DeWitt and DeWitt [62] and Smith and Will [57] [4],

$$\boldsymbol{F}_{\text{tail}} \sim \frac{q^2 M}{r^3}\hat{r} , \tag{2.79}$$

and then comparing it to the Newtonian expression for the gravitational force, with respect to which it is often negligible.

The estimate of the tail term in Eq. (2.79) was shown in Ref. [57] to be the expression for the radiation reaction force acting upon a static charge outside a Schwarzschild BH, as seen by an instantaneously comoving inertial observer at the position of the particle. However, in Ref. [62] it had already been shown that, even in the weak field limit, this does not account for the radiation reaction force completely, as another term exists which is non-zero only if the particle is moving. So the question is clear: if the charge is moving, can the tail term still be neglected? More precisely, can it be neglected if the particle is moving in a circular orbit?

If the tail term is indeed neglected, the equation of motion is just Eq. (2.78) without the last term on the RHS, with the EM field replaced by the result Eq. (2.47), explicitly given by

$$F_{r\phi} = Br\sin^2\theta, \quad F_{\theta\phi} = Br^2\sin\theta\cos\theta , \tag{2.80}$$

[3] We report that the equations of motion we obtained differ from theirs by a factor of 3 and a factor of $u^\phi$ in Eq. (2.82), and by a minus sign in Eq. (2.83).

[4] The radiation reaction force is often called the particle's self-force. This is because that force can be seen as arising from the interaction of the particle with its own EM field [59].

with all other independent components of $F_{\mu\nu}$ equal to zero. Consider now the motion of a particle in the equatorial plane ($\theta = \pi/2$) [5] , in which case $F_{r\phi} = Br$ is the only non-zero component of the EM field. Then the equations of motion can be written explicitly as

$$\frac{du^t}{d\tau} = -\frac{2M}{r^2 f(r)} u^t u^r - \frac{2q^2}{3m}\frac{\omega_c u^t}{r}\left[\omega_c\, r f(r)\left(f(r)\left(u^t\right)^2 - 1\right) - M u^\phi\right] , \tag{2.81}$$

$$\frac{du^r}{d\tau} = u^\phi\left(\omega_c\, r f(r) + (r-3M)u^\phi\right) - \frac{M}{r^2} - \frac{2q^2}{3m}\frac{\omega_c u^r}{r}\left[\omega_c r f(r)^2\left(u^t\right)^2 - M u^\phi\right] , \tag{2.82}$$

$$\frac{du^\phi}{d\tau} = -\frac{2u^r\left(u^\phi + \omega_c/2\right)}{r} + \frac{2q^2}{3m}\frac{\omega_c}{r^3}\left[M r^2\left(u^\phi\right)^2 - \omega_c\, r^3 f(r)^2\left(u^t\right)^2 u^\phi + M\right] . \tag{2.83}$$

If we now look at the kinematic variables of the charged particles in the equatorial plane (Eq. (2.56)) we find the rate of energy loss is

$$\frac{dE}{dt} = -\frac{2q^2}{3}\omega_c f(r)\left[\omega_c \mathcal{E}^2 - \left(\omega_c f(r) + \frac{M}{r}u^\phi\right)\right] , \tag{2.84}$$

while that of angular momentum loss becomes

$$\frac{dL}{dt} = \frac{2q^2}{3}\frac{\omega_c}{u^t}\left[M r\left(u^\phi\right)^2 - \omega_c r^2 f(r)^2\left(u^t\right)^2 u^\phi + \frac{M}{r}\right] . \tag{2.85}$$

An interesting feature of Eq. (2.84) is that it allows for the particle to gain energy, that is, it is possible to have $dE/dt > 0$. If we restrict to circular orbits of radius $r_0$, the condition for $dE/dt > 0$ can be written as

$$\omega_c > 0 \quad \wedge \quad 0 < f(r_0)u^\phi/\Omega_{\text{PC}} < 1 . \tag{2.86}$$

This condition can only ever be satisfied in PC orbits, as $u^\phi$ and $\omega_c$ must have the same sign. If we replace the value of $u^\phi$ corresponding to PC orbits, that is,

$$u^\phi \to \frac{\Omega_0}{\sqrt{1 - 2M/r_0 - v_0^2}} , \tag{2.87}$$

where $\Omega_0$ was given in Eq. (2.65), then we find that for all PC orbits outside the light ring ($r_0 > 3M$) this condition is satisfied, so that the particle gains energy instead of losing.

Since, as we discussed in Sec. 2.2.3, the energy of circular orbits increases with the radius of the orbit, we expect the orbital radius of a particle in a PC orbit to increase as it gains energy according to Eq. (2.84). By numerically integrating Eqs. (2.81), (2.82) and (2.83), we found this orbit widening effect does take place (see Fig. 2.5). Since the energy gain holds for all orbits with $r_0/M > 3$, so does the orbit widening.

This result is counterintuitive: there seems to be a violation of energy conservation since there is no clear source of energy in the system that could be feeding the orbit widening. The BH is not rotating, so it cannot be superradiance, and the EM field is purely magnetic, so it cannot be the EM field either.

This apparent incoherence was the main motivation for this thesis, where we tried to understand how

[5] For consistency, it is important to note that when we take a particle with $u^\theta = 0$ in the equatorial plane, then $du^\theta/d\tau = 0$, so that the motion will remain in the equatorial plane.

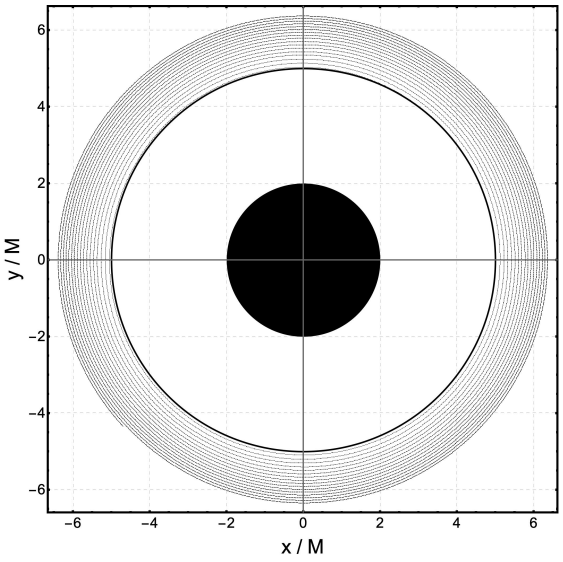


Figure 2.5: Motion of a radiating charged particle in the equatorial plane of a Schwarzschild BH surrounded by an asymptotically uniform magnetic field with $M = 1$, $M\omega_c = 0.2$ and $2q^2/3m = 0.1\,M$, neglecting the tail term. The particle is initially in a PC orbit, but the radiation reaction force causes the radius of the orbit to increase adiabatically, while the particle gains energy. The black circle in the center represents the BH region; the black ring at $r/M = 5$ represents the initial circular orbit.

EM radiation reaction affects the motion of charged particles around magnetized Schwarzschild BHs, focusing on the simplest case of circular orbits. We will try to establish if this orbit-widening effect can indeed happen, and, more generally, if there is any scenario where the tail term can be neglected, which would mean the Eqs. (2.81), (2.82) and (2.83) are the correct equations of motion of the system.

# Chapter 3

# Radiating charged particle orbiting a magnetized Schwarzschild black hole - Newtonian Limit

The results in this chapter were published in [54].

In this chapter, the main aim is to employ the Newtonian limit to try and understand if the energy gain and associated orbit widening that we found in Sec. 2.3.2 does indeed take place. Just as an initial sanity check, we replaced the BH with a static charge at the origin and found that this phenomenon no longer took place (Appendix C). In the Newtonian limit, the charge and BH cases should give rise to the same results, as long as the value of the static charge is chosen appropriately.

The system is exactly the one studied in Sec. 2.2.3 but including radiation reaction so that the equation of motion is Eq. (2.78). To obtain the Newtonian limit, we start by recalling the expression for the gravitational potential of a pointlike particle of mass $M$ placed at the origin:

$$\Phi(r) = -\frac{M}{r} \,. \tag{3.1}$$

Let $u^\mu$ be the 4-velocity of the charged test particle:

$$u^\mu = u^t \left(1, \boldsymbol{v}\right) \,, \quad u^t = \frac{dt}{d\tau} \sim \left(1 - v^2\right)^{-\frac{1}{2}} \,, \tag{3.2}$$

where $\boldsymbol{v}$ is the coordinate 3-velocity and $v$ is its norm. We now must impose that the particle is moving slowly through a weak gravitational field, which can be written as

$$|\Phi| \sim v^2 \sim r^2 \omega_c^2 \sim \mathcal{O}\left(\varepsilon\right) \ll 1 \,. \tag{3.3}$$

The first condition implies a weak gravitational field, the second condition states that the particle is slow-

moving, and the third condition means that the magnetic field is also weak[1]. From this point onward we neglect terms which are $\mathcal{O}(\varepsilon)^2$ or smaller. The metric (2.24) is then approximated by

$$g_{\text{Newton}} = -(1+2\Phi)\,dt^2 + (1-2\Phi)\,d\boldsymbol{r}^2\,. \tag{3.4}$$

If we calculate the action for timelike geodesics using this metric, we retrieve the appropriate Newtonian action

$$S = \int \sqrt{-g_{\mu\nu}u^\mu u^\nu}d\tau = \int \left(1 - \frac{v^2}{2} - \frac{M}{r}\right) dt\,, \tag{3.5}$$

up to $\mathcal{O}(\varepsilon)^2$ terms. Now consider a particle in a circular orbit in the equatorial plane with radial coordinate $r_0$. Note that we will parameterize the motion using the coordinate time $t$ rather than the proper time $\tau$, since the $\mathcal{O}(\varepsilon)$ term in (3.2) always leads to $\mathcal{O}(\varepsilon)^2$ terms in the equation of motion. With that in mind, we use $u^t \approx 1$ from here on, consistently with the pre-relativistic idea that proper time is the same as coordinate time.

## 3.1 Analytical results in the adiabatic approximation

We assume the effects of radiation are small enough for the particle to always be in a circular orbit, but that the radius $r_0$ of the latter changes adiabatically. In that case the position $\boldsymbol{x}(t)$ and the 3-velocity, $\boldsymbol{v}(t)$ of the charged particle are

$$\boldsymbol{x}(t) = r_0\left(\cos(\Omega_0 t)\,,\,\sin(\Omega_0 t)\,,\,0\right)\,, \tag{3.6}$$

$$\boldsymbol{v}(t) = \frac{d\boldsymbol{x}(t)}{dt} \approx r_0\Omega_0\left(-\sin(\Omega_0 t)\,,\,\cos(\Omega_0 t)\,,\,0\right)\,, \tag{3.7}$$

where the angular velocity $\Omega_0$ also changes adiabatically. We assume that the orbit satisfies all the conditions for the Newtonian limit to hold. In that case, the limit of Eq. (2.78) for these circular orbits is easy to find:

$$m\frac{d\boldsymbol{v}}{dt} = \boldsymbol{F}_{\text{N}} + \boldsymbol{F}_{\text{L}} + \boldsymbol{F}_{\text{RR}} + \boldsymbol{F}_{\text{tail}}\,. \tag{3.8}$$

Here, the first two forces on the RHS are, respectively, the Newtonian gravitational force and the Lorentz force, which, in this case, take the form

$$\boldsymbol{F}_{\text{N}} = -m\frac{M}{r_0^2}\hat{\boldsymbol{r}}\,, \quad \boldsymbol{F}_{\text{L}} = qv_0B_0\hat{\boldsymbol{r}}\,, \tag{3.9}$$

where $\hat{\boldsymbol{r}}$ is the unit radial vector and $v_0 = r_0\Omega_0$. The third force comes from the Abraham–Lorentz–Dirac term in Eq. (2.78). For the particle orbits we are studying, it is

$$\boldsymbol{F}_{\text{RR}} = \frac{2q^2}{3}\omega_c\frac{v_0^2}{r_0}\hat{\boldsymbol{\phi}}\,, \tag{3.10}$$

[1] This condition may also be stated as "all the typical velocities of the problem are much smaller than the speed of light".

where $\hat{\phi}$ is the unit tangent vector. This is the first dissipative term we encounter. It is parallel to the velocity in PC orbits, hence doing positive work, and anti-parallel to the velocity in MC orbits, where it does negative work. Finally, we have the tail term, which was estimated for the weak field, slow motion regime in Refs. [62, 63]:

$$\boldsymbol{F}_{\text{tail}} = q^2 \frac{M}{r_0^3}\hat{\boldsymbol{r}} - \frac{2q^2}{3}\frac{d}{dt}\left(\boldsymbol{\nabla}\Phi\right) = q^2 \frac{M}{r_0^3}\hat{\boldsymbol{r}} - \frac{2q^2}{3}\frac{M}{r_0^3}v_0\hat{\boldsymbol{\phi}}\,, \tag{3.11}$$

where $\boldsymbol{\nabla}$ is the gradient with respect to the spatial coordinates. We can distinguish two components of the tail: a conservative part, $F^r_{\text{tail}}$, and a dissipative part, $F^\phi_{\text{tail}}$. We will now determine whether or not these tail terms must be included to adequately describe the motion of the charged particle.

The conservative part, $F^r_{\text{tail}}$, was originally derived in Ref. [62] (see also Ref. [57]), and can be compared to the gravitational force as it points in the radial direction. If this comparison is done at the BH horizon $(r = 2M)$ we obtain

$$\frac{F^r_{\text{tail}}}{F_{\text{N}}} \approx 10^{-19}\left(\frac{q}{e}\right)^2\left(\frac{m_e}{m}\right)\left(\frac{10M_\odot}{M}\right)\,, \tag{3.12}$$

where $e$ and $m_e$ are, respectively, the electron charge and mass, and $M_\odot$ is the mass of the sun. This ratio is very small for astrophysically relevant scenarios, which means the conservative part of the tail term can be neglected. Note that it may seem odd that the comparison is performed at the BH horizon since a weak field approximation is assumed; however, the tail term decays faster with $r$ than $F_{\text{N}}$, and so this is, in fact, an upper bound. This was the comparison used in Refs. [52, 53] to ignore the tail term; however, in the process they also neglected the dissipative part of the tail term, which we will see cannot generally be neglected.

Regarding the dissipative part, $F^\phi_{\text{tail}}$, we start by noting it always does negative work, since it points in the opposite direction to the particle's velocity. To see if it must be included, we should compare it with the other dissipative term, $F_{\text{RR}}$, which is also tangent to the particle's velocity. We find

$$\frac{F^\phi_{\text{tail}}}{F_{\text{RR}}} = \frac{\omega_K^2}{|\omega_{\text{c}}|\Omega_0} = \frac{F_{\text{N}}}{F_{\text{L}}}\,, \tag{3.13}$$

(where $\omega_{\text{c}}$ is the cyclotron frequency, and $\omega_{\text{K}}$ is the Keplerian frequency). Thus, neglecting the dissipative part of the tail term and keeping the radiation reaction due to the Lorentz force is equivalent to neglecting the gravitational force while keeping the Lorentz force.

In Sec. 2.2.3 we found the orbital frequency of PC orbits asymptotically approaches $\Omega_{\text{PC}} = \omega_K^2/\omega_c$ for large orbital radius. Thus, in the Newtonian limit, this is the orbital frequency in PC orbits, which would mean the ratio of Eq. (3.13) goes to $1$. We conclude that neglecting the tail term while keeping $\boldsymbol{F}_{\text{RR}}$ in PC orbits is not consistent.

For vacuum spacetimes, therefore, the conservative part of the tail term can be neglected in the Newtonian limit. However, the dissipative part can only be neglected consistently if either of the following is true:

**(i)** Radiation reaction due to the Lorentz force is neglected as well, and the equation of motion is just Eq. (2.75) with all terms $\propto q^2$ set to zero;

**(ii)** the gravitational force is neglected as well, and a flat-space description using the Abraham-Lorentz-Dirac equation is valid.

In other words, in situations where the gravitational force dominates, such as the PC orbits, the tail term *must* be included, since $F^{\phi}_{\text{tail}}$ also dominates $F_{\text{RR}}$. In particular, the particle will *always* lose energy. This is the main result of this chapter.

As an additional check on the calculation presented above, we can see if it allows us to recover the results for the Lorentz self-force and Larmor power formula, which we derived in Appendix B). Indeed, those results are only recovered if the dissipative part of the tail term is included. The results of Ref. [87] for a charged particle orbiting a Kerr BH in the Newtonian limit are also only recovered if both $\boldsymbol{F}_{\text{RR}}$ and $\boldsymbol{F}^{\phi}_{\text{tail}}$ are included in the equations of motion. We have shown that to adequately recover the non-relativistic Larmor formula (Eq. (2.22)) from the DeWitt–Brehme equation (Eq. (2.75)), in all setups where EM radiation reaction and gravity are relevant, the tail term must *always* be included[2].

## 3.2 Numerical simulation of plus configuration orbits

To visualize the effects of the tail term in the dynamics, we have also studied numerically the evolution of particles in the plus configuration, with and without the inclusion of the tail. For the numerical evolution, we did not restrict ourselves to the adiabatic approximation (i.e. did not assume the orbit is circular with slowly varying parameters). This is still, of course, within the framework of the Newtonian limit.

Using Cartesian coordinates $(x, y)$ in the equatorial plane, the equation of motion is still Eq. (3.8), but now the expressions for the forces on the RHS are given by [42, 62, 63]

$$\boldsymbol{F}_N = -\frac{Mm}{r^3}x\hat{\boldsymbol{x}} - \frac{Mm}{r^3}y\hat{\boldsymbol{y}}\,, \tag{3.14}$$

$$\boldsymbol{F}_L = qv_yB_0\hat{\boldsymbol{x}} - qv_xB_0\hat{\boldsymbol{y}}\,, \tag{3.15}$$

$$\boldsymbol{F}_{\text{RR}} = -\frac{2q^3}{3m^2}\left(\left(qv_xB_0^2 + \frac{Mm}{r^3}yB_0\right)\hat{\boldsymbol{x}} + \left(qv_yB_0^2 - \frac{Mm}{r^3}yB_0\right)\hat{\boldsymbol{y}}\right), \tag{3.16}$$

$$\boldsymbol{F}_{\text{tail}} = \frac{q^2M}{r^3}\left(\left(\frac{x}{r} - \frac{2}{3}v_x\right)\hat{\boldsymbol{x}} + \left(\frac{y}{r} - \frac{2}{3}v_y\right)\hat{\boldsymbol{y}}\right). \tag{3.17}$$

We recall that $B_0$ is the magnetic field intensity.

These equations were used to numerically simulate the motion of particles in plus configuration orbits, using the parameters given in Table 3.1. To illustrate the importance of the tail term, we present two simulations, with and without including the term $\boldsymbol{F}_{\text{tail}}$ in the equations of motion (Fig. 3.1). Since $\boldsymbol{F}_{\text{RR}}$ is doing positive work, when the tail is excluded the particle starts drifting away from the BH, as a result of gaining energy. By opposition, as expected from our analytical results, the particle starts falling into the BH when the tail term is included.

[2] Interestingly, even when this limit is recovered, the conservative part of the tail term, $F^{r}_{\text{tail}}$, is still present; it is a completely new term which was not predicted before GR. This term was calculated in the general case, without requiring the Newtonian limit, but instead having the particle be held static, in [57]. Since it is an intrinsically general relativistic effect, it must be tied to the notion of spacetime curvature. Heuristically, the presence of the BH deforms the electrostatic field lines generated by a point charge in such a way as to mimic the presence of a second charged particle between the original point charge and the BH.

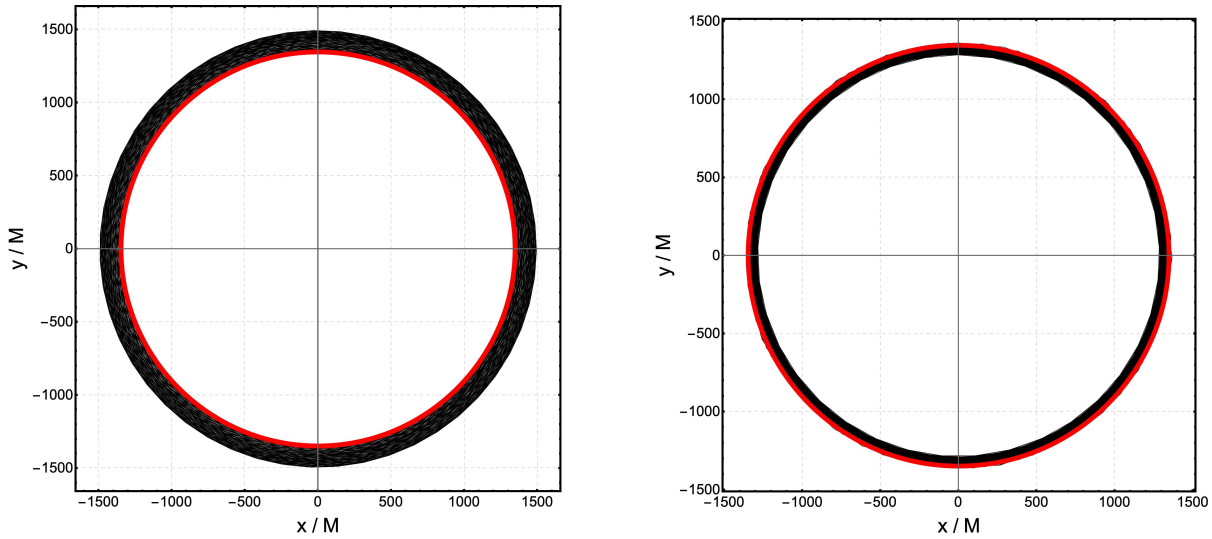


Figure 3.1: Trajectories of a charged particle in a plus configuration orbit, with the parameters given in Table 3.1. The red circle represents the initial orbit, with the subsequent particle motion plotted in black. *Left panel* – motion without the inclusion of $\boldsymbol{F}_{\text{tail}}$. *Right panel* – motion with the inclusion of $\boldsymbol{F}_{\text{tail}}$. We can see that if the tail is neglected then the particle gains energy and the orbit drifts away from the BH, as a consequence of the positive work done by $\boldsymbol{F}_{\text{RR}}$ (left). By contrast, if the tail term $\boldsymbol{F}_{\text{tail}}$ is included then it does enough negative work so that the particle loses energy and starts falling into the BH (right).

| Qty | Value | Simulation |
|---|---|---|
| $M$ | $10\,M_{\odot}$ | $1$ |
| $B_0$ | $10^8\,G$ | $1.20 \times 10^{-11}$ |
| $q$ | $7 \times 10^{15}\,C$ | $1.44 \times 10^{-5}$ |
| $m$ | $10^{20}\,kg$ | $5 \times 10^{-12}$ |
| $r_0$ | $2 \times 10^7\,m$ | $1.35 \times 10^3$ |

Table 3.1: Parameters used in our simulations. The second column gives values in SI units and solar masses ($M_{\odot}$), while the third column gives the values used in the actual simulation (after normalizing to the BH mass).

This clearly illustrates that the orbit widening effects reported in [52, 53] result from incorrectly excluding the tail term from the equation motion, at least in the Newtonian limit.

## 3.3 Discussion of the Newtonian limit

Our results disagree with those in Ref. [53]. In the latter, the dissipative part of the tail term is neglected altogether, and the equation of motion used to study charged particle dynamics is (2.78) without the tail term. This implies, in particular, that a particle in a plus configuration orbit will gradually gain energy, given that $\boldsymbol{F}_{\text{RR}}$ will do positive work, as evidenced in (3.10) and the subsequent discussion. This energy extraction is accompanied by a "orbital widening" effect. Such a result cannot be correct, as there is no possible source of energy for these particles (in fact, it was this counter-intuitive claim that led us to investigate the tail term). We find that not only does such an energy-generating process disappear when the tail is included, but also that it must *always* be included, at least in the Newtonian limit.

But why is the tail term and its complicated expression (2.76) so important? Imagine we could indeed neglect it, so the equation of motion after order reduction would be

$$\frac{Du^\mu}{d\tau} = \frac{q}{m}F^\mu{}_\nu u^\nu + \frac{2q^2}{3m}\left(\frac{q}{m}\nabla_\alpha F^\mu{}_\nu u^\alpha u^\nu\right) \frac{2q^2}{3m}\left(\frac{q^2}{m^2}\left(F^{\mu\nu}F_{\nu\rho} + F^{\nu\alpha}F_{\alpha\rho}u_\nu u^\mu\right)u^\rho\right) . \tag{3.18}$$

This equation states that if no EM field is present then the particle will simply follow a geodesic of space-time, meaning it does not radiate. This would also mean that the gravitational force is fundamentally different from any other, as Eq. (2.22) would have to be corrected so that it only includes acceleration arising from all forces other than the gravitational force. In GR, gravity is indeed a fundamentally different force; however, it still must make orbiting particles radiate, as their position varies periodically. This can also be seen from a calculation using the conformal invariance of Maxwell's equations (see Appendix D).

# Chapter 4

# Electromagnetic fields as perturbations of Schwarzschild spacetime

We now turn our attention to the general strong field case, so we drop the assumptions of Eq. (3.3) and study the full GR case. We want to include radiation reaction in our description of the motion of a charged particle around a magnetized Schwarschild BH and will do so by studying the radiation field itself, which is taken to be small enough for BH perturbation theory to be valid. We must note that we considered no perturbations on the background magnetic field, which is kept constant throughout the analysis (see Sec. 2.2.2).

The study of perturbations of the Schwarzschild geometry is a very rich one, dating back to the historic works by Regge and Wheeler [65], Vishveshwara [103], Zerilli [66, 104] and others [9, 77, 105], but also with more recent developments [106–108]. We choose to employ the Teukolsky equation [68], which describes perturbations of the Kerr family of solutions, but taking the spin of the BH to zero ($a = 0$), so that we get the Bardeen-Press equation [69] – an equivalent formulation of perturbations of the Schwarzschild geometry to that given by the Regge-Wheeler and Zerilli equations, as shown by Chandrasekhar in [70].

The idea now is the following: we will first look at the formalism of the Teukolsky equation and some key components needed for our analysis. Next, we will take a charged particle in a circular orbit around a Schwarzschild BH surrounded by an asymptotically uniform magnetic field (see Sec. 2.2.3) and use Teukolsky's equation to study the radiation field it creates; from that, we will obtain the amount of energy $E$ and angular momentum $L$ lost to infinity, as well as that which is absorbed by the BH. Since the motion in the equatorial plane is entirely determined by the value of these two quantities, knowing how they evolve allows us to study how the orbit changes with time. The assumption that the particle is always in a circular orbit is called the adiabatic approximation and it states that if the parameters vary slowly enough we can assume that the particle is always in a circular orbit, and its radius $r_0$ is varying slowly.

There is an important caveat, however: for a given value of energy and radius of the orbit, the angular momentum is uniquely determined (see Sec. 2.2.3). Thus, for the adiabatic approximation to be valid, the rate of change of energy and angular momentum must be compatible with the particle remaining in a circular orbit. There is a general result relating the energy and angular momentum carried by EM waves [109] across any sphere centered at the BH:

$$dL = \frac{m}{\omega} dE = \frac{1}{\Omega_0} dE \,, \tag{4.1}$$

which is precisely what we had found in flat space (see Eq. (2.23)). It turns out that if we replace the expressions for $E$ and $L$ for a particle in a circular orbit around a magnetized Schwarzschild BH (Eqs. (2.29) and (2.30)), the result is indeed compatible with the particle remaining in a circular orbit. Furthermore, this result is also valid for scalar and gravitational waves, so the adiabatic approximation can also be used in those cases. With this in mind, we will only calculate energy fluxes, because the angular momentum fluxes can be easily calculated using Eq. (4.1).

## 4.1 The Teukolsky equation

### 4.1.1 Newman-Penrose formalism

The Teukolsky equation is derived within the framework of the Newman-Penrose formalism [110]. Take a null tetrad composed of two real vectors $l^\mu$ and $n^\mu$ as well as a complex conjugate pair $m^\mu$ and $\overline{m}^\mu$, satisfying

$$l_\mu n^\mu = -m_\mu \overline{m}^\mu = -1, \tag{4.2}$$

with all other inner products vanishing. It is well known that locally we can always give a spinorial structure to a Lorentzian manifold as there exists an isomorphism between real spinorial 2-tensors in a spinor space and vectors in the tangent space at each point of the manifold (Ch. 13 of Wald [99]). The idea of the Newman-Penrose formalism is to express the connection of the spacetime manifold in terms of 12 complex scalars – the spin coefficients – which come up naturally within the spinorial formalism. Because of the properties of the spinor space, null vectors are the simplest to represent using spinors, and so the easiest way to write these spin coefficients in vector notation is through contractions of the connection with a complex null tetrad satisfying the orthogonality relations of Eq. (4.2).

The null tetrad we use should evidence the algebraic properties of the solution. It is well known from the Petrov classification [111, 112] that Schwarzschild is a type D algebraically special spacetime with repeated null directions given by the ingoing and outgoing null vectors. Thus, using standard Schwarzschild $\{t, r, \theta, \phi\}$ coordinates, we choose for our basis the null tetrad initially proposed by Kin-

nersley [113] :

$$
\begin{aligned}
l^{\mu} &= \left(f(r)^{-1}, 1, 0, 0\right), \\
n^{\mu} &= \frac{1}{2}\left(1, -f(r), 0, 0\right), \\
m^{\mu} &= \frac{1}{\sqrt{2}r}\left(0, 0, 1, i/\sin\theta\right),
\end{aligned}
\tag{4.3}
$$

with $f(r) = (1 - 2M/r)$, where $M$ is the mass of the BH. This basis is also particularly interesting because it transforms in a specific way under rotations, as we show in the following subsection.

### 4.1.2 Spin weighted spherical harmonics

Following Ref. [114], the idea of spin-weighted functions arises as follows: consider an orthonormal tetrad in a point of Schwarzschild spacetime, with vectors pointing in the direction induced by radial coordinates, that is

$$
e_t^{\mu} = \frac{1}{\sqrt{f(r)}}\,\delta_t^{\mu}\,, \quad e_r^{\mu} = \sqrt{f(r)}\,\delta_r^{\mu}\,, \quad e_{\theta}^{\mu} = \frac{1}{r}\,\delta_{\theta}^{\mu}\,, \quad e_{\phi}^{\mu} = \frac{1}{r\sin\theta}\,\delta_{\phi}^{\mu}\,. \tag{4.4}
$$

If we rotate around $e_r^{\mu}$ by an angle $\alpha$ then we find the new vectors tangent to the sphere are linear combinations of $e_{\theta}^{\mu}$ and $e_{\phi}^{\mu}$. Now imagine that, instead, we use $m^{\mu}$ and its complex conjugate (see Eq.(4.3)) as a basis for vectors tangent to the sphere. Now, $m^{\mu}$ transforms in a very specific way under rotations: if we rotate by the same angle $\alpha$ around the radial direction then

$$
m^{\mu} \to e^{i\alpha} m^{\mu}. \tag{4.5}
$$

This allows us to introduce the notion of spin weight: a quantity $\eta$ is said to have spin weight $s$ if it follows the following transformation law under rotations by an angle $\alpha$ about the radial direction:

$$
\eta \to e^{is\alpha}\eta. \tag{4.6}
$$

As an example, we have that for any real vector $v^{\mu}$, the scalar product with the basis vectors of (4.3) have the following spin weights:

$$
v_{\mu}l^{\mu} \to s = 0\,, \quad v_{\mu}n^{\mu} \to s = 0\,, \quad v_{\mu}m^{\mu} \to s = +1\,, \quad v_{\mu}\overline{m}^{\mu} \to s = -1. \tag{4.7}
$$

Finally, we want to tie everything back with the Newman-Penrose formalism and the introduction of a spinor structure to our spacetime. We said that the choice of a null tetrad naturally induces a basis of spinor space; furthermore, the choice of the null tetrad of (4.3) introduces a particularly special basis of that space, one which transforms in a specific way under rotations, i.e a basis of spinors with a defined spin weight. Following the discussion above about the spinor space and the isomorphism with the tangent space of our manifold, it is not surprising that the spinors have spin weight $\pm 1/2$.

Having described what spin weight is with a reasonable level of detail, we can now introduce the

"*edth*" operators, which are a pair of differential operators on the sphere that can be written in standard spherical coordinates as

$$\eth\eta = -\left(\partial_\theta + \frac{i}{\sin\theta}\partial_\phi - s\cot\theta\right)\eta, \tag{4.8}$$

$$\bar{\eth}\eta = -\left(\partial_\theta - \frac{i}{\sin\theta}\partial_\phi + s\cot\theta\right)\eta. \tag{4.9}$$

It turns out that these operators are raising and lowering operators for the spin weight of a given quantity, that is, if $\eta$ has spin weight $s$, then $\eth\eta$ will have spin weight $s+1$ and $\bar{\eth}\eta$ will have spin weight $s-1$. We may ask which set of functions ${}_sP_{\ell m}$ solve the eigenvalue problems

$$\left(\bar{\eth}\eth - \lambda_1\right)\ {}_sP_{\ell m}(\theta,\phi) = 0, \tag{4.10}$$

$$\left(\eth\bar{\eth} - \lambda_2\right)\ {}_sQ_{\ell m}(\theta,\phi) = 0. \tag{4.11}$$

The labels $s$, $\ell$, and $m$ are integers corresponding to the spin weight, angular number, and azimuthal number. When we consider $s=0$, we get $\eth\bar{\eth} = \bar{\eth}\eth = -L^2$, the square angular momentum operator. So, in that case, the basis of spherical harmonics, $Y_{\ell m}(\theta,\phi)$ provides a solution to the eigenvalue problem, with $\lambda_1 = \lambda_2 = \ell(\ell+1)$.

For the case of general $s$, the adequate basis functions are called spin-weighted spherical harmonics. The corresponding eigenvalue equations are

$$\bar{\eth}\eth\ {}_sY_{\ell m}(\theta,\phi) = -\left(\ell(\ell+1) - s(s+1)\right)\ {}_sY_{\ell m}, \tag{4.12}$$

$$\eth\bar{\eth}\ {}_sY_{\ell m}(\theta,\phi) = -\left(\ell(\ell+1) - s(s-1)\right)\ {}_sY_{\ell m}. \tag{4.13}$$

Note that, like the ordinary spherical harmonics, spin-weighted spherical harmonics have a dependence on $\phi$ which goes like $e^{im\phi}$, where $-\ell \leq m \leq \ell$. Furthermore, they are only defined for $\ell \geq |s|$, and for each value of $s$ they are a complete orthonormal set of functions on the sphere, in the sense that any function defined on the sphere with spin weight $s$ may be expanded as a series in ${}_sY_{\ell m}$ and

$$\int d\Omega\ {}_sY_{\ell m}\ {}_s\overline{Y}_{\ell' m'} = \delta_{\ell\ell'}\delta_{mm'}. \tag{4.14}$$

The last important relations regarding spin-weighted spherical harmonics are

$$\eth\ {}_sY_{\ell m} = \left((\ell-s)(\ell+s+1)\right)^{\frac{1}{2}}\ {}_{s+1}Y_{\ell m}, \tag{4.15}$$

$$\bar{\eth}\ {}_sY_{\ell m} = -\left((\ell+s)(\ell-s+1)\right)^{\frac{1}{2}}\ {}_{s-1}Y_{\ell m}. \tag{4.16}$$

One may ask what is the connection between this notion of spin weight and the notion of spin in physics as intrinsic angular momentum. Consider, for example, a photon: in quantum field theory, the photon field is a massless vector field, which in turn implies it must have two independent polarizations (left- and right- circularly polarized), carrying angular-momentum $L = \pm 1$ (in natural units). By looking at (4.7), we see that a vector may be decomposed into components of spin weight $-1 \leq s \leq 1$. In

fact, in quantum field theory, vector fields are always associated with particles that carry intrinsic angular momentum $L = \pm 1$, precisely because of the way vectors behave under rotations, as encapsulated in (4.7). Similarly, an electron has spin $L = \pm 1/2$, because it is represented by a spinor field which has spin weight $s = \pm 1/2$, and a graviton has intrinsic angular momentum $L = \pm 2$, because it is represented by a 2-tensor field, which may be decomposed into components with spin weight $-2 \leq s \leq 2$.

This will be important because the Teukolsky equation uses the Newman-Penrose formalism with the null tetrad of (4.3). This means that all the perturbation fields (Weyl tensor, EM field, or scalar field) are written in their spin-weighted components so that the angular dependence is naturally expressed in terms of spin-weighted spherical harmonics.

### 4.1.3 The master equation

The Teukolsky equation [68] governs perturbations of the Kerr metric, and hence can also be used to study perturbations of the Schwarzschild metric by simply taking $a = 0$. We will not deduce Teukolsky's equation here, but simply give an overview of the idea. In his 1973 paper, Teukolsky starts by proving that, for all algebraically special Petrov type D spacetimes, the Newman-Penrose formalism leads to a separated form of the field equations for the gauge invariant components of the Weyl and Faraday tensors. Then, taking the spacetime to be Kerr as well and using Boyer-Lindquist coordinates and the Kerr version of the null tetrad in (4.3), Teukolsky manages to write a general equation that describes both scalar ($s = 0$), EM ($s = 1$) and gravitational ($s = 2$) perturbations. Taking that equation and setting $a = 0$ gives us the Bardeen-Press equation [69], written in Schwarzschild coordinates as

$$\begin{aligned}\left(\frac{r^2}{f}\right)\partial_t^2\psi - \frac{1}{\sin^2\theta}\partial_\phi^2\psi - \left(\frac{1}{r^2 f}\right)^s \partial_r\left(\left(r^2 f\right)^{s+1}\partial_r\psi\right) - \frac{1}{\sin\theta}\partial_\theta\left(\sin\theta\,\partial_\theta\psi\right) \\ -2is\left(\frac{\cos\theta}{\sin^2\theta}\right)\partial_\phi\psi - 2s\left(\frac{M}{f} - r\right)\partial_t\psi + \left(s^2\cot^2\theta - s\right)\psi = 4\pi r^2 T\,,\end{aligned} \tag{4.17}$$

where $\psi$ is the perturbation field and $T$ is a source term, which in general is not the trace of the energy-momentum tensor or any other familiar quantity. Using the differential operators defined in the previous subsection (4.8) and (4.9), this equation can be re-written as

$$\left(\frac{r^2}{f}\right)\partial_t^2\psi - \left(\frac{1}{r^2 f}\right)^s \partial_r\left(\left(r^2 f\right)^{s+1}\partial_r\psi\right) - 2s\left(\frac{M}{f} - r\right)\partial_t\psi - \bar{\eth}\eth\psi = 4\pi r^2 T\,, \tag{4.18}$$

where now all the angular dependence is encapsulated by the $\eth$ and $\bar{\eth}$ operators. When $T$ and $\psi$ are expanded in spin-weighted spherical harmonic components, the angular and radial parts will nicely decouple, because ${}_sY_{\ell m}$ are eigenfunctions of the operator $\bar{\eth}\eth$.

For now, we will focus on the homogeneous equation ($T = 0$), as the solution to that equation will be needed to construct the solutions of the equation with a source (see Appendix E). We start by expanding the field in terms of its Fourier-harmonic components: if $\psi$ has spin weight $s$ then it may be expanded as

$$\psi = \int_{-\infty}^{\infty} d\omega \sum_{\ell,m}^{\infty} R_{\omega\ell m}(r)\,{}_sY_{\ell m}(\theta,\phi)e^{-i\omega t}. \tag{4.19}$$

Replacing this in (4.18) and decoupling the radial and angular parts yields the equation for the mode amplitudes $R_{\omega\ell m}$:

$$\left(r^2 f\frac{d^2}{dr^2}+2(s+1)(r-M)\frac{d}{dr}-V_s(r)\right)R_{\omega\ell m}=0\,, \tag{4.20}$$

$$V_s(r)=-\frac{(r\omega)^2}{f}+2i\omega s\left(\frac{M}{f}-r\right)+(\ell-s)(\ell+s+1)\,. \tag{4.21}$$

As it stands, this equation is difficult to solve, so we define the function $S(r)$ as the new unknown and introduce the usual tortoise coordinate $r_\star$:

$$S(r)=r\left(r^2 f\right)^{\frac{s}{2}}R_{\omega\ell m}\,, \tag{4.22}$$

$$r_\star=r+2M\log\left|\frac{r}{2M}-1\right|\,,\quad \frac{dr_\star}{dr}=f^{-1}\,. \tag{4.23}$$

The equation for $S(r)$ is then:

$$\frac{d^2S}{dr_\star^2}+K(r)S=0\,, \tag{4.24}$$

where

$$K(r)=\frac{1}{r^4}\Big[r^4\omega^2+2ir^2\omega s(r-3M)-M^2s^2+(2Mr-r^2)\ell(\ell+1)+2M(2M-r)\Big]\,. \tag{4.25}$$

We now want to find asymptotic solutions to the equation written in this form. We start by looking at the limit $r\to\infty$ ($r_\star\to\infty$), in which case the equation reduces to

$$\frac{d^2S}{dr_\star^2}+\left(\omega^2+\frac{2i\omega s}{r}\right)S=0\,, \tag{4.26}$$

with linearly independent solutions

$$S(r)\sim r^{\pm s}e^{\mp i\omega r_\star}\iff R_{\omega\ell m}\sim\frac{e^{-i\omega r_\star}}{r}\quad\text{or}\quad R_{\omega\ell m}\sim\frac{e^{i\omega r_\star}}{r^{2s+1}}\,. \tag{4.27}$$

As for the horizon limit, $r\to 2M$ ($r_\star\to-\infty$), the equation becomes

$$\frac{d^2S}{dr_\star^2}+\left(\omega-\frac{is}{4M}\right)^2S=0\,, \tag{4.28}$$

with linearly independent solutions

$$S(r)\sim\left(r^2f\right)^{\pm s/2}e^{\pm i\omega r_\star}\iff R_{\omega\ell m}\sim e^{i\omega r_\star}\quad\text{or}\quad R_{\omega\ell m}\sim\frac{e^{-i\omega r_\star}}{(r^2f)^s}\,. \tag{4.29}$$

## 4.2 Electromagnetic perturbations of Schwarzschild spacetime

We are interested in studying EM perturbations on top of a Schwarzschild background. In general, the topic of using BH perturbation theory to study the motion of point particles around Schawrzschild BHs is immensely vast; here we mention some of the more noteworthy examples like the benchmark

works dating back to the 1970s by Marc Davis, Remo Ruffini, and collaborators [9, 77, 86], as well as a complete series by Poisson and collaborators [80–82]. In recent years, similar methods have been used, for example, to study exotic compact objects [83]. For our analysis, we will follow mainly Refs. [81–83].

To use the Teukolsky equation (Eq. (4.18)) we must first decompose the EM field into its projections in the null tetrad of (4.3), namely three complex scalars with well-defined spin weight $s$:

$$\begin{aligned} (s=1) \quad \phi_0 &= F_{\mu\nu} l^\mu m^\nu \,, \\ (s=0) \quad \phi_1 &= \frac{1}{2} F_{\mu\nu} \left( l^\mu n^\nu + \overline{m}^\mu m^\nu \right) \,, \\ (s=-1) \quad \phi_2 &= F_{\mu\nu} \overline{m}^\mu n^\nu \,. \end{aligned} \tag{4.30}$$

We can use the Teukolsky equation to find both $\phi_0$ and $\phi_2$, but it turns out we only have to solve for $\phi_2$, since, as we will see, this quantity gives us all the information we need regarding the energy carried away in the radiation field. With that in mind, the equation we have to solve is Eq.(4.18), with the substitutions

$$\psi = r^2 \phi_2 \,, \quad s = -1 \,, \quad \text{and} \quad T = r^2 J_2 \,, \tag{4.31}$$

where $J_2$ is given in Eq. (3.8) of Ref. [68]:

$$J_2 = \left( n^\alpha \partial_\alpha - \frac{3f}{2r} \right) J_{\overline{m}} - \overline{m}^\alpha \partial_\alpha J_n \,, \tag{4.32}$$

with $J_{\overline{m}} = \overline{m}^\alpha J_\alpha$, $J_n = n^\alpha J_\alpha$. Based on the results of Appendix E, we start by defining solutions to the homogeneous equation (4.20) for $s = -1$. We define the solutions $R^H$ and $R^\infty$ using the results in Eqs. (4.27) and (4.29), with their asymptotic behavior corresponding to purely ingoing waves at the horizon and purely outgoing waves at infinity, respectively [1].

$$R^H_{\omega\ell m} \to \frac{A_{\text{in}}}{r} \, e^{-i\omega r_\star} + A_{\text{out}} \, r \, e^{i\omega r_\star} \,, \qquad R^\infty_{\omega\ell m} \to r \, e^{i\omega r_\star} \qquad (r \to \infty) \,, \tag{4.33}$$

$$R^H_{\omega\ell m} \to (r^2 f) \, e^{-i\omega r_\star} \,, \qquad R^\infty_{\omega\ell m} \to B_{\text{in}} (r^2 f) e^{-i\omega r_\star} + B_{\text{out}} e^{i\omega r_\star} \qquad (r \to 2M) \,. \tag{4.34}$$

Looking at the source again, we may expand the scalars we constructed from $J_\mu$ (Eq. (4.32)) in their Fourier-harmonic components, as we did for $\psi$ in Eq. (4.19), that is:

$$J_n = \int_{-\infty}^{\infty} d\omega \sum_{\ell,m}^{\infty} {}_nJ_{\omega\ell m} Y_{\ell m}(\theta,\phi) e^{-i\omega t} \,, \tag{4.35}$$

$$J_{\overline{m}} = \int_{-\infty}^{\infty} d\omega \sum_{\ell,m}^{\infty} {}_{\overline{m}}J_{\omega\ell m} \, {}_{-1}Y_{\ell m}(\theta,\phi) e^{-i\omega t} \,, \tag{4.36}$$

[1] We should include factors of $M$ in these solutions to ensure that $R$ has units of $L^2$ and that the coefficients are all dimensionless. This was not done because the final result is always a dimensionless energy flux, so the factors of $M$ all cancel out.

after which we may re-write Eq. (4.32) as

$$\begin{aligned} J_2 =& \frac{1}{2}\left(\partial_t - f\partial_r - \frac{3f}{r}\right) J_{\overline{m}} + \frac{1}{\sqrt{2}r}\overline{\eth} J_n \\ =& \int_{-\infty}^{\infty} d\omega \sum_{\ell,m}^{\infty} \left[ -\frac{1}{2}\left(i\omega + f\frac{d}{dr} + \frac{3f}{r}\right) {}_{\overline{m}}J_{\omega\ell m} - \frac{\sqrt{\ell(\ell+1)}}{\sqrt{2}r}\, {}_nJ_{\omega\ell m}\right] {}_{-1}Y_{\ell m}(\theta,\phi)e^{-i\omega t}\,. \end{aligned} \tag{4.37}$$

Thus, replacing this result in (4.31) and then plugging that into (4.18), along with (4.19), and performing the inverse Fourier transform together with the projection into a particular harmonic (using the orthogonality of spin weighted spherical harmonics [114]), we get the Teukolsky equation for the Fourier-harmonic components of $\psi = r^2\phi_2$:

$$\left[r^2 f\frac{d^2}{dr^2} - V_{-1}(r)\right] R_{\omega\ell m} = 4\pi r^4 \left[\frac{1}{2}\left(i\omega + f\frac{d}{dr} + \frac{3f}{r}\right) {}_{\overline{m}}J_{\omega\ell m} + \frac{\sqrt{\ell(\ell+1)}}{\sqrt{2}r}\, {}_nJ_{\omega\ell m}\right]. \tag{4.38}$$

## 4.3 Energy radiated by a charged particle in a circular orbit

We now must make a statement about the 4-current, $J_\mu$, which for a single particle of charge $q$ takes the form

$$J_\mu(x) = q\int d\tau\; u_\mu(\tau)\delta^{(4)}(x - z(\tau))\,, \tag{4.39}$$

where $z(\tau)$ is the particle's trajectory, $\tau$ is the proper time and $u^\mu = dz^\mu/d\tau$ is the 4-velocity. In the particular case of a circular orbit of radius $r_0$ with orbital angular velocity $\Omega_0 = d\phi/dt$ in the equatorial plane, we get, using Schwarzschild $\{t, r, \theta, \phi\}$ coordinates,

$$z(\tau) = (u^t\tau\,,\, r_0\,,\, \pi/2\,,\, u^t\Omega_0\tau) \quad \text{and} \quad u^\mu = u^t\,(1, 0, 0, \Omega_0)\,, \tag{4.40}$$

$$u^t = \frac{E_0}{mf(r_0)} = \left(1 - \frac{2M}{r_0} - (v_0)^2\right)^{-\frac{1}{2}}, \tag{4.41}$$

with $E_0$, $m$, and $v_0$ being, respectively, the energy, mass, and 3-velocity of the particle (see Eqs. (2.56) and (2.11)). In the particular case of the charged particle moving in an asymptotically uniform magnetic field, $\Omega_0$ is given in Eq. (2.65).

Putting everything together and using the delta function in time to get rid of the integral in (4.39) yields

$$J_\mu(x) = q\frac{u_\mu}{u^t}\frac{\delta(r - r_0)}{r^2}\frac{\delta(\cos\theta)}{\sin\theta}\delta(\phi - \Omega_0 t)\,. \tag{4.42}$$

To find the Fourier-harmonic components of $J_n$ and $J_{\overline{m}}$ (see Eqs. (4.35) and (4.36)), we must replace the 4-velocity in the expression above, contract that with the corresponding tetrad vector, $n^\mu$ or $\overline{m}^\mu$, perform the inverse Fourier transform and finally project onto the spin weighted spherical harmonic basis, yielding

$${}_nJ_{\omega\ell m} = -\frac{q}{2}f(r_0)\;\overline{Y}_{\ell m}(\pi/2, 0)\frac{\delta(r - r_0)}{r^2}\delta(\omega - m\Omega_0)\,, \tag{4.43}$$

$${}_{\overline{m}}J_{\omega\ell m} = -i\frac{q}{\sqrt{2}}\,v_0\;{}_{-1}\overline{Y}_{\ell m}(\pi/2, 0)\frac{\delta(r - r_0)}{r^2}\delta(\omega - m\Omega_0)\,. \tag{4.44}$$

Now that the sources are completely determined we can obtain a solution to Eq. (4.38) using the result of Appendix E. Using the previously defined solutions to the homogeneous equation (Eqs. (4.33) and (4.34)) to impose physical boundary conditions at infinity and at the horizon, the final result for the Fourier-harmonic components of $\psi = r^2\phi_2$ (see Eq. (4.19)) is

$$R_{\omega\ell m}(r) = \frac{1}{\mathcal{W}}\left(R^{\infty}_{\omega\ell m}(r)\int_{r_+}^{r}\frac{T(r')R^{H}_{\omega\ell m}(r')}{r'^2 f(r')}dr' + R^{H}_{\omega\ell m}(r)\int_{r}^{\infty}\frac{T(r')R^{\infty}_{\omega\ell m}(r')}{r'^2 f(r')}dr'\right), \tag{4.45}$$

where

$$\mathcal{W} = R^{\infty}_{\omega\ell m}\frac{dR^{H}_{\omega\ell m}}{dr} - R^{H}_{\omega\ell m}\frac{dR^{\infty}_{\omega\ell m}}{dr} = -2i\omega A_{\text{in}} \tag{4.46}$$

and

$$T = -4\pi r^4\left[\frac{1}{2}\left(i\omega + f\frac{d}{dr} + \frac{3f}{r}\right)\,{}_{\overline{m}}J_{\omega\ell m} + \frac{\sqrt{\ell(\ell+1)}}{\sqrt{2}r}\,{}_{n}J_{\omega\ell m}\right]. \tag{4.47}$$

Since the sources (Eqs. (4.43) and (4.44)) are proportional to $\delta(r - r_0)$, the integrals in Eq. (4.45) are easy to solve.

### 4.3.1 Radiated energy flux at infinity

Having found a solution to Teukolsky's equation in Eq. (4.45), we now have to finally come around to understand how that translates to energy flux. We start by looking at the power lost to radiation which goes away to infinity. To do that, we have to look at the energy-momentum tensor of the EM field, which is written in a particularly useful form in Ref. [68]:

$$\begin{aligned}4\pi T_{\mu\nu} = \Big[&|\phi_0|^2 n_\mu n_\nu + |\phi_2|^2 l_\mu l_\nu + 2|\phi_1|^2\left(l_{(\mu}n_{\nu)} + m_{(\mu}\overline{m}_{\nu)}\right)\\ &- 4\overline{\phi_0}\phi_1 n_{(\mu}m_{\nu)} - 4\overline{\phi_1}\phi_2 l_{(\mu}m_{\nu)} + 2\phi_2\overline{\phi_0}m_\mu\overline{m}_\nu\Big] + c.c.\,,\end{aligned} \tag{4.48}$$

where $c.c.$ stands for complex conjugate. To look at the energy current at infinity we must contract this tensor with the timelike Killing vector field of the spacetime, which defines a conserved current, corresponding to energy as seen by observers at infinity. In Schwarzschild coordinates, the timelike Killing vector field is $X^\mu = \delta^\mu_t$, so the conserved current is just $T^\mu{}_t$. Thus, the energy flux at infinity can be defined as the flux of $T^\mu{}_t$ across a sphere of radius $r$ in the limit where $r \to \infty$. Doing so and taking into account the asymptotic form of the solutions of Teukolsky's equation (Eq. (4.27)) yields the result below [68, 71]:

$$\left.\frac{d^2E}{dt\,d\Omega}\right|_{\infty} = \lim_{r\to\infty} -r^2 T^r{}_t = \lim_{r\to\infty}\frac{r^2}{2\pi}|\phi_2|^2\,, \tag{4.49}$$

which shows that $\phi_2$ carries all the information concerning outgoing radiation at infinity. Furthermore, we only need to find the Fourier-harmonic components of the field at infinity which, following Eqs. (4.45),

(4.46) and (4.47), yield

$$R_{\omega\ell m}(r\to\infty) = i\frac{\pi q}{\sqrt{2}\omega A_{\rm in}}\left[\frac{R^H_{\omega\ell m}(r_0)}{f_0}\left(\left(i\omega+\frac{3f_0}{r_0}\right)iv_0\ {}_{-1}\overline{Y}_{\ell m}(\pi/2,0)+\frac{\sqrt{\ell(\ell+1)}}{r_0}f_0\ {}_0\overline{Y}_{\ell m}(\pi/2,0)\right)\right.$$
$$\left.-iv_0\frac{d}{dr}\left(R^H_{\omega\ell m}\right)_{r=r_0}\ {}_{-1}\overline{Y}_{\ell m}(\pi/2,0)\right]re^{i\omega r_\star}\delta(\omega-m\Omega_0)\,, \tag{4.50}$$

where $f_0\equiv f(r_0)$. If we replace this result in the expansion of $\phi_2$ (Eq. (4.19) with $\psi=r^2\phi_2$) we find

$$\phi_2(r\to\infty) = \frac{1}{r}\sum_{\ell,m}\ {}_{-1}Y_{\ell m}(\theta,\phi)Z^\infty_{\ell m}e^{-im\Omega_0(t-r_\star)}\,, \tag{4.51}$$

where $Z^\infty_{\ell m}$ is just the part of (4.50) that does not depend on $r$ and with $\omega$ replaced by $m\Omega_0$:

$$Z^\infty_{\ell m} = i\frac{\pi q}{\sqrt{2}\,m\Omega_0 A_{\rm in}}\left[\frac{R^H_{m\Omega_0\ell m}(r_0)}{f_0}\left(\left(im\Omega_0+\frac{3f_0}{r_0}\right)iv_0\ {}_{-1}\overline{Y}_{\ell m}(\pi/2,0)+\frac{\sqrt{\ell(\ell+1)}}{r_0}f_0\ {}_0\overline{Y}_{\ell m}(\pi/2,0)\right)\right.$$
$$\left.-iv_0\frac{d}{dr}\left(R^H_{m\Omega_0\ell m}\right)_{r=r_0}\ {}_{-1}\overline{Y}_{\ell m}(\pi/2,0)\right]. \tag{4.52}$$

Finally, replacing this in (4.49), integrating over the sphere and using the orthogonality of ${}_sY_{\ell m}$ yields the energy radiated away to infinity in EM waves:

$$\dot{E}^\infty \equiv \left.\frac{dE}{dt}\right|_\infty = \frac{1}{2\pi}\sum_{\ell,m}|Z^\infty_{\ell m}|^2\,. \tag{4.53}$$

### 4.3.2 Radiated energy flux on the horizon

If we were studying radiation reaction in flat space we would now be done, as the energy that is radiated away would all have to eventually end up at infinity. However, since we are studying this phenomenon in a BH spacetime, we must also consider the energy absorbed by the BH.

The analog of (4.49) for the flux that crosses the horizon is a lot more complicated to find, as the timelike Killing vector of the spacetime becomes null there. The general problem was solved by Hawking and Hartle [115], but here we will give a simpler argument: consider the flux of $T^\mu{}_t$ across a sphere of radius $r$ and naively take the limit where $r\to 2M$:

$$\left.\frac{d^2E}{dt\,d\Omega}\right|_H = \lim_{r\to 2M}\frac{1}{2\pi}r^2\left[|\phi_2|^2-\frac{f^2}{4}|\phi_0|^2\right] = -\lim_{r\to 2M}\frac{1}{2\pi}\frac{1}{16M^2}\left|(r^2f)\phi_0\right|^2\,, \tag{4.54}$$

where we use the asymptotic behavior of the solutions of the Teukolsky equation as presented in Eq. (4.29) and the minus sign simply indicates that the energy is flowing inwards. Note how the $(r^2f)$ factor exactly cancels out the divergence in the $\phi_0$ mode at the horizon (Eq. (4.29)). This recovers the result obtained by Teukolsky and Press in Ref. [71].

Still on the topic of Eq. (4.54), it is clear that the relevant Newman-Penrose component of the EM field for ingoing radiation at the horizon is $\phi_0$, which would naively be expected given it is also the quantity that governs ingoing radiation at infinity. This is unfortunate, as we have only solved Teukolsky's equation for

$\phi_2$. Luckily, we can look back at the coupled Maxwell equations (2.38) to find $\phi_0$ once $\phi_2$ is found using Teukolsky's equation. This is precisely what Teukolsky and Press did in Ref. [71], and in the same article they go on to use this to rewrite Eq. (4.54) in terms of $\phi_2$, obtaining

$$\left.\frac{d^2E}{dt\,d\Omega}\right|_{\text{horizon}} = \lim_{r\to 2M} \frac{32\,\omega^2 M^6(16\,\omega^2+1/M^2)}{\pi\left[\ell(\ell+1)\right]^2}\left|\frac{\phi_2}{f}\right|^2 , \tag{4.55}$$

where again, the $r^2 f$ factor compensates for the fact that $\phi_2$ goes to zero at the horizon (Eq. (4.29)). Once this is done, the situation is now very similar to the one we had for the flux at infinity. Again we only need to solve for the radial functions at the horizon $R_{\omega\ell m}(r\to 2M)$. Thus from Eqs. (4.45), (4.46) and (4.47) we get

$$\begin{aligned} R_{\omega\ell m}(r\to 2M) = i\frac{\pi q}{\sqrt{2}\omega A_{\text{in}}}\Bigg[\frac{R^{\infty}_{\omega\ell m}(r_0)}{f_0}\left(\left(i\omega+\frac{3f_0}{r_0}\right) iv_0\,{}_{-1}\overline{Y}_{\ell m}(\pi/2,0) + \frac{\sqrt{\ell(\ell+1)}}{r_0} f_0\,{}_0\overline{Y}_{\ell m}(\pi/2,0)\right) \\ - iv_0\frac{d}{dr}\left(R^{\infty}_{\omega\ell m}\right)_{r=r_0}\,{}_{-1}\overline{Y}_{\ell m}(\pi/2,0)\Bigg] r^2 f e^{-i\omega r_\star}\delta(\omega-m\Omega_0)\,, \end{aligned} \tag{4.56}$$

which is the same as (4.50), except that the solution to the homogeneous Teukolsky equation that must be found is now $R^{\infty}_{\omega\ell m}$. If we replace this result in the Fourier expansion of $\psi = r^2\phi_2$ (Eq. (4.19)) and perform the integral over $\omega$ we find

$$\phi_2(r\to 2M) = f\sum_{\ell,m}\,{}_{-1}Y_{\ell m}(\theta,\phi) Z^H_{\ell m} e^{-im\Omega_0(t+r_\star)}\,, \tag{4.57}$$

where $Z^H_{\ell m}$ is just the part of (4.56) that does not depend on $r$ with $\omega$ replaced by $m\Omega_0$:

$$\begin{aligned} Z^H_{\ell m} = i\frac{\pi q}{\sqrt{2}m\Omega_0 A_{\text{in}}}\Bigg[\frac{R^{\infty}_{m\Omega_0\ell m}(r_0)}{f_0}\left(\left(im\Omega_0+\frac{3f_0}{r_0}\right) iv_0\,{}_{-1}\overline{Y}_{\ell m}(\pi/2,0) + \frac{\sqrt{\ell(\ell+1)}}{r_0} f_0\,{}_0\overline{Y}_{\ell m}(\pi/2,0)\right) \\ - iv_0\frac{d}{dr}\left(R^{\infty}_{m\Omega_0\ell m}\right)_{r=r_0}\,{}_{-1}\overline{Y}_{\ell m}(\pi/2,0)\Bigg]\,. \end{aligned} \tag{4.58}$$

Finally, replacing this in (4.55), integrating over the sphere and using the orthogonality of ${}_sY_{\ell m}$ yields the energy absorbed by the BH in EM waves:

$$\dot{E}^H \equiv \left.\frac{dE}{dt}\right|_H = \sum_{\ell,m}\frac{32\,(m\Omega_0)^2 M^6(16(m\Omega_0)^2+1/M^2)}{\pi\left[\ell(\ell+1)\right]^2}\left|Z^H_{\ell m}\right|^2 . \tag{4.59}$$

# Chapter 5

# Analytical results - low frequency limit

We have established that if a particle is in a circular orbit with radius $r_0$ and orbital frequency $\Omega_0$ around a Schwarzschild BH, the energy it loses through radiation either to infinity or into the BH can be found from Eqs. (4.52), (4.53), (4.58) and (4.59). Although these seem very complicated at first glance, the problem boils down to solving for three quantities :

- $R^H_{m\Omega_0\ell m}(r_0)$: the solution of the homogeneous Teukolsky equation (Eq. (4.20)), with boundary conditions corresponding to purely ingoing waves at the horizon (see Eqs. (4.33) and (4.34)), evaluated at the orbital radius $r_0$;
- $R^\infty_{m\Omega_0\ell m}(r_0)$: the solution of the homogeneous Teukolsky equation (Eq. (4.20)), with boundary conditions corresponding to purely outgoing waves at infinity (see Eqs. (4.33) and (4.34)), evaluated at the orbital radius $r_0$;
- $A_{\text{in}}$: the coefficient for the ingoing mode at infinity for the solution $R^H_{m\Omega_0\ell m}(r)$ (see Eq. (4.33)).

Finding all these quantities reduces to solving the homogeneous Teukolsky equation with physical boundary conditions. This is, in general, a very difficult endeavor, but if we take the small frequency limit, $M\omega \ll 1$, and focus on slow orbits, $v_0 = r_0\Omega_0 \ll 1$, this can indeed be done; a detailed discussion of that calculation is presented in Appendix F. All of this means we can get analytical expressions for the energy flux at infinity and on the horizon for slow orbits in terms of $(\ell, m)$ modes, where $M\omega = Mm\Omega_0 \ll 1$. From here on we set $M = 1$ in all the results we show, for simplicity. The analytical formulas presented here will be compared with numerical results in Ch. 6.

## 5.1 Energy flux at infinity

We start by commenting on the energy flux at infinity of the dipole mode $\ell = 1$, $m = \pm 1$, obtained from Eqs. (4.52) and (4.53), which yields a generalized Larmor formula (GLF):

$$\dot{E}^\infty_{11} = 2\frac{1}{2\pi}|Z^\infty_{11}|^2 \approx \frac{2}{3}q^2(r_0-2)^2\Omega_0^4\,, \tag{5.1}$$

where in the first equality we use the fact that the $m = -1$ mode contributes the same as the $m = 1$ mode (the general transformation formula for $m \to -m$ is given after Eq. (B12) of Ref. [83]). We will use this from here on, always treating modes with symmetric values of $m$ together, and denoting by $\dot{E}^{\infty}_{\ell m}$ the sum of the energy flux at infinity for the pair of modes $(\ell, \pm m)$; the only potential problem with that would be in the $m = 0$ mode, which is not excited by the system.

We call Eq. (5.1) a generalized Larmor formula because if we look at slow orbits with $r_0 \gg 2$, *i.e.* the Newtonian limit, we recover the Larmor power formula (2.22). The only difference between the expression for general slow orbits and Newtonian limit orbits is in taking $r_0 \to r_0 - 2$. This means that when the orbits approach the horizon, which can happen for stable orbits in the PC (see Fig. 2.2), the dipole mode radiation that goes away to infinity goes to zero.

It is well known that for Newtonian limit orbits the radiation is dominated by the dipole mode, but it could be that in the strong gravity regime, the curvature of spacetime causes higher multipole terms to be excited, even if the orbits are slow. In those cases, the GLF (Eq. (5.1)) would not be useful by itself as the energy radiated in other modes would have to be included. To check whether such a regime exists we must start by finding a general expression for the energy radiated to infinity in any given mode $(\ell,\, m)$.

The energy radiated for modes with even and odd values of $\ell+m$ must be calculated separately. This is because in Eq. (4.52) the dominant term would usually be the one proportional to ${}_0\bar{Y}_{\ell m}(\pi/2, 0)$, as the term in ${}_{-1}\bar{Y}_{\ell m}(\pi/2, 0)$ is of higher order in $v_0$. However, ${}_0\bar{Y}_{\ell m}(\pi/2, 0)$ is identically zero for odd values of $\ell + m$, so the energy radiated in those modes is suppressed by a factor $(v_0)^2$. With that in mind, using analytic expressions for the spherical harmonics read off from a similar analysis done by Poisson and Sasaki in Ref. [82], we have

$$\begin{aligned}\dot{E}^{\infty}_{\ell m} =& 2^{4l-3} q^2 (r_0-2)^2 (m\Omega_0)^{2(\ell+1)} \frac{(\ell+1)\,(2\ell+1)\,\Gamma(l)^2\,\Gamma(\ell+1)^2\,\Gamma(\ell+2)^2\,(\ell-m)!\,(\ell+m)!}{\ell\,\Gamma(2\ell)^2\,\Gamma(2\ell+2)^2\,((\ell-m)!!)^2\,((\ell+m)!!)^2} \\ &\times\ {}_2F_1\left(1-\ell, \ell+2; 2; 1-\frac{r_0}{2}\right)^2\end{aligned} \tag{5.2}$$

for even values of $\ell + m$, and

$$\begin{aligned}\dot{E}^{\infty}_{\ell m} =& 2^{4\ell-7} q^2 (v_0)^2 (m\Omega_0)^{2(\ell+1)}\ \frac{(2\ell+1)\,\Gamma(\ell)^2\,\Gamma(\ell+1)^2\,\Gamma(\ell+2)^2\,((\ell-m)!!)^2\,((\ell+m)!!)^2}{\ell^3\,(\ell+1)\,\Gamma(2\ell)^2\,\Gamma(2\ell+2)^2\,(\ell-m)!\,(\ell+m)!} \\ &\times \left(\left(\ell^2+\ell-2\right) r_0(r_0-2)\,{}_2F_1\left(2-\ell, \ell+3; 3; 1-\frac{r_0}{2}\right) - 4(r_0-4)\,{}_2F_1\left(1-\ell, \ell+2; 2; 1-\frac{r_0}{2}\right)\right)^2\end{aligned} \tag{5.3}$$

for odd values of $\ell + m$.

Going back to the question of whether or not higher multipoles are important, we must compare the energies radiated for two different modes $(\ell, m)$ and $(\ell', m')$. To simplify the analysis, we start by answering the following question: given a value of $\ell$, what is the dominant $m$ mode? Naively, one would think odd modes can be discarded right away, but the non-trivial dependence in $r_0$ calls for further inspection. Thus, we choose to compare $(\ell, m)$ and $(\ell, m-2)$, separating the even and odd values of

$\ell+m$; after some careful manipulation we obtain the following bounds for the ratios:

$$\frac{\dot{E}^{\infty}_{\ell\, m-2}}{\dot{E}^{\infty}_{\ell m}} = \left(\frac{m-2}{m}\right)^{2\ell+2}\left(1-\frac{2m-2}{(\ell-m+2)(\ell+m-1)}\right) < \left(\frac{\ell-2}{\ell}\right)^{2\ell+2} < \frac{1}{e^4} \approx 1.8\times 10^{-2}\,, \tag{5.4}$$

$$\frac{\dot{E}^{\infty}_{\ell\, m-2}}{\dot{E}^{\infty}_{\ell m}} = \left(\frac{m-2}{m}\right)^{2\ell+2}\left(1+\frac{2m-2}{(\ell-m+1)(\ell+m)}\right) < \left(\frac{\ell-3}{\ell-1}\right)^{2\ell+2}\left(\frac{3}{2}\right) < \frac{3}{2e^4} \approx 2.7\times 10^{-2}\,, \tag{5.5}$$

where $e$ is Euler's number. This establishes that the modes with $m=\ell$ and $m=\ell-1$ are the strongest ones for the even and odd cases, respectively, with smaller $m$ modes becoming exponentially less important. To reinforce this point, we look at the first few $\ell$ modes in Table 5.1; the results therein agree with the bounds above, and show that the suppression can be even stronger.

| $m$ | $\ell=3$ | $\ell=4$ | $\ell=5$ | $\ell=6$ | $\ell=7$ |
|---|---|---|---|---|---|
| $\ell$ | $10^{-4}$ | $10^{-3}$ | $10^{-3}$ | $10^{-3}$ | $10^{-3}$ |
| $\ell-1$ | 0 | $10^{-5}$ | $10^{-3}$ | $10^{-3}$ | $10^{-3}$ |
| $\ell-2$ | - | 0 | $10^{-6}$ | $10^{-3}$ | $10^{-4}$ |
| $\ell-3$ | - | - | 0 | $10^{-7}$ | $10^{-5}$ |
| $\ell-4$ | - | - | - | 0 | $10^{-8}$ |
| $\ell-5$ | - | - | - | - | 0 |

Table 5.1: Order of magnitude of the ratio of EM energy flux at infinity for different modes, $\dot{E}^{\infty}_{\ell\, m-2}/\dot{E}^{\infty}_{\ell m}$, corresponding to different values of $\ell$ and $m$, as emitted by a charged particle in a circular orbit around a Schwarzschild BH. These values are obtained analytically for slow orbits, $v_0 \ll 1$, in the low-frequency limit, $M\omega \ll 1$, and they do not depend on the orbital radius nor the orbital frequency. We use different expressions for modes with even and odd values of $\ell+m$.

Given the above, we just have to compare the modes $m=\ell$ and $m=\ell-1$. We do it by defining a quantity $\alpha_\ell$ below (explicit expression in Eq. (G.1)), corresponding to the ratio of the modes normalized to $(v_0)^2$:

$$\alpha_\ell(r_0) \equiv \frac{1}{(v_0)^2}\frac{\dot{E}^{\infty}_{\ell\,\ell-1}}{\dot{E}^{\infty}_{\ell\ell}}\,. \tag{5.6}$$

We plot $\alpha_\ell$ for the few $\ell$ modes in Fig. 5.1 and conclude that for $r_0 > 2.1$ we have $\alpha_\ell < 1$, so, if the orbits are slow, we can say with confidence that the mode $m=\ell$ dominates and carries almost all the energy radiated to infinity for that value of $\ell$; closer to the BH, the mode with $m=\ell-1$ eventually becomes dominant and has to be included. The divergence at $r_0 \to 2$ in Fig. 5.1 is just a result of $\dot{E}^{\infty}_{\ell\ell} \to 0$ in that limit, while $\dot{E}^{\infty}_{\ell\,\ell-1}$ approaches a finite value.

All of this implies that, if we restrict ourselves to $r_0 > 2.1$, we can use the mode with $m=\ell$ as a benchmark to see if the higher $\ell$ modes are important or not. Thus, we will now look at the comparison between a mode $(\ell,\ell)$ and a mode $(\ell+1,\ell+1)$. By renormalizing the ratio to the square of the orbital velocity $v_0$, we obtain the quantity $\zeta_\ell(r_0)$, given by (explicit expression in Eq. (G.2)):

$$\zeta_\ell(r_0) \equiv \frac{1}{(v_0)^2}\frac{\dot{E}^{\infty}_{\ell+1\,\ell+1}}{\dot{E}^{\infty}_{\ell\ell}}\,. \tag{5.7}$$

We find that $\zeta_\ell$ is of the order of unity for $\ell=1,2,3,4,5$ (Fig. 5.2), which means that, since the orbits are

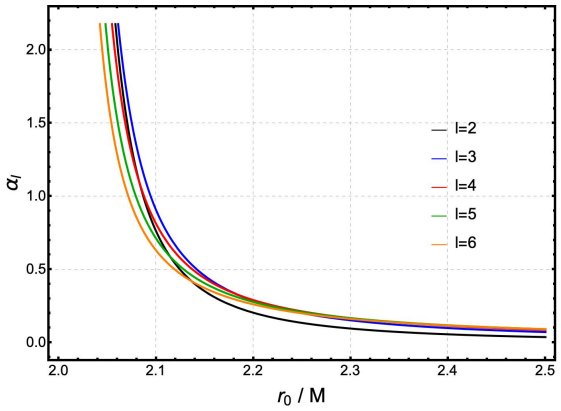


Figure 5.1: $\alpha_\ell\, v_0^2 = \dot{E}^\infty_{\ell\,\ell-1}/\dot{E}^\infty_{\ell\ell}$ – ratio of EM energy fluxes at infinity, as seen by stationary observers at infinity, for different modes, normalized to the square of the orbital velocity; the radiation is emitted by a charged particle in a circular orbit of radius $r_0$ around a Schwarzschild BH. These results are obtained analytically in the slow motion and low-frequency regime. The black, blue, red, green, and orange curves represent the cases $\ell = 2,\, 3,\, 4,\, 5,\, 6$ respectively.

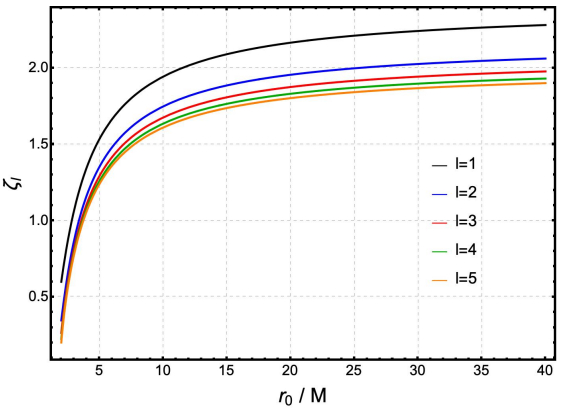


Figure 5.2: $\zeta_\ell\, v_0^2 = \dot{E}^\infty_{\ell+1\,\ell+1}/\dot{E}^\infty_{\ell\ell}$ – ratio of EM energy fluxes at infinity for different modes as a function of the orbital radius $r_0$. The black, blue, red, green, and orange curves represent the cases $\ell = 2,\, 3,\, 4,\, 5,\, 6$ respectively.

slow, $v_0 \ll 1$, the dipole term is dominant and enough to capture the energy flux at infinity. Looking at Fig 5.2, we also see that $\zeta_\ell$ appears to be approaching a constant for $r_0 \to \infty$; indeed, we have

$$\lim_{r_0\to\infty} \zeta_\ell(r_0) = \left(\frac{\ell}{\ell+1}\right)^{-2\ell-1} \frac{(\ell+2)}{2(2\ell+3)}\,. \tag{5.8}$$

This is an interesting result, as it shows us that, for $r_0 \to \infty$, the higher multipoles are all suppressed by a factor $(v_0)^2$. This suppression is much more general as if we compare an arbitrary $(\ell, m)$ mode with the dipole we find

$$\dot{E}^\infty_{\ell m} \sim \left[3\, 4^l m^{2\ell+2}\, \frac{l\,(\ell+1)\,(2\ell+1)\,\Gamma(l)^2\,\Gamma(\ell-m+1)\,\Gamma(\ell+m+1)}{((\ell-m)!!)^2\,((\ell+m)!!)^2\,\Gamma(2\ell+2)^2}(v_0)^{2\ell-2}\right]\dot{E}^\infty_{11} \qquad (r_0\to\infty) \tag{5.9}$$

for even values of $\ell+m$, and

$$\dot{E}^{\infty}_{\ell m} \sim \left[3\,4^{\ell+1} m^{2\ell+2} \frac{(l-2)^2(\ell+1)(2\ell+1)\Gamma(l)^2((\ell-m)!!)^2((\ell+m)!!)^2}{\ell\,\Gamma(2\ell+3)^2\,\Gamma(\ell-m+1)\,\Gamma(\ell+m+1)}(v_0)^{2\ell}\right]\dot{E}^{\infty}_{11} \qquad (r_0\to\infty) \tag{5.10}$$

for odd values of $\ell+m$. This result establishes the dominance of the dipole term for large orbital radius while also recovering the scaling with $v_0$ obtained by Poisson and Sasaki [82] for gravitational radiation.

From the results in this section, we conclude that, within the domain of validity of the slow motion and low frequency approximation, the dipole term dominates the energy flux at infinity, even in the strong field regime, up to about $r_0 \approx 2.1$. Beyond that value, modes with odd $\ell+m$ must be included to get an accurate estimate of the energy flux at infinity.

## 5.2 Energy flux on the horizon

We now turn to the energy flux on the BH horizon. Again, we start by looking at the dipole mode by substituting $\ell=1$, $m=\pm1$ in Eqs. (4.58) and (4.59), yielding

$$\dot{E}^{H}_{11} = 3q^2\Omega_0^2 \frac{\left(-2r_0+(r_0-2)r_0\log\left(\frac{r_0}{r_0-2}\right)+2\right)^2}{2r_0^2}\,. \tag{5.11}$$

Note that now, in opposition to what we saw for the flux at infinity in Eq. (5.1), the flux on the horizon goes to a finite value when $r_0\to 2$.

For a generic $(\ell,\,m)$, the energy radiated into the BH is given by

$$\begin{aligned}\dot{E}^{H}_{\ell m} =& 2^{2\ell+3} q^2 (r_0-2)^{-2(\ell+1)} (m\Omega_0)^4 \frac{(2\ell+1)\,\Gamma(\ell+1)^2\,\Gamma(\ell+2)^2\,(\ell-m)!\,(\ell+m)!}{\ell\,(\ell+1)\,\Gamma(2\ell+2)^2\,((\ell-m)!!)^2\,((\ell+m)!!)^2} \\ &\times {}_2F_1\left(\ell+1,\ell+2;2(\ell+1);-\frac{2}{r_0-2}\right)^2\end{aligned} \tag{5.12}$$

for even values of $\ell+m$, and

$$\begin{aligned}\dot{E}^{H}_{\ell m} =& 2^{2\ell+3} q^2 (r_0-2)^{-2(\ell+3)} (m\Omega_0)^4 (v_0)^2 \frac{(2\ell+1)\Gamma(\ell+1)^2\Gamma(\ell+2)^2((\ell-m)!!)^2((\ell+m)!!)^2}{\ell^3(\ell+1)^3\Gamma(2\ell+2)^2(\ell-m)!(\ell+m)!} \\ &\times\left((r_0-2)((\ell+3)r_0-4)\,{}_2F_1\left(\ell+1,\ell+2;2(\ell+1);-\frac{2}{r_0-2}\right)\right. \\ &\left.-(\ell+2)r_0\,{}_2F_1\left(\ell+2,\ell+3;2\ell+3;-\frac{2}{r_0-2}\right)\right)^2\end{aligned} \tag{5.13}$$

for odd values of $\ell+m$. We will now use these expressions to try and ultimately understand if we can accurately describe radiation reaction using only a finite number of modes. We start by looking at the following question: given a value of $\ell$, what is the dominant $m$ mode? To answer that, we again choose to compare $(\ell,m)$ and $(\ell,m-2)$, separating the modes with even and odd values of $\ell+m$, yielding

$$\frac{\dot{E}^{H}_{\ell\,m-2}}{\dot{E}^{H}_{\ell m}} = \left(\frac{m-2}{m}\right)^2\left(1-\frac{2m-2}{(\ell-m+2)(\ell+m-1)}\right)\left(\frac{\ell-2}{\ell}\right)^2 < 1 \tag{5.14}$$

for even values of $\ell+m$, and

$$\frac{\dot{E}^H_{\ell\, m-2}}{\dot{E}^H_{\ell m}} = \left(\frac{m-2}{m}\right)^2 \left(1+\frac{2m-2}{(\ell-m+1)(\ell+m)}\right)\left(\frac{\ell-3}{\ell-1}\right)^2\left(\frac{3}{2}\right) < \frac{3}{2} \tag{5.15}$$

for odd values of $\ell+m$. These bounds establish that the mode with $m=\ell$ is the strongest one for the even case; on the contrary, the mode with $m=\ell-1$ is not necessarily the strongest of all modes with odd $m+l$. We investigated this further by looking at the first few $\ell$ modes in Table 5.2; the results therein agree with the bounds obtained above, and show that indeed, for odd $\ell+m$, it is difficult to establish which mode is dominant.

| $m$ | $\ell=3$ | $\ell=4$ | $\ell=5$ | $\ell=6$ | $\ell=7$ |
|---|---|---|---|---|---|
| $\ell$ | $10^{-1}$ | $10^{-1}$ | $10^{-1}$ | $10^{-1}$ | $10^{-1}$ |
| $\ell-1$ | 0 | $10^{-1}$ | 1 | 1 | 1 |
| $\ell-2$ | - | 0 | $10^{-1}$ | $10^{-1}$ | $10^{-1}$ |
| $\ell-3$ | - | - | 0 | $10^{-1}$ | $10^{-1}$ |
| $\ell-4$ | - | - | - | 0 | $10^{-1}$ |
| $\ell-5$ | - | - | - | - | 0 |

Table 5.2: Order of magnitude of the ratio of EM energy flux on the horizon in different modes, $\dot{E}^H_{\ell\, m-2}/\dot{E}^H_{\ell m}$, for different values of $\ell$ and $m$. These values are obtained analytically for slow orbits in the low-frequency limit.

With this in mind, we still choose to compare the modes $m=\ell$ and $m=\ell-1$, as Eq. (5.15) shows that, even if the latter is not dominant, it is of the same order of magnitude as the dominant mode with odd $\ell+m$. The comparison is done through the ratio $\beta_\ell$ (explicit expression in Eq. (G.3)):

$$\beta_\ell(r_0) \equiv \frac{1}{(v_0)^2}\frac{\dot{E}^H_{\ell\,\ell-1}}{\dot{E}^H_{\ell\ell}}\,. \tag{5.16}$$

We plot $\beta_\ell$ for the first few $\ell$ modes in Fig. 5.3 and conclude that for $r_0 > 2.1$ we have $\beta_\ell < 5$, which is a lot less convincing than what we got for the ratio to infinity in Fig 5.1; still, it allows us to say with confidence that for slow orbits the mode $m=\ell$ dominates and carries almost all the energy radiated to the BH for that value of $\ell$; closer to the BH, the mode with $m=\ell-1$ eventually becomes dominant and has to be included, most likely together with other modes with odd values of $\ell+m$, as was hinted by Eq. (5.15). The divergence at $r_0\to 2$ in Fig. 5.3 is a result of an actual divergence in $\dot{E}^H_{\ell\,\ell-1}$ as $r_0\to 2$, while $\dot{E}^H_{\ell\ell}$ approaches a finite value. For $r_0 > 2.5$, we checked $\beta_\ell$ decreases monotonically to a constant value smaller than $1$ but different for each value of $\ell$.

The takeaway of the previous analysis is that we can (and will) still use $m=\ell$ as the dominant term for each value of $\ell$, keeping in mind that we restrict ourselves to $r_0 > 2.1$. Thus, keeping to the goal of understanding if a finite number of modes can be enough to describe the energy carried by radiation going into the BH, we will compare a mode $(\ell,\ell)$ with the neighboring $(\ell+1,\ell+1)$; we call this ratio $\xi_\ell(r_0)$, defining it below (explicit expression in (G.4)):

$$\xi_\ell(r_0) \equiv \frac{\dot{E}^H_{\ell+1\,\ell+1}}{\dot{E}^H_{\ell\ell}}\,. \tag{5.17}$$

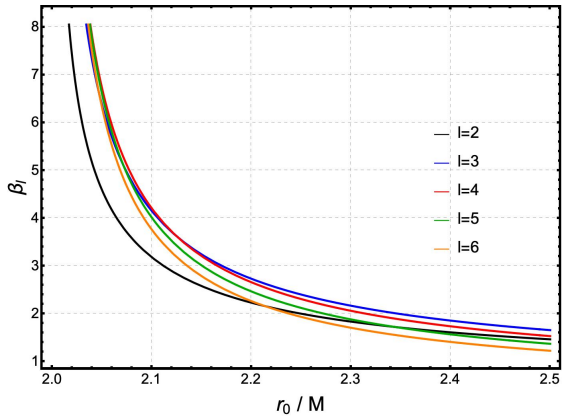


Figure 5.3: $\beta_\ell\, v_0^2 = \dot{E}^H_{\ell\,\ell-1}/\dot{E}^H_{\ell\ell}$ – ratio of EM energy fluxes on the horizon for different modes as a function of the orbital radius $r_0$. The black, blue, red, green, and orange curves represent the cases $\ell = 2,\, 3,\, 4,\, 5,\, 6$ respectively.

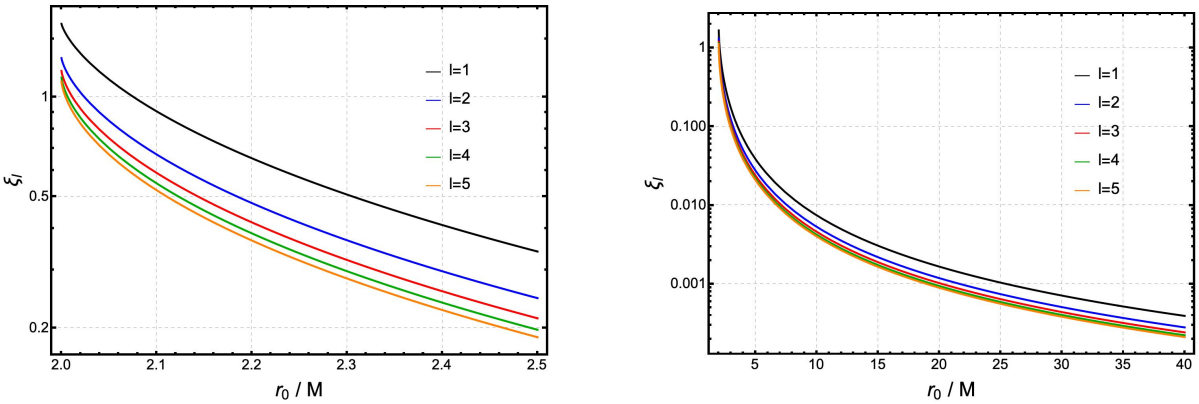


Figure 5.4: $\xi_\ell = \dot{E}^H_{\ell+1\,\ell+1}/\dot{E}^H_{\ell\ell}$ – ratio of EM energy fluxes on the horizon for different modes as a function of the orbital radius $r_0$. The black, blue, red, green, and orange curves represent the cases $\ell = 2,\, 3,\, 4,\, 5,\, 6$ respectively. *Left panel* – comparison for smaller values of $r_0$. *Right panel* – comparison for larger values of $r_0$.

While in the case of the flux at infinity, there was a dependency of the ratio in $\Omega_0$, which made the analysis way simpler, in this case, there is only a dependency on $r_0$, which makes it so that when $r_0 \to \infty$ infinity, the energy radiated in the dipole mode is indeed the dominant one. To understand what happens in the strong gravity regime though, we plotted $\xi_\ell$ for the first few modes and the results are given in Fig. 5.4.

We found that for large enough $r_0$, going well into the strong gravity regime, the higher multipoles are suppressed exponentially and so the dipole is dominant. But for $r_0 < 2.1$ we start to see the higher multipoles becoming more important, to a point where they cannot be neglected; eventually, arbitrarily close to the horizon, the modes with higher $\ell$ are even more important than those with lower $\ell$.

This establishes that for $r_0 > 2.1$ the first few modes with $m = \ell$ should be enough to capture the radiation absorbed by the BH, provided, of course, the orbits are slow. On the contrary, very close to the BH ($r_0 < 2.1$), even if the orbits are slow, to obtain the total energy flux on the horizon we must include more and more modes, eventually leading to $\omega = m\Omega_0 \sim 1$, thus breaking our approximation.

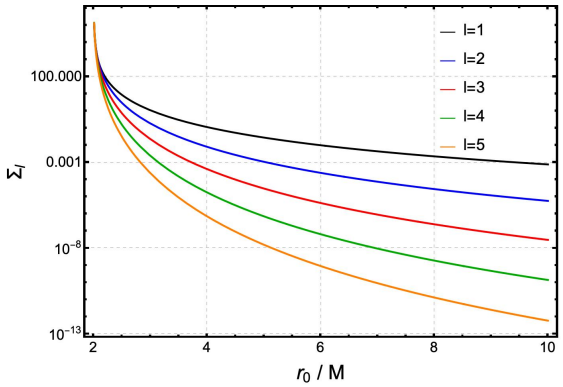


Figure 5.5: $\Sigma_\ell = \dot{E}^H_{\ell\ell}/\dot{E}^\infty_{\ell\ell}$ – ratio of EM energy fluxes on the horizon and at infinity for different modes as a function of the orbital radius $r_0$. The black, blue, red, green, and orange curves represent the cases $\ell = 2,\ 3,\ 4,\ 5,\ 6$ respectively.

## 5.3 Comparing energy flux on the horizon and at infinity

Next, it is important to compare the energy flux on the horizon and at infinity. Using Eqs. (5.1) and (5.12) we choose to study the ratio $\Sigma_\ell$ (explicit expression in Eq. (G.5)):

$$\Sigma_\ell(r_0) \equiv (v_0)^2 \frac{\dot{E}^H_{\ell\ell}}{\dot{E}^\infty_{11}}\,. \tag{5.18}$$

This choice is motivated by the previous result that the dipole mode dominates the energy flux at infinity in the region $r_0 > 2.1$. We plotted $\Sigma_\ell$ for the first few modes in Fig. 5.5. Because of the normalization of $\Sigma_\ell$, it is difficult to make any definite remarks as for very small $v_0$, we can always get $\Sigma_\ell \gtrsim 1$; we can only state with confidence that the energy flux on the horizon should always be investigated, especially in the $r_0 < 10$ region. Very close to the horizon, BH absorption is the dominant effect, as one would naively expect.

To complete this analysis, we investigate the ratio between the energy flux on the horizon for a mode $(\ell, m)$ and the energy radiated to infinity in the same mode for orbits with $r_0 \gg 1$:

$$\dot{E}^H_{\ell m} \sim 4\, r_0^{-4l-2} (m\Omega_0)^{-2\ell}\, (l\,\Gamma(l))^2\, \dot{E}^\infty_{\ell m} \qquad (r_0 \to \infty) \tag{5.19}$$

for even values of $l+m$, and

$$\dot{E}^H_{\ell m} \sim 4\, r_0^{-4l-2} (m\Omega_0)^{-2\ell} \left(\frac{\ell\,(\ell+3)\,\Gamma(l)}{(l-2)}\right)^2 \dot{E}^\infty_{\ell m} \qquad (r_0 \to \infty) \tag{5.20}$$

for odd values of $l+m$. Together with Eqs. (5.9) and (5.10), these establish that, in the limit $r_0 \to \infty$, the energy lost to radiation in the dipole mode is the dominant one, be it to infinity or the BH. Furthermore, if we take Keplerian orbits, $\Omega_0 = r_0^{-3/2}$, these results recover the scaling with $v_0$ obtained by Poisson and Sasaki in Ref. [82] for gravitational radiation.

Having established that for orbits with $r_0 \gg 1$ the dipole mode dominates both the energy flux on the horizon and at infinity, we can now look at the ratio of the two using Eq. (5.19). In particular, we can

look at what happens when the particle is in free fall ($\omega_c = 0$) so that the angular frequency is that of Keplerian orbits (see Sec. 2.2.1):

$$\frac{\dot{E}^H_{11}}{\dot{E}^\infty_{11}} \sim \frac{4}{r_0^6\Omega_0^2} \xrightarrow{\Omega_0=\omega_K} \frac{4}{r_0^3} \qquad (r_0 \to \infty)\,. \tag{5.21}$$

It is clear that for this type of orbit, the flux at infinity greatly dominates the flux on the horizon. For gravitational radiation, the dominant mode has $\ell = 2$, so the scaling law for the ratio of energy absorbed by the BH and going to infinity in the quadrupole mode is faster, $\propto r_0^{-4}$, as shown below.

More interestingly, Eq. (5.21) tells us that if the angular frequency decays faster than $1/r_0^3$ then the flux on the horizon can be the dominant effect; this was pointed out by Gal'tsov in 1982 [87]. The bordering case $\Omega_0 \propto r_0^{-3}$ is precisely what we got for charged particles in PC orbits in the presence of an asymptotically uniform magnetic field in the region $r_0 \gg r_c$ (see Eqs. (2.67), (2.68) and (2.70)). This means that for PC orbits in a region where $r_0 \gg \max(r_c\,,\,1)$, the ratio of the energy fluxes on the horizon and at infinity in the dipole mode does not decay with the radius, and instead goes to a constant:

$$\frac{\dot{E}^H_{11}}{\dot{E}^\infty_{11}} \sim \frac{4}{r_0^6\Omega_0^2} \xrightarrow{\Omega_0=\omega_K^2/\omega_c} 4\omega_c^2 \qquad (r_0 \to \infty)\,. \tag{5.22}$$

The validity of this relies on the orbits being slow-moving and the radiation having a small frequency, both of which hold here (see studies of PC orbits in Sec. 2.2.3). For modes with higher $(\ell, m)$, Eqs. (5.19) and (5.20) show that the flux on the horizon always becomes dominant for very wide orbits, although still subdominant when compared to $\dot{E}^\infty_{11}$.

This concludes the analytical results concerning EM radiation, where we found that, provided the orbits are slow: in the region $r_0 > 2.1$ it is possible to estimate the total rate of energy loss; this is done through the calculation of the energy lost both to infinity and through BH absorption, for a finite number of $(\ell, m)$ modes; for very wide orbits the dipole mode is dominant, but closer to the BH other modes with $\ell = m$ may become relevant as well. Outside this region, infinitely many terms may have to be included, and our approximation breaks for some of them, so we can make no statements.

## 5.4 Scalar and gravitational radiation

As we said in the beginning of this chapter, the main task in finding the energy flux formulas for the EM case was solving the homogeneous Teukolsky equation with physical boundary conditions. In Appendix F we did that not only for $s = -1$ (corresponding to the EM perturbations we studied) but for arbitrary $s$. As it turns out, solving the homogeneous Teukoslky equation is always the most difficult task in obtaining the energy flux formulas, independently of the value of $s$; this means that the methods developed in Appendix F also took care of the hardest step in obtaining the energy fluxes in the scalar ($s = 0$) and gravitational ($s = -2$) cases, in the low frequency and slow motion limit. Because of this, we go over these cases briefly.

### 5.4.1 The scalar case

First, consider a scalar field $\Phi$ minimally coupled to gravity and to matter which is being excited by the motion of a point-particle of mass $m_0$ around a BH; the corresponding action can be written as [83]

$$S = \int d^4x\sqrt{-g}\left(\frac{R}{16\pi} - g^{\mu\nu}\partial_\mu\Phi\partial_\nu\Phi - 2\gamma\Phi T\right), \tag{5.23}$$

where $\gamma$ is a coupling constant and $T$ is the trace of the energy-momentum tensor of the particle. The particle will be radiating scalar waves and we can proceed identically to what we did for EM radiation in Secs. 4.2 and 4.3 to find the energy flux at infinity and on the horizon in scalar waves, that is the equivalents of (4.52), (4.53), (4.58), and (4.59). The main differences are the value of $s$, the source (which is now the trace of the energy-momentum tensor) and the flux formulas of Eqs. (4.49) and (4.55), whose analog can be read off from Ref. [71].

In the end, we find expressions where the only unknowns are, once again, the quantities listed at the beginning of this chapter: $R^\infty(r_0)$, $R^H(r_0)$ and $A_{\text{in}}$. Thus we just have to replace $s = 0$ in the analytical results of Appendix F and we are done. The result for the energy flux in scalar waves at infinity and at the horizon in the dipole term $\ell = 1$, $m = \pm 1$, emitted by a particle in a circular orbit is

$${}_0\dot{E}^\infty_{11} = \frac{\gamma^2 m_0^2}{12\pi}\frac{(r_0-2)(r_0-1)^2}{r_0}\Omega_0^4\,, \tag{5.24}$$

$${}_0\dot{E}^H_{11} = \frac{3\gamma^2 m_0^2(r_0-2)\Omega_0^2\left((r_0-1)\log\left(\frac{r_0}{r_0-2}\right)-2\right)^2}{4\pi r_0}\,. \tag{5.25}$$

If we take the limit $r_0 \to \infty$, we find

$${}_0\dot{E}^\infty_{11} \sim \frac{\gamma^2 m_0^2 r_0^2\Omega_0^4}{12\pi} \xrightarrow{\Omega_0 = r_0^{-3/2}} \frac{\gamma^2 m_0^2}{12\pi r_0^4} \qquad (r_0 \to \infty)\,, \tag{5.26}$$

$$\frac{{}_0\dot{E}^H_{11}}{{}_0\dot{E}^\infty_{11}} \sim \frac{4}{r_0^6\Omega_0^2} \xrightarrow{\Omega_0 = r_0^{-3/2}} \frac{4}{r_0^3} \qquad (r_0 \to \infty)\,, \tag{5.27}$$

where the results after the arrow correspond to Keplerian orbits, $\Omega_0 = r_0^{-3/2}$. What we got for the energy flux to infinity in that limit is a standard result [83]. Regarding the flux into the BH, we find that the ratio is the same as for EM waves (see Eq. (5.21)). Furthermore, we find that once again, if the orbital velocity decays fast enough with $r_0$, the energy flux on the horizon can become the dominant effect; in the particular case of PC orbits, for sufficiently large orbital radius we have $\Omega_0 \sim r_0^{-3}$ (see Sec. 2.2.3), meaning that the ratio goes to a constant.

### 5.4.2 The gravitational case

We can also use the results of Appendix F to study gravitational radiation. Again, we just need to find the equivalents of Eqs. (4.52), (4.53), (4.58), and (4.59). To do so, in this case, we did not perform the calculations ourselves but instead read off the relevant quantities from Refs. [71, 83]. Once we have those, we just need to employ the analytical results of this section with $s = -2$ and any $(\ell\,,\, m)$ values we

wish. Looking at the dominant quadrupole term $\ell = 2$, $m = \pm 2$ yields, for the energy flux in gravitational waves at infinity and on the horizon, generated by a particle of mass $m_0$ in a circular orbit of radius $r_0$:

$$ {}_{-2}\dot{E}^{\infty}_{22} = \frac{32 m_0^2 (r_0-2)^2 r_0 (r_0(9r_0-20)+36)\Omega_0^6}{45(r_0-3)} \tag{5.28} $$

$$ \begin{aligned} {}_{-2}\dot{E}^{H}_{22} = \frac{5 m_0^2 \Omega_0^2}{72(r_0-3)r_0^4} \Big[ & 4\left(81r_0^7 - 342r_0^6 + 657r_0^5 - 588r_0^4 - 180r_0^3 + 400r_0^2 + 164r_0 + 64\right) \\ & - 12\left(27r_0^5 - 141r_0^4 + 324r_0^3 - 386r_0^2 + 104r_0 + 136\right) r_0^3 \log\left(\frac{r_0}{r_0-2}\right) \\ & + 9(r_0-2)^2\left(9r_0^2 - 20r_0 + 36\right) r_0^5 \log^2\left(\frac{r_0}{r_0-2}\right) \Big] . \end{aligned} \tag{5.29} $$

If we take the limit $r_0 \to \infty$, we find

$$ {}_{-2}\dot{E}^{\infty}_{22} \sim \frac{32\, m_0^2 r^4 \Omega_0^6}{5} \xrightarrow{\Omega_0 = r_0^{-3/2}} \frac{32\, m_0^2}{5 r_0^5} \qquad (r_0 \to \infty) , \tag{5.30} $$

$$ \frac{{}_{-2}\dot{E}^{H}_{22}}{{}_{-2}\dot{E}^{\infty}_{22}} \sim \frac{1}{r_0^{10}\Omega_0^4} \xrightarrow{\Omega_0 = r_0^{-3/2}} \frac{1}{r_0^4} \qquad (r_0 \to \infty) , \tag{5.31} $$

where the results after the arrow correspond to Keplerian orbits, $\Omega_0 = r_0^{-3/2}$. What we got for the energy flux to infinity in that limit is the standard quadrupole formula [81, 116]. Regarding the flux into the BH, we find that the ratio for Keplerian orbits scales differently from what it does for EM waves (see Eq. (5.21)). In this case, it decays more quickly as $r_0$ increases; the $r_0^{-4}$ scaling is also a standard result [82]. We also see that the gravitational radiation absorbed by the BH can become dominant when compared to the energy escaping to infinity in the quadruple mode if the orbital velocity decays quickly enough with the orbital radius. In this case, the ratio of the two effects goes to a constant if $\Omega_0 \sim r_0^{-5/2}$; if we consider wide enough PC orbits with $\Omega_0 \sim r_0^{-3}$ (see Sec. 2.2.3), we find the energy absorbed by the BH actually becomes more and more dominant the further the particle is from the BH.

# Chapter 6

# Numerical results

We now aim to study the EM energy flux at infinity and on the horizon emitted by a charged particle in a circular orbit around a Schwarschild BH surrounded by an asymptotically uniform magnetic field. We do so by solving Eqs. (4.52), (4.53), (4.58) and (4.59) numerically rather then analytically. The great advantage of the numerical solutions is that we don't need to restrict to small wave frequency or slow orbits anymore, and can study the energy radiated in any mode for any particular orbit, provided the method converges. We never took into account the numerical error of the simulations, which of course exists and could be very important; still, throughout the analysis, we assume the numerical results are accurate.

The method used is described in Appendix H, where we also explain why all our results depend on one parameter only: the cyclotron frequency $\omega_c$. Thus we will vary its value to test previous analytical results and generally obtain a better understanding of the system under study. Based on the analytical results obtained in the previous section, we always studied the same three modes: the dipole ($\ell = m = 1$), quadrupole ($\ell = m = 2$), and octupole ($\ell = m = 3$). Note that we always include both positive and negative $m$ modes, which contribute equally, as discussed after Eq. (5.1).

## 6.1 No magnetic field: $\omega_c = 0$

We start with the simplest case: a normal Schwarzschild BH ($\omega_c = 0$). In Fig. 6.1, we show the comparison of the numerical results for the energy flux at infinity, normalized to the GLF (see Eq. (5.1)), as well as analytical predictions obtained using Eq. (5.2). We found that numerical and analytical results are in agreement for orbital radii satisfying $r_0 > 30$, which roughly corresponds to orbital velocities $v_0 < 0.2$ (see Fig. 2.4). This leads us to conclude that the slow motion approximation taken in Sec. 5 is valid for $v_0 < 0.2$, which from now on we call the "slow orbits". With that in mind, in the region of "slow orbits", the dipole term is dominant and approaches the prediction given by the GLF. This is even more evident on the right panel, where we only show the results for the dipole, which reaches $.999$ of the analytical result; this had to be the case, as the Newtonian limit applies in the right panel, so we had to recover the Larmor formula following our results of Sec. 3. Contrarily, for $r_0 < 30$ the dipole is no longer as dominant,

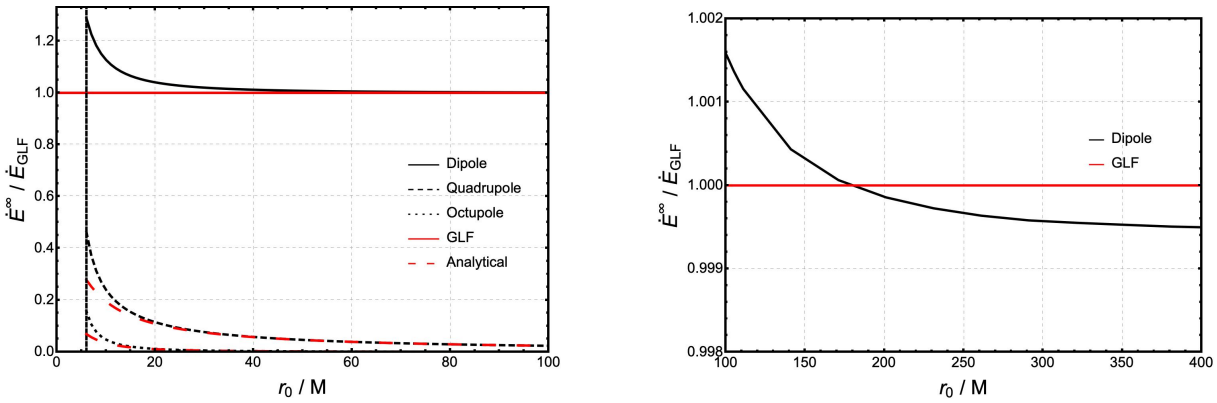


Figure 6.1: Energy flux of EM radiation at infinity, as seen by stationary observers at infinity, normalized to the generalized Larmor formula (GLF – Eq. (5.1)), in different $(\ell\,,\,m)$ modes, emitted by a charged particle in a circular orbit of radius $r_0$ around a Schwarzschild BH. The solid, dashed, and dotted black curves correspond to numerical results for the dipole ($\ell = m = 1$), quadrupole ($\ell = m = 2$), and octupole ($\ell = m = 3$) modes. The solid red line is the prediction of the RLF, while the dashed red lines represent the predictions obtained with Eq. (5.2) for the quadrupole and octupole. The vertical black dashed line indicates the ISCO, $r_{\rm ISCO}/M = 6$. *Left panel* – all modes for $r_0/M < 100$. *Right panel* – dipole mode for $r_0/M > 100$. We found good agreement between numerical and analytical results in the region of slow orbits ($v_0 < 0.2$), which is roughly $r_0/M > 30$, where we also see the dipole is dominant.

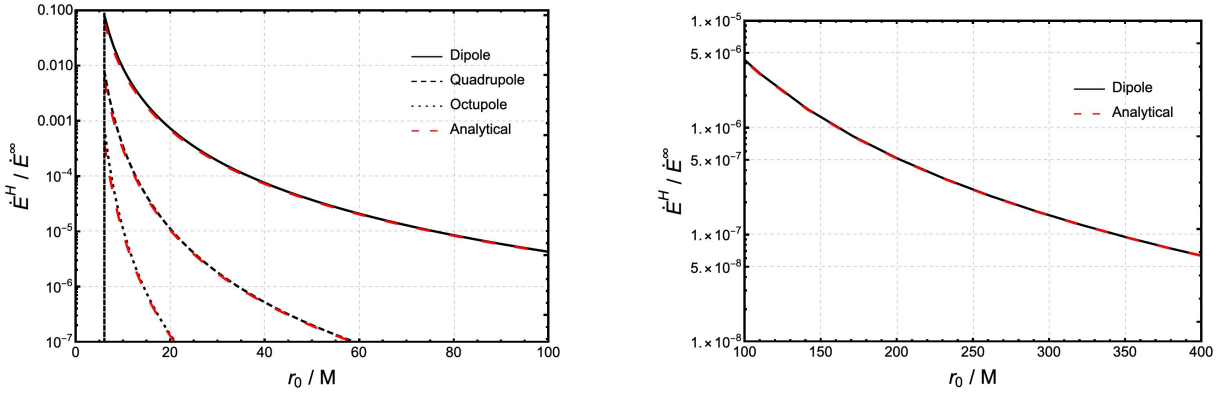


Figure 6.2: Ratio between the energy flux of EM radiation on the horizon and at infinity, for a charged particle in a circular orbit of radius $r_0$ around a Schwarzschild BH. The solid, dashed, and dotted black curves correspond to the dipole, quadrupole, and octupole modes. The dashed red lines are the predictions for the three modes obtained analytically using Eqs. (5.2) and (5.12). The vertical black dashed line indicates the ISCO, $r_{\rm ISCO}/M = 6$. *Left panel* – all modes for $r_0/M < 100$. *Right panel* – dipole mode for $r_0/M > 100$. We found good agreement between numerical and analytical results. The dipole term dominates the energy flux on the horizon but is still subdominant when compared to the energy flux at infinity.

and our analytical results don't give good predictions.

As for the energy flux on the horizon, in Fig. 6.2 we show the ratio of energy radiated to the BH and to infinity in the same $(\ell\,,\,m)$ mode; we compare numerical and analytical results, where the latter were obtained using Eqs. (5.2) and (5.12). There is good agreement between numerical and analytical results, especially in the "slow orbit" region. In terms of energy flux on the horizon, the dipole mode is generally dominant by at least a full order of magnitude when compared to other modes. The energy flux on the horizon in the dipole mode reaches a maximum of about $10\%$ of flux at infinity in the same mode (for $r_0 = r_{\text{ISCO}}$), but can generally be neglected for $r_0 > 10$.

We conclude that for $r_0 > 30$, we can use only the energy radiated to infinity in the dipole mode to capture the radiation reaction completely. Furthermore, our analytical and numerical results, as well as standard literature results, are all in agreement in this region, which inspires confidence in both. Closer to the BH, the energy radiated to infinity and into the BH in higher multipoles has to be considered. Still, even at the ISCO, we can obtain a good approximation using only finitely many modes (for a more rigorous argument see Table 6.1 of the next section).

## 6.2 Minus configuration orbits: $\omega_c < 0$

Having established a good level of confidence in our analytical results, we ask ourselves what happens when we include a magnetic field. Allowing $\omega_c \neq 0$ influences PC and MC orbits distinctly; we start by studying MC orbits (see Fig. 2.1), which have velocity profiles of the types shown in the left panels of Fig. 2.4.

We take $\omega_c = -10^{-3}$, which corresponds to a non-monotonic velocity profile (Fig. 6.3), with a minimum value for $r_0 \sim r_c = 100$. This motivates the definition of three different regions with distinct properties: the "Kepler" ($r_0 < 30$), "slow orbits" ($30 < r_0 < 180$), and "MC" ($r_0 > 180$) regions. We give more complete definitions of the three regions at the end of this section, along with a discussion of the results in light of these definitions.

Due to the relativistic nature of the asymptotic orbits in the MC, the energy flux at infinity was normalized to the RLF (see Eq. (2.21))[1]. The result of comparing the energy flux at infinity in different modes is presented in Fig. 6.4. Just as in the case of $\omega_c = 0$, we found good agreement between numerical and analytical results, as well as the dominance of the dipole, for "slow orbits". However, the relativistic nature of the orbits with $r_0 > 180$ causes the dipole to drift away from the RLF result, as higher multipoles become more important due to beaming.

In view of this, we compare in Fig. 6.5 the energy flux to infinity just in the dipole mode to that given by the sum of the first three modes with $\ell = m$. Furthermore, since we now included a magnetic field, we can also compare the result obtained with Eq. (2.84) (see Sec. 2.3.2 for a derivation). We obtained that equation from the generalization of the Abraham-Lorentz-Dirac force, which is also present in flat

[1] It is important to note two things about the RLF: it is a flat space expression, contrary to the GLF, so it is only valid for $r_0 \gg 1$; within its domain of validity, it includes the energy flux in all multipolar modes. This would always have to be true for the RLF to be valid for highly relativistic speeds, as in that case the particle experiences beaming, which causes all the multipoles to be nontrivially excited [42].

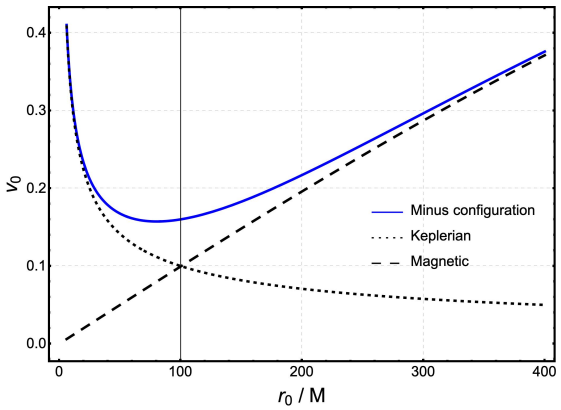


Figure 6.3: Velocity profile of MC circular orbits with radius $r_0$ and $M\omega_c = 10^{-3}$. The blue curve corresponds to the actual velocity profile, the black dotted curve is the "Keplerian" result, the black dashed curve is the "Magnetic" result and the black vertical line indicates the position of the critical radius $r_c = 100M$ (cf. caption of Fig. 2.4). The "Keplerian" result is roughly recovered for $r_0/M < 30$, and the "Magnetic" for $r_0/M > 180$. We have "slow orbits" ($v_0 < 0.2$) around $30 < r_0/M < 180$.

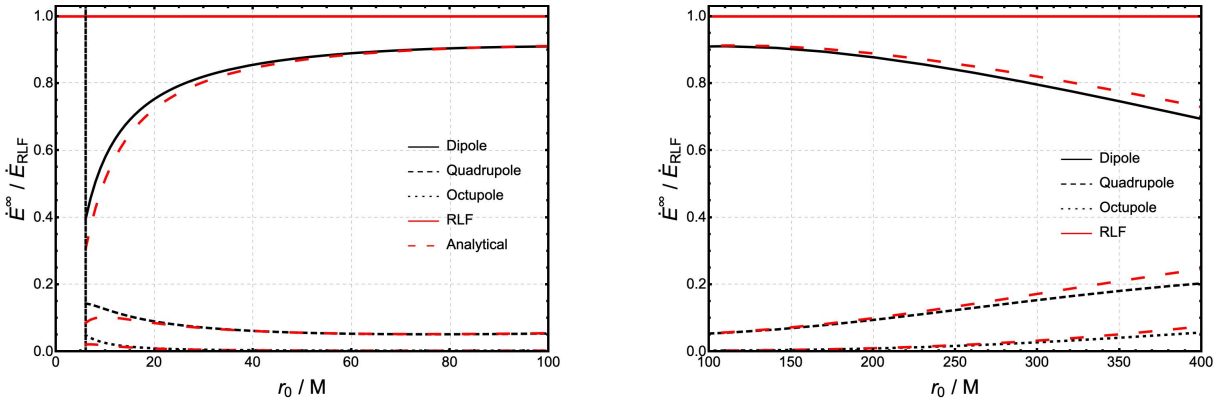


Figure 6.4: Energy flux of EM radiation at infinity normalized to the relativistic Larmor formula (RLF – Eq. (2.21)), for a charged particle in an MC circular orbit of radius $r_0$ around a Schwarzschild BH with $M\omega_c = -10^{-3}$. The solid, dashed, and dotted black curves correspond to numerical results for the dipole, quadrupole, and octupole modes. The solid red line is the prediction of the RLF, while the dashed red lines represent the predictions obtained analytically for all three modes. The vertical black dashed line indicates the ISCO, $r_{\rm ISCO}/M \lesssim 6$. *Left panel* – all modes for $r_0/M < 100$. *Right panel* – all modes for $r_0/M > 100$. We found good agreement between numerical and analytical results in the region $30 < r_0/M < 180$, where the dipole term is dominant. Outside this region, higher multipoles become more relevant and the analytical predictions become less accurate. The dipole never recovers the RLF beyond about 90%.

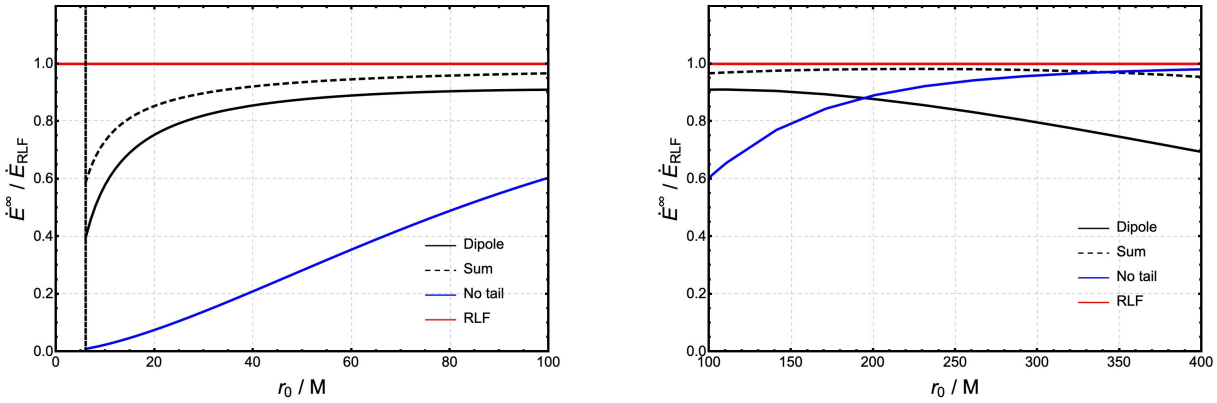


Figure 6.5: Energy flux of EM radiation at infinity normalized to the RLF, for a charged particle in an MC circular orbit of radius $r_0$ around a Schwarzschild BH with $M\omega_c = -10^{-3}$. The solid black curve corresponds to the dipole mode, while the dashed black curve includes also the sum of the quadrupole and octupole modes. The solid red line is the prediction of the RLF. The blue curve is the prediction obtained if we neglect the tail term, that is Eq. (2.84). The vertical black dashed line indicates the ISCO, $r_{\rm ISCO}/M \lesssim 6$. *Left panel* – all modes for $r_0/M < 100$. *Right panel* – all modes for $r_0/M > 100$. When compared to Fig. 6.4, the sum of modes allows us to recover the RLF with very good accuracy, in a wide range of orbits. The "no tail" curve gives very bad results for small $r_0/M$ while it completely recovers the RLF for very large enough values of $r_0/M$.

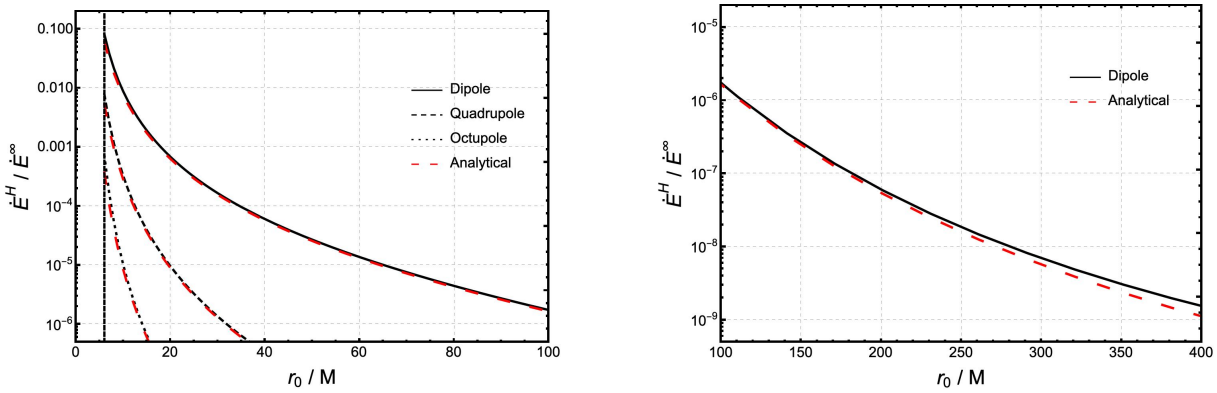


Figure 6.6: Ratio between the energy flux of EM radiation on the horizon and at infinity, for a charged particle in an MC circular orbit of radius $r_0$ around a Schwarzschild BH with $M\omega_c = -10^{-3}$. The solid, dashed, and dotted black curves correspond to the dipole, quadrupole, and octupole modes. The dashed red lines are the predictions for the three modes obtained analytically. The vertical black dashed line indicates the ISCO, $r_{\rm ISCO}/M \lesssim 6$. *Left panel* – all modes for $r_0/M < 100$. *Right panel* – dipole mode for $r_0/M > 100$. We find good agreement between numerical and analytical results up to $r_0/M \sim 180$. The dipole term dominates the energy flux on the horizon but is still subdominant when compared to the energy flux at infinity.

space, and so naively is not expected to describe the energy absorbed by the BH. Therefore, it can only result from an energy flux to infinity, so we choose to include it in Fig. 6.5 and call it the "no tail" curve. By considering the sum of multipoles, we successfully recover the RLF in a wide range of orbits ($80 < r_0 < 350$), beyond which beaming intensifies and other modes would have to be added up. As we discussed in Sec. 2.3.2, the "no tail" expression only sees the acceleration of the particle due to the Lorentz force; indeed, in the magnetic region, that is practically the sole source of acceleration, which is why that expression agrees with the RLF. But for smaller values of $r_0$ that is never the case, and as gravitational effects become more important, that expression gives an ever worse underestimation of the energy flux.

Next, in Fig. 6.6 we look at the ratio of the energy flux on the horizon and at infinity. In broad terms, the energy absorbed by the BH in the dipole mode is relevant at the ISCO, coming to about $10\%$ of the energy radiated to infinity, but it then decays with $r_0$, quickly becoming negligible; the other modes never reach $1\%$ so they can generally be neglected. We find that the analytical predictions were in agreement with numerical results in the up to about $r_0 \sim 180$.

Summing up, we looked at MC orbits for $M\omega_c = -10^{-3}$ and found that the analysis can be divided into three distinct regions, which are defined relative to the critical radius $r_c = 100$ (see Eq. (2.67)):

- "Kepler" region ($r_0 < 30$) – these orbits are dominated by gravitational effects and are faster closer to the ISCO (Fig. 6.3). Here the results are very similar to what we found for $\omega_c = 0$. Our analytical formulas fail to give very accurate predictions, the "no tail" expression is catastrophically bad, and not even the RLF is valid in this region. Still, it seems that by adding up numerical results for different modes, taking into account both flux at infinity and on the horizon, we can obtain an accurate value for the total energy flux. We confirmed this for the first $(\ell\,,\,m)$ modes at $r_0 = r_{\rm ISCO}$ in Table 6.1 and found that higher order modes were exponentially suppressed, so using a finite number allows for arbitrarily small errors.

- "Slow orbit" region ($30 < r_0 < 180$) – these are the slowest orbits, with $v_0 < 0.2$, located around the critical radius $r_c = 100$ (Fig. 6.3). Here the dipole mode is dominant, but adding up numerical results for the first three $\ell = m$ modes was needed to get good agreement with the RLF. The energy flux on the horizon is always negligible in this region. Our analytical formulas give accurate predictions in this region, while the "no tail" expression underestimates the energy flux.

- "Magnetic" region ($r_0 > 180$) – as orbits become dominated by magnetic effects and the velocity becomes higher (Fig. 6.3), the dipole mode becomes less dominant, and even more modes have to be included to adequately describe the energy flux to infinity. Adding up the numerical results for the first three $\ell = m$ modes still gives good agreement with the RLF, but only up to $r_0 \approx 350$, after which it also falls short; if more modes are included, we extend the validity further away, but, eventually, it will always fall short. The energy flux on the horizon is always negligible in this region, and our analytical formulas fail to make accurate predictions, but the "no tail" expression is very successful.

Changing $\omega_c$ leads to a change in $r_c$, which in turn leads to a shift in these regions, but the results for

| $\ell$ | $m$ | $\dot{E}^{\infty}_{\ell m}/\dot{E}^{\infty}_{11}$ (%) | $\dot{E}^{H}_{\ell m}/\dot{E}^{\infty}_{11}$ (%) |
|---|---|---|---|
| 1 | 1 | 100 | 8.2 |
| 2 | 2 | 36.3 | 0.28 |
| 2 | 1 | $< 10^{-2}$ | $< 10^{-1}$ |
| 3 | 3 | 12.4 | $< 10^{-2}$ |
| 3 | 2 | $< 10^{-1}$ | $< 10^{-3}$ |
| 4 | 4 | 4.12 | $< 10^{-3}$ |
| 5 | 5 | 1.3 | $< 10^{-5}$ |
| 6 | 6 | 0.43 | $< 10^{-6}$ |
| 7 | 7 | 0.14 | $< 10^{-8}$ |
| 8 | 8 | $< 10^{-1}$ | $< 10^{-9}$ |

Table 6.1: Numerical results for the comparison of the energy flux on the horizon ($\dot{E}^{H}_{\ell m}$) and to infinity ($\dot{E}^{\infty}_{\ell m}$), normalized to the energy flux at infinity in the dipole mode ($\dot{E}^{\infty}_{\ell m}$) generated by a charged particle at the ISCO in the MC, around a Schwarzschild BH with $M\omega_c = -10^{-3}$. It seems clear that with finitely many modes, one can obtain arbitrarily small errors in the total energy flux.

each should be qualitatively the same; keep in mind that the "Kepler" and even the "slow orbits" region could be pulled in beyond the ISCO (see bottom right panel of Fig. 2.4).

## 6.3 Plus configuration orbits: $\omega_c > 0$

We now proceed to study orbits in the PC (see Fig. 2.1). In this configuration, having $\omega_c \neq 0$ does not alter the monotonicity of the velocity profile, but instead just decreases the orbital velocity for all values of $r_0$ (see Fig. 2.4). This means that now the analytical results obtained before may be used to study a larger set of orbits, as they are only valid if the orbital velocity is small.

We will start by looking at $\omega_c = 10^{-2}$, and only after that will we look at greater values of $\omega_c$, which will allow us to find slow orbits closer to the event horizon[2].

### 6.3.1 $M\omega_c = 10^{-2}$

Consider first the case $\omega_c = 10^{-2}$, which corresponds to the velocity profile shown in Fig. 6.7, with $r_c \approx 21.5$. Again, we start by looking at the energy flux to infinity, normalized to the GLF, in different modes, and we show the results in Fig. 6.8. We find, as would be expected, that in the region of "slow orbits" the dipole mode dominates and our numerical and analytical results are in agreement. Outside this region, both of these properties fail.

Regarding the "no tail" expression of Eq. (2.84), in Sec. 2.3.2 we showed that it leads to particles gaining energy in all orbits beyond the light ring, $r_0 > 3$. Since this is not what we obtain with our analytical or numerical results, we completely exclude the "no tail" expression from the PC analysis hereinafter.

Looking at the ratio of energy flux on the horizon and at infinity (Fig. 6.9), we find very good agreement between numerical and analytical results for "slow orbits"; we also find that the dipole mode is

[2]The reason for this separation, as well as for the values chosen for $\omega_c$, is that it becomes harder to get numerical results for very small orbital frequencies, meaning that as we increase $\omega_c$ in PC orbits we are decreasing the domain that can be studied.

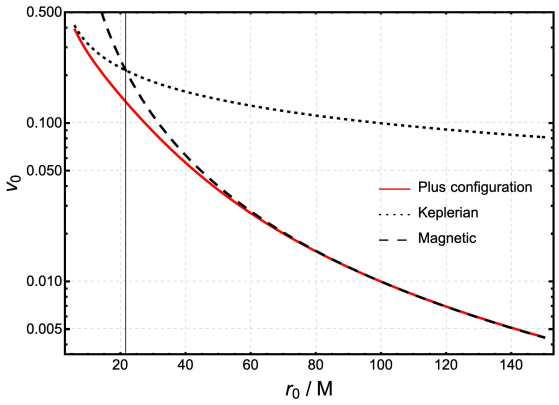


Figure 6.7: Velocity profile of PC circular orbits with radius $r_0$ and $M\omega_c = 10^{-2}$. The red curve corresponds to the actual velocity profile, the black dotted curve is the "Keplerian" result, the black dashed curve is the "Magnetic" result, and the black vertical line indicates the position of the critical radius $r_c/M \approx 21.5$. The "Magnetic" result is recovered for $r_0/M > 40$. We have "slow orbits" for $r_0/M > 15M$.

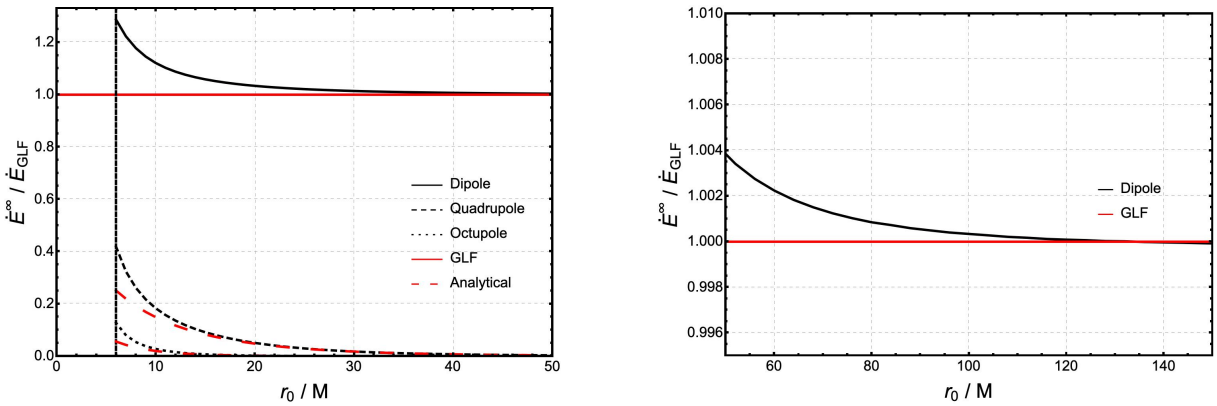


Figure 6.8: Energy flux of EM radiation at infinity, normalized to the GLF, for a charged particle in a PC circular orbit of radius $r_0$ around a Schwarzschild BH with $M\omega_c = 10^{-2}$. The solid, dashed, and dotted black curves correspond to numerical results for the dipole, quadrupole, and octupole modes. The solid red line is the prediction of the GLF, while the dashed red lines represent the predictions obtained analytically for the quadrupole and octupole. The vertical black dashed line indicates the ISCO, $r_{\rm ISCO}/M \lesssim 6$. *Left panel* – all modes for $r_0/M < 100$. *Right panel* – dipole mode for $r_0/M > 100$. We find good agreement between numerical and analytical results in the region $r_0/M > 15$, where the dipole is dominant.

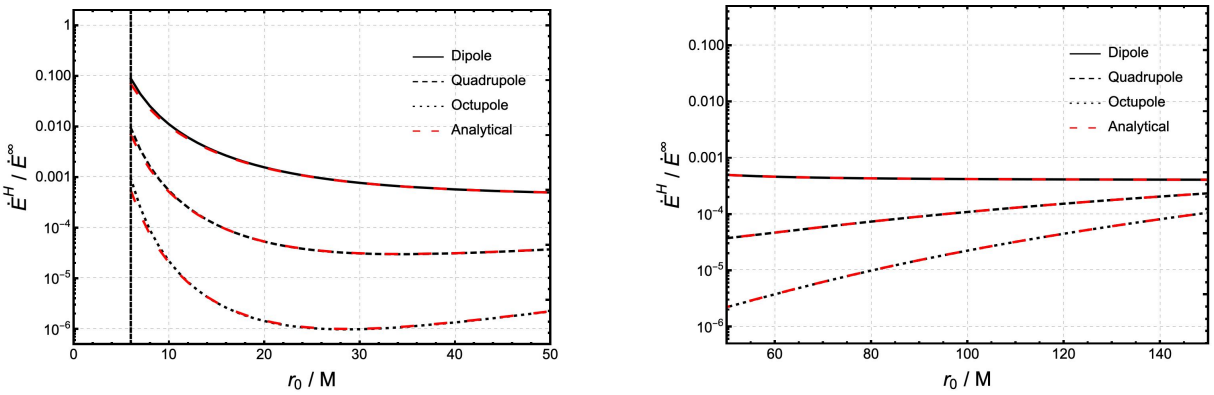


Figure 6.9: Ratio between the energy flux of EM radiation on the horizon and at infinity, for a charged particle in a PC circular orbit of radius $r_0$ around a Schwarzschild BH with $M\omega_c = 10^{-2}$. The solid, dashed, and dotted black curves correspond to the dipole, quadrupole, and octupole modes. The dashed red lines are the predictions for the three modes obtained analytically. The vertical black dashed line indicates the ISCO, $r_{\rm ISCO}/M \lesssim 6$. *Left panel* – all modes for $r_0/M < 50$. *Right panel* – all modes for $r_0/M > 50$. We find good agreement between numerical and analytical results. The dipole term still dominates, as does the energy flux on the horizon; however, for $r_0/M > 40$ we see the ratio go to a constant for the dipole, and start growing for the higher multipoles.

dominant, as is the energy flux to infinity, although the flux on the horizon in the dipole mode is non-negligible for $r_0 < 10$. However, contrary to what we saw for orbits in the MC, now the ratio in the dipole mode goes to a constant for $r_0 \gtrsim 40$; according to the analytical result of Eq. (5.22), the constant is $4\omega_c^2 = 4 \times 10^{-4}$, which is compatible with what we see in the plot. We also see that in the higher multipoles, the ratio is actually growing, showing increasing importance of the flux on the horizon; this is also something we were expecting according to the discussion following Eq. (5.22).

### 6.3.2 $M\omega_c = 2 \times 10^{-1}$

For this value of $\omega_c$ the velocity profile is given in Fig. 6.10 and it corresponds to a critical radius of $r_c \approx 2.9$, which lies beyond the ISCO. Regarding the energy flux to infinity, we see in Fig. 6.11 that we have good agreement between numerical and analytical results but only for orbits with $v_0 \lesssim 0.1$, which corresponds to $r_0 \gtrsim 8$. The dominance of the dipole is also clear in this region, so it adequately describes all the energy flux at infinity.

Regarding the energy flux on the horizon, in Fig. 6.12, we see that our numerical simulations recover the analytical results with good accuracy. Once again, we also find that when $r_0 \gg r_c$ the ratio of energy flux on the horizon and at infinity goes to a constant for the dipole, while it keeps growing for the higher multipoles; in this case, the analytical prediction for the constant is $4\omega_c^2 = 0.16$, which is consistent with the numerical result. We also compare the energy flux on the horizon in the three modes to the energy flux to infinity in the dipole mode, and find the former are still negligible for $r_0 > 10$. For $r_0 < 10$, the flux on the horizon can no longer be completely neglected, and at the ISCO the energy flux on the horizon in the dipole mode is actually the dominant effect, but all three modes should be included (a more systematic study of this is done presented in Table 6.2).

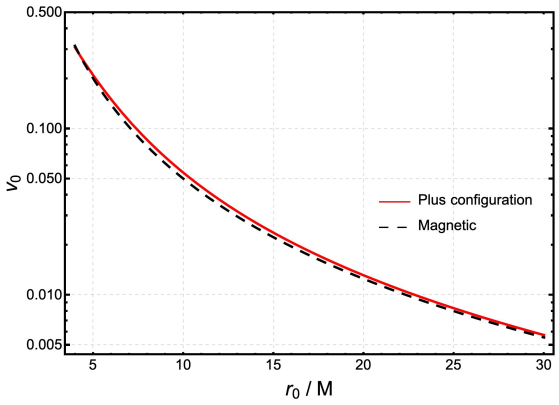


Figure 6.10: Velocity profile of PC circular orbits with radius $r_0$ and $M\omega_c = 2\times10^{-1}$. The red curve corresponds to the actual velocity profile and the black dashed curve is the "Magnetic" result. The critical radius $r_c/M \approx 2.9$ lies beyond the ISCO so it is not shown. The "Magnetic" result is always recovered and we have "slow orbits" for $r_0/M > 5M$.

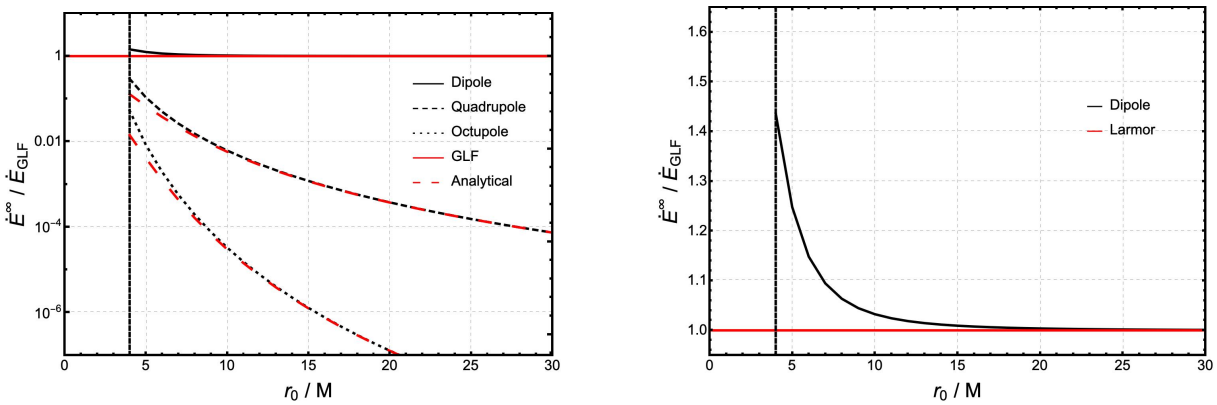


Figure 6.11: Energy flux of EM radiation at infinity, normalized to the GLF, for a charged particle in a PC circular orbit of radius $r_0$ around a Schwarzschild BH with $M\omega_c = 2\times10^{-1}$. The solid, dashed, and dotted black curves correspond to numerical results for the dipole, quadrupole, and octupole modes. The solid red line is the prediction of the GLF, while the dashed red lines represent the predictions obtained analytically for the quadrupole and octupole. The vertical black dashed line indicates the ISCO, $r_{\rm ISCO}/M \approx 4$. *Left panel* – all modes. *Right panel* – dipole mode. We find good agreement between numerical and analytical results, and the dipole term is clearly dominant.

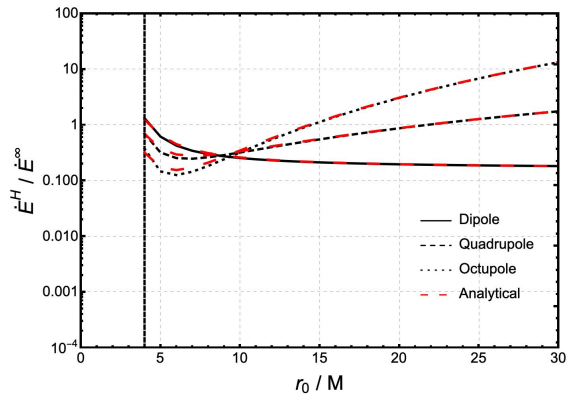


Figure 6.12: Ratio between the energy flux of EM radiation on the horizon and at infinity, for a charged particle in a PC circular orbit of radius $r_0$ around a Schwarzschild BH with $M\omega_c = 2 \times 10^{-1}$. The solid, dashed, and dotted black curves correspond to the dipole, quadrupole, and octupole modes. The dashed red lines are the predictions for the three modes obtained analytically. The vertical black dashed line indicates the ISCO, $r_{\rm ISCO}/M \approx 4$. We find good agreement between numerical and analytical results. The dipole term is still dominant, but now the energy flux on the horizon is already larger than the flux at infinity very close to the BH, although the latter is dominant for $r_0/M > 5$. The ratio goes to a constant for the dipole and grows for the higher multipoles, to the point where the energy flux on the horizon is greater than the flux at infinity in the quadrupole and octupole modes.

### 6.3.3 $M\omega_c = 2$

For this value of $\omega_c$, the velocity profile is given in Fig. 6.13, and corresponds to a critical radius of $r_c \approx 0.6$, which lies beyond the event horizon. The energy flux to infinity is depicted in Fig. 6.14, and even though now $v_0 < 0.2$ for all orbits, the numerical simulations are unable to recover the analytical results for $r_0 < 5$. Other than that, the analysis is qualitatively similar to that of Fig. 6.11.

Finally, in Fig. 6.15 we show that for this value of $\omega_c$ the energy flux on the horizon is orders of magnitude greater than that to infinity, so it cannot be neglected. Furthermore, we once again see the ratio go to a constant for the dipole mode while it keeps growing for the higher multipoles; in this case, the constant would be $4\omega_c^2 = 16$, which is consistent with the numerical result. Again, we also compare the energy flux on the horizon in all three modes to the energy flux to infinity in the dipole mode to see if a finite number of modes is sufficient to describe the total energy flux; we find that with increasing $r_0$ the energy flux to infinity for the dipole mode becomes more relevant, but the dominant effect is always BH absorption of the dipole mode. The orbit for which the most modes have to be included is thus the ISCO, so we look at the energy flux in multiple $(\ell\,,\,m)$ modes for that orbit in Table 6.2. We find that, although many terms have to be included, the importance of higher multipoles appears to decay fast enough so that one can use a finite number of modes and still obtain an arbitrarily small error in the total energy radiated. For higher values of $r_0$, the problem only becomes easier, and fewer and fewer terms are needed.

### 6.3.4 Summary of plus configuration

Summing up, we looked at PC orbits for 3 different values of the cyclotron frequency and concluded that:

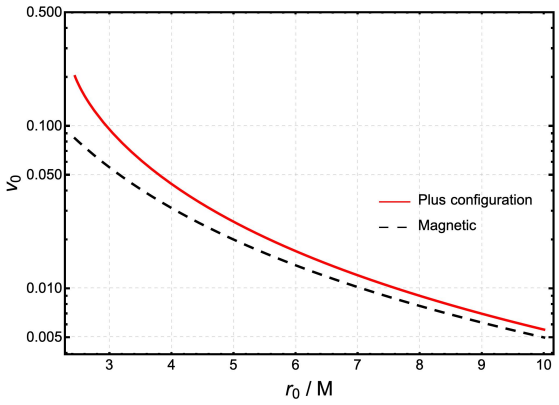


Figure 6.13: Velocity profile of PC circular orbits with radius $r_0$ and $M\omega_c = 2$. The red curve corresponds to the actual velocity profile and the black dashed curve is the "Magnetic" result. The critical radius $r_c/M \approx 0.63$ lies beyond the ISCO so it is not shown. The "Magnetic" result is always roughly recovered and all orbits are "slow orbits".

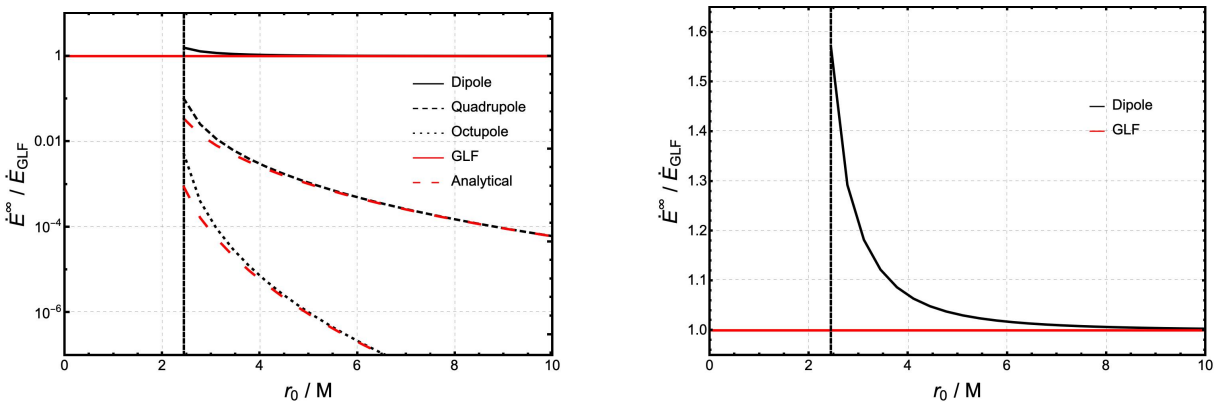


Figure 6.14: Energy flux of EM radiation at infinity, normalized to the generalized Larmor formula GLF, for a charged particle in a PC circular orbit of radius $r_0$ around a Schwarzschild BH with $M\omega_c = 2$. The solid, dashed, and dotted black curves correspond to numerical results for the dipole, quadrupole, and octupole modes. The solid red line is the prediction of the GLF, while the dashed red lines represent the predictions obtained from Eq. (5.2) for the quadrupole and octupole. The vertical black dashed line indicates the ISCO, $r_{\rm ISCO}/M \approx 2.4$. *Left panel* – all modes. *Right panel* – dipole mode. We find good agreement between numerical and analytical results, and the dipole term is clearly dominant.

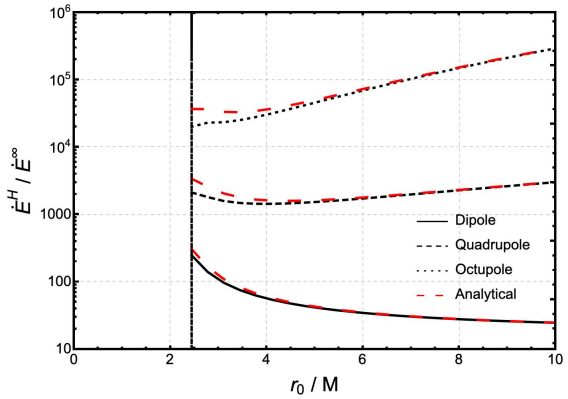


Figure 6.15: Ratio between the energy flux of EM radiation on the horizon and at infinity, for a charged particle in a PC circular orbit of radius $r_0$ around a Schwarzschild BH with $M\omega_c = 2$. The solid, dashed, and dotted black curves correspond to the dipole, quadrupole, and octupole modes. The dashed red lines are the predictions for the three modes obtained analytically using Eqs. (5.2) and (5.12). The vertical black dashed line indicates the ISCO, $r_{\rm ISCO}/M \approx 2.4$. We find good agreement between numerical and analytical results for $r_0/M > 5M$.The dipole term still dominates, but now the energy flux on the horizon is the dominant effect; the ratio goes to a constant for the dipole and grows for the higher multipoles.

| $\ell$ | $m$ | $\dot{E}^\infty_{\ell m}/\dot{E}_{11}$ (%) | $\dot{E}^H_{\ell m}/\dot{E}^\infty_{11}$ (%) |
|---|---|---|---|
| 1 | 1 | $0.4$ | $100$ |
| 2 | 2 | $< 10^{-1}$ | $54.5$ |
| 2 | 1 | $< 10^{-4}$ | $2.2$ |
| 3 | 3 | $< 10^{-2}$ | $26.3$ |
| 3 | 2 | $< 10^{-6}$ | $1.1$ |
| 4 | 4 | $< 10^{-4}$ | $12.5$ |
| 5 | 5 | $< 10^{-5}$ | $5.8$ |
| 6 | 6 | $< 10^{-6}$ | $2.7$ |
| 7 | 7 | $< 10^{-8}$ | $1.2$ |
| 8 | 8 | $< 10^{-9}$ | $0.6$ |

Table 6.2: Numerical results for the comparison of the energy flux on the horizon ($\dot{E}^H_{\ell m}$) and to infinity ($\dot{E}^\infty_{\ell m}$), normalized to the energy flux at infinity in the dipole mode ($\dot{E}^\infty_{\ell m}$) generated by a charged particle at the ISCO in the PC, around a Schwarzschild BH with $M\omega_c = 2$. It appears clear that with finitely many modes, one can obtain arbitrarily small errors in the total energy flux.

- For these orbits, the domain of validity of our analytical expressions is far greater than in the absence of a magnetic field, as including it results in slower orbits for all orbital radii. Still, very close to the BH we require far lower velocities for the analytical expressions to be valid, as even for $v_0 < 0.1$, which would usually be enough, the analytical formulas still give bad predictions for $r_0 < 5$ when $\omega_c = 2$.

- Generally, out of the values tested, we found that it is possible to describe the total energy flux in all the orbits using only a finite number of modes. For high $\omega_c$, the ISCO is very close to the event horizon and so the energy flux on the horizon must be calculated for many modes, but a finite number of modes is still enough to get arbitrarily high accuracy.

- For large enough values of orbital radius, the ratio of the energy flux on the horizon and to infinity

goes to a constant ($4\omega_c^2$) for the dipole mode and grows to arbitrarily large values for the higher-order multipoles. For a fixed, but large enough, value of $r_0$, this ratio grows with $\ell$. This happens for even smaller values of $r_0$ than we had anticipated when we derived Eq. (5.22). Even though this trend is transversal in our results, we find that asymptotically the energy flux on the horizon in the higher-order multipoles goes to zero when compared to the energy flux at infinity in the dipole mode.

Further increasing $\omega_c$ would pull the ISCO even closer to the event horizon, and we would have to include even more modes to describe the energy flux adequately, but a finite number should still be enough, at least until $r_0 \approx 2.1$, as discussed in Sec. 5.

The result reported in the third point above has several interesting implications: First, it takes place asymptotically far away from the BH, for orbits so wide that BH absorption should naively be very small, given that the wave frequency is so large it shouldn't even see the BH; this argument must however be taken with a grain of salt, as it is not the particle that is radiating, but the binary particle + BH. Second, it gives a non-ambiguous way of distinguishing a BH from other astrophysical objects even if we are very far away from it. Finally, an observer at infinity looking at a particle orbiting the BH with $r_0 \gg 1$ would at best be able to realize that the ratio of energy flux on the horizon and at infinity in the dipole mode is going to a constant, since the energy flux in higher multipoles is completely negligible in such scenario.

# Chapter 7

# Conclusions

In this thesis, we aimed to give a detailed and consistent analysis of the radiation reaction force acting on a charged particle in a circular orbit around a Schwarzschild BH immersed in an asymptotically uniform magnetic field. This work was motivated by the prospect of energy extraction mechanisms relying on radiation reaction [29].

Regarding the dynamics of charged particles in this system without radiation reaction, it is important to note that circular motion exists only in the equatorial plane and that its analysis can be split into MC (angular momentum and cyclotron frequency have opposite signs) and PC (angular momentum and cyclotron frequency have the same sign) orbits. MC orbits approach flat space cyclotron motion at infinity. As the absolute value of the cyclotron frequency increases, all MC orbits become more relativistic, while the ISCO grows closer to the horizon (but never going below $r \approx 4.3M$). The PC orbits, on the other hand, do not approach flat space cyclotron motion at infinity. As the absolute value of the cyclotron frequency increases, PC orbits become less and less relativistic, while the ISCO approaches the event horizon at $r = 2M$.

If we include radiation, the equation of motion is the DeWitt–Brehme equation (Eq. (2.75)), which is very complicated to solve, especially because of the existence of a non-local term — the tail (Eq. (2.76)). Some authors have delved into the task of brute-force calculating the radiative Green's functions needed to evaluate the tail integral [64]; others have also tried neglecting it from the analysis altogether [53]. However, neglecting the tail leads to a seemingly unphysical "orbit widening" in PC orbits [52], resulting in the particle gaining energy without any clear source; this caught our attention and was the starting point for this work.

We started by looking at the Newtonian limit of the DeWitt–Brehme equation; the results of that analysis were published in Ref. [54]. In this case, the tail term has an analytical expression [55], so including it poses no problem whatsoever. We found that, for the calculation to be consistent with neglecting the tail term, one of two scenarios had to take place: either the radiation reaction is neglected altogether, or the gravitational force can be neglected, and so a flat space description of the phenomenon using the Abraham–Lorentz–Dirac equation is valid. This happens because the Abraham–Lorentz–Dirac force only accounts for the radiation reaction due to the covariant acceleration, that is, to the external

forces; the radiation reaction to gravity is entirely captured by the tail. We also found that we could only recover standard literature results by including the tail and that the "orbit widening" ceases to exist if it is included. This established that neglecting the tail is often not a valid approximation, at least in the Newtonian limit, but a strong-field calculation was still missing.

As stated above, calculating the tail term in the strong field case is a very difficult task, so instead we consider the simpler formalism of BH perturbation theory, namely the Bardeen–Press equation [68, 69]. We considered a charged particle in a circular orbit around a magnetized Schwarzschild BH and using BH perturbation theory we obtained the multipolar expansion of its radiation field; this allows us to obtain the energy flux at infinity and on the horizon [71], and thus infer the energy lost by the particle through radiation reaction. Even assuming that the particle is always in a circular orbit, it is possible to study the orbit's evolution by using the adiabatic approximation. Generally, the motion of the particle in the equatorial plane is entirely determined by the value of its energy and angular momentum; by knowing how those evolve in time, we can evolve the orbit of the particle. In the case of circular orbits, a single parameter — the energy — suffices to determine the orbit, and so evolving the energy is equivalent to evolving the orbit (provided, of course, that radiative effects are small enough so that saying that the particle is in a circular orbit remains a good approximation — adiabatic approximation).

Once the expressions for the energy flux at infinity and on the horizon were obtained, it became clear that there was only one hard task to overcome: solving the homogeneous Teukolsky radial equation with physical boundary conditions, corresponding to purely ingoing waves at the horizon and to purely outgoing waves at infinity. We did so in two different and independent ways, first through analytical methods, valid in the low frequency and slow motion regime, and then through numerical methods. The results of this analysis are being prepared for publication. It is important to note that now the low frequency and slow motion approximations are not equivalent to the Newtonian limit, since PC orbits can be slow very close to the event horizon.

On the analytical front, we established that for orbital radius $r_0 \gtrsim 2.1M$ the total energy flux can be calculated using a finite number of multipolar modes. In that region, the dipole is the dominant mode for both energy flux on the horizon and at infinity, with the latter being described by the GLF, which reduces to the standard Larmor power formula for large enough orbital radius. However, determining which effect is dominant, flux on the horizon or at infinity is more complicated than one would naively expect. Indeed, we found that for Keplerian orbits, where the angular velocity behaves as $\Omega_0 \sim 1/r_0^{3/2}$, the further the particle is from the BH, the lesser energy it absorbs, meaning the total energy flux is determined by the flux at infinity and approaches the prediction of the Larmor formula. However, for PC orbits, the ratio of energy flux on the horizon and at infinity in the dipole mode goes to a constant $4\omega_c^2$, where $\omega_c$ is the cyclotron frequency; for the higher order multipoles, the same ratio goes to infinity with increasing orbital radius. This is a direct result of the decay of the angular velocity in PC orbits, $\Omega_0 \sim 1/r_0^3$; in fact, if the angular velocity were to decay even faster with orbital radius, then the ratio for the dipole would also grow indefinitely with the orbital radius. Regarding the MC orbits, we did not perform any specific analytical study because those orbits are relativistic for large enough orbital radius, thus falling outside the domain of our approximation. We also took the chance to see what happens for scalar and

gravitational radiation; in those cases, we only looked at the dominant dipole and quadrupole modes, respectively. For the scalar case, the qualitative analysis is identical to the EM case; for the gravitational case, since the dominant mode is now the quadrupole, we found that the ratio of energy flux on the horizon and at infinity in that mode goes to infinity with increasing orbital radius, provided the particle is in a PC orbit. We found that all our analytical results were compatible with the available literature [82, 83, 87].

Our numerical analysis was restricted to the EM case, and, when the orbits were slow and the mode frequency was small, it completely corroborated the previously obtained analytical results. Generically, we found dominance of the dipole for slow orbits. In PC orbits, we recovered that, for increasing orbital radius, the ratio of energy flux on the horizon and at infinity goes to $4\omega_c^2$ in the dipole mode, and goes to infinity for higher order multipoles; moreover, for a fixed and sufficiently large value of orbital radius, this ratio grows with the angular number $\ell$. Still in regards to PC orbits, out of all the values tested, a finite number of modes was always enough to capture the total energy lost by the particle.

We also obtained numerical results for MC orbits. We found that, for a given value of $\omega_c$, the analysis can be split into three regions: the "Kepler" region, where the orbits are Keplerian, our analytical results are not valid, and neither is the RLF; the "slow orbit" region, where the RLF is valid, as are our analytical results (namely the dipole is dominant); and the "Magnetic" region, where the motion approaches flat space cyclotron motion, the RLF is valid, but our analytical formulas fail because of the relativistic nature of these orbits. It is a general result that when the orbit of a particle is extremely relativistic, the higher order multipoles are excited and must be included to obtain a rigorous account of the energy flux; we recovered this result and found that, in the "slow orbits" and "Magnetic" regions, adding up the contributions from the dipole, quadrupole and octupole modes allows for a much more trustworthy estimate of the energy flux when compared to the prediction of the RLF; still, for sufficiently large orbital radius, the sum of modes always falls short, as beaming intensifies and more and more modes would have to be included. Nevertheless, it seems that for finite orbital radius, a finite number of modes is enough to account for the energy lost by the particle.

In regards to the importance of the tail term in the strong field regime: we had seen that for PC orbits, neglecting the tail predicts that the particle will always gain energy in PC orbits outside the light ring ($r_0 > 3M$). Our analytical and numerical results clearly state that this is not true, so we conclude that neglecting the tail is never a valid method to study radiation reaction in PC orbits. As for the MC orbits, what we found is compatible with the results we had obtained in the Newtonian limit: neglecting the tail is only valid in the "Magnetic region", which is dominated by magnetic effects and so the curvature can be neglected there; indeed, neglecting the tail is a very good approximation in this region, because it describes the radiation reaction due to the external force, which in this case is the dominant force. Thus, when it comes to using the DeWitt–Brehme equation of motion, we can say with confidence that: *To adequately describe the dynamics of a radiating pointlike charge in a vacuum spacetime, the tail term must be included, unless radiation reaction is neglected altogether, or the spacetime curvature can be ignored, in which case a flat space description of radiation, based on the Abraham-Lorentz-Dirac equation, is sufficient.*

With all of this, we believe to have successfully completed the task at hand, not only clearing up a confusion in the literature but also giving a detailed account of the phenomenon of radiation reaction in magnetized BHs. Before ending, we want to point out important possibilities for future work: first, it is well known that radiation reaction in curved space is not purely dissipative, but also contains a conservative counterpart, which we left out of our analysis; including it would be interesting, as it could provide interesting changes to the velocity profiles. Second, it would also be interesting to see if these orbits are stable to small eccentric perturbations, performing an analysis akin to that in Ref. [117]. Finally, it would also be of great importance to generalize the results to the rotating Kerr BH case, as superradiance and other energy extraction mechanisms could produce very interesting dynamics in the presence of magnetic fields. The last point is the subject of ongoing work.

# Bibliography


[1] A. Einstein, “Zur Allgemeinen Relativitätstheorie”, *Sitzungsber. Preuss. Akad. Wiss. Berlin (Math. Phys. )* **1915**, *1915*, [Addendum: Sitzungsber.Preuss.Akad.Wiss.Berlin (Math.Phys.) 1915, 799–801 (1915)], 778–786.

[2] B. P. Abbott et al., “Observation of Gravitational Waves from a Binary Black Hole Merger”, *Phys. Rev. Lett.* **2016**, *116*, 061102.

[3] B. P. Abbott et al., “GW150914: First results from the search for binary black hole coalescence with Advanced LIGO”, *Phys. Rev. D* **2016**, *93*, 122003.

[4] K. Schwarzschild, “On the gravitational field of a mass point according to Einstein’s theory”, *Sitzungsber. Preuss. Akad. Wiss. Berlin (Math. Phys. )* **1916**, *1916*, 189–196.

[5] J. R. Oppenheimer, H. Snyder, “On Continued Gravitational Contraction”, *Phys. Rev.* **1939**, *56*, 455–459.

[6] R. Penrose, “Gravitational collapse and space-time singularities”, *Phys. Rev. Lett.* **1965**, *14*, 57–59.

[7] S. Hawking, “The occurrence of singularities in cosmology. III. Causality and singularities”, *Proc. Roy. Soc. Lond. A* **1967**, *300*, 187–201.

[8] S. W. Hawking, R. Penrose, “The Singularities of gravitational collapse and cosmology”, *Proc. Roy. Soc. Lond. A* **1970**, *314*, 529–548.

[9] R. Ruffini, *Black Holes: les Astres Occlus*, Gordon and Breach Science Publishers, New York, **1973**.

[10] R. P. Kerr, “Gravitational Field of a Spinning Mass as an Example of Algebraically Special Metrics”, *Phys. Rev. Lett.* **1963**, *11*, 237–238.

[11] R. Penrose, “Gravitational collapse: The role of general relativity”, *Riv. Nuovo Cim.* **1969**, *1*, 252–276.

[12] R. Ruffini, J. R. Wilson, “Relativistic magnetohydrodynamical effects of plasma accreting into a black hole”, *Phys. Rev. D* **1975**, *12*, 2959–2962.

[13] R. D. Blandford, R. L. Znajek, “Electromagnetic extraction of energy from Kerr black holes.”, *Monthly Notices of the Royal Astronomical Society* **1977**, *179*, 433–456.

[14] R. Brito, V. Cardoso, P. Pani, "Superradiance: New Frontiers in Black Hole Physics", *Lect. Notes Phys.* **2015**, *906*, pp.1–237.

[15] J. a. R. T. de Mello Neto, "Physics and Astrophysics of Ultra-High Energy Cosmic Rays: Recent Results from the Pierre Auger Observatory", *Phys. Part. Nucl.* **2022**, *53*, 224–232.

[16] Y. Tsunesada et al. in Proceedings of 37th International Cosmic Ray Conference — PoS(ICRC2021), *Vol. 395*, **2021**, p. 337.

[17] R. Abbasi et al., "Joint analysis of the energy spectrum of ultra-high-energy cosmic rays as measured at the Pierre Auger Observatory and the Telescope Array", *PoS* **2021**, *ICRC2021*, 337.

[18] M. Kachelriess, "Extragalactic cosmic rays", *PoS* **2022**, *ICRC2021*, 018.

[19] R. M. Wald, "Energy Limits on the Penrose Process", *The Astrophysical Journal* **1974**, *191*, 231–234.

[20] J. M. Bardeen, W. H. Press, S. A. Teukolsky, "Rotating black holes: Locally nonrotating frames, energy extraction, and scalar synchrotron radiation", *Astrophys. J.* **1972**, *178*, 347.

[21] T. Piran, J. Shaham, J. Katz, "High Efficiency of the Penrose Mechanism for Particle Collisions", *The Astrophysical Journal* **1975**, *196*, L107.

[22] T. Piran, J. Shaham, "Upper bounds on collisional Penrose processes near rotating black-hole horizons", *Phys. Rev. D* **1977**, *16*, 1615–1635.

[23] J. D. Schnittman, "Revised Upper Limit to Energy Extraction from a Kerr Black Hole", *Phys. Rev. Lett.* **2014**, *113*, 261102.

[24] E. Berti, R. Brito, V. Cardoso, "Ultrahigh-Energy Debris from the Collisional Penrose Process", *Phys. Rev. Lett.* **2015**, *114*, 251103.

[25] S. M. Wagh, S. V. Dhurandhar, N. Dadhich, "Revival of the Penrose Process for Astrophysical Applications", *The Astrophysical Journal* **1985**, *290*, 12.

[26] S. M. Wagh, S. V. Dhurandhar, N. Dadhich, "Revival of the Penrose Process for Astrophysical Applications: Erratum", *The Astrophysical Journal* **1986**, *301*, 1018.

[27] S. Parthasarathy, S. M. Wagh, S. V. Dhurandhar, N. Dadhich, "High Efficiency of the Penrose Process of Energy Extraction from Rotating Black Holes Immersed in Electromagnetic Fields", *The Astrophysical Journal* **1986**, *307*, 38.

[28] A. Tursunov, N. Dadhich, "Fifty years of energy extraction from rotating black hole: revisiting magnetic Penrose process", *Universe* **2019**, *5*, 125.

[29] M. Kološ, A. Tursunov, Z. Stuchlík, "Radiative Penrose process: Energy Gain by a Single Radiating Charged Particle in the Ergosphere of Rotating Black Hole", *Phys. Rev. D* **2021**, *103*, 024021.

[30] Z. Stuchlík, M. Kološ, A. Tursunov, "Penrose Process: Its Variants and Astrophysical Applications", *Universe* **2021**, *7*, 416.

[31] A. Tursunov, Z. Stuchlík, M. Kološ, N. Dadhich, B. Ahmedov, "Supermassive Black Holes as Possible Sources of Ultrahigh-energy Cosmic Rays", *Astrophys. J.* **2020**, *895*, 14.

[32] K. Gupta, Y. T. A. Law, J. Levin, "Penrose process for a charged black hole in a uniform magnetic field", *Phys. Rev. D* **2021**, *104*, 084059.

[33] C. Dyson, D. Pereñiguez, "Magnetic Black Holes: from Thomson Dipoles to the Penrose Process and Cosmic Censorship", **2023**.

[34] J. A. Rueda, R. Ruffini, "Extracting the energy and angular momentum of a Kerr black hole", **2023**.

[35] M. Y. Piotrovich, N. A. Silant'ev, Y. N. Gnedin, T. M. Natsvlishvili, "Magnetic fields and quasi-periodic oscillations of black hole radiation", *Astrophysical Bulletin* **2011**, *66*, 320–324.

[36] R. P. Eatough et al., "A strong magnetic field around the supermassive black hole at the centre of the Galaxy", *Nature* **2013**, *501*, 391–394.

[37] A. K. Baczko et al., "A Highly Magnetized Twin-Jet Base Pinpoints a Supermassive Black Hole", *Astron. Astrophys.* **2016**, *593*, A47.

[38] R. A. Daly, "Black Hole Spin and Accretion Disk Magnetic Field Strength Estimates for more than 750 AGN and Multiple GBH", *Astrophys. J.* **2019**, *886*, 37.

[39] M. Abraham, "Prinzipien der Dynamik des Elektrons", *Annalen der Physik* **1902**, *315*, 105–179.

[40] P. A. M. Dirac, "Classical theory of radiating electrons", *Proc. Roy. Soc. Lond. A* **1938**, *167*, 148–169.

[41] E. Poisson, "An Introduction to the Lorentz-Dirac equation", **1999**.

[42] J. D. Jackson, *Classical Electrodynamics*, Wiley, **1998**.

[43] V. P. Frolov, A. A. Shoom, "Motion of charged particles near weakly magnetized Schwarzschild black hole", *Phys. Rev. D* **2010**, *82*, 084034.

[44] V. P. Frolov, "Weakly magnetized black holes as particle accelerators", *Phys. Rev. D* **2012**, *85*, 024020.

[45] A. M. A. Zahrani, V. P. Frolov, A. A. Shoom, "Critical escape velocity for a charged particle moving around a weakly magnetized Schwarzschild black hole", *Phys. Rev. D* **2013**, *87*, 084043.

[46] M. Kološ, Z. Stuchlík, A. Tursunov, "Quasi-harmonic oscillatory motion of charged particles around a Schwarzschild black hole immersed in a uniform magnetic field", *Class. Quant. Grav.* **2015**, *32*, 165009.

[47] N. P. Baker, V. P. Frolov, "Charged Particle Motion Near a Magnetized Black Hole: A Near-Horizon Approximation", **2023**.

[48] F. Abdulxamidov, J. Rayimbaev, A. Abdujabbarov, Z. Stuchlík, "Spinning magnetized particles orbiting magnetized Schwarzschild black holes", *Phys. Rev. D* **2023**, *108*, 044030.

[49] M. Qi, J. Rayimbaev, B. Ahmedov, "Charged particles and quasiperiodic oscillations around magnetized Schwarzschild black holes", *Eur. Phys. J. C* **2023**, *83*, 730.

[50] A. N. Aliev, D. V. Galtsov, "Magnetized Black Holes", *Sov. Phys. Usp.* **1989**, *32*, 75.

[51] A. N. Aliev, N. Ozdemir, "Motion of charged particles around a rotating black hole in a magnetic field", *Mon. Not. Roy. Astron. Soc.* **2002**, *336*, 241–248.

[52] A. Tursunov, M. Kološ, Z. Stuchlík, "Orbital widening due to radiation reaction around a magnetized black hole", *Astron. Nachr.* **2018**, *339*, 341–346.

[53] A. Tursunov, M. Kološ, Z. Stuchlík, D. V. Gal'tsov, "Radiation Reaction of Charged Particles Orbiting a Magnetized Schwarzschild Black Hole", *The Astrophysical Journal* **2018**, *861*, 2.

[54] J. S. Santos, V. Cardoso, J. Natário, "Electromagnetic radiation reaction and energy extraction from black holes: The tail term cannot be ignored", *Phys. Rev. D* **2023**, *107*, 064046.

[55] B. S. DeWitt, R. W. Brehme, "Radiation damping in a gravitational field", *Annals of Physics* **1960**, *9*, 220–259.

[56] J. Hobbs, "A vierbein formalism of radiation damping", *Annals of Physics* **1968**, *47*, 141–165.

[57] A. G. Smith, C. M. Will, "FORCE ON A STATIC CHARGE OUTSIDE A SCHWARZSCHILD BLACK HOLE", *Phys. Rev. D* **1980**, *22*, 1276–1284.

[58] T. C. Quinn, R. M. Wald, "An Axiomatic approach to electromagnetic and gravitational radiation reaction of particles in curved space-time", *Phys. Rev. D* **1997**, *56*, 3381–3394.

[59] E. Poisson, A. Pound, I. Vega, "The Motion of point particles in curved spacetime", *Living Rev. Rel.* **2011**, *14*, 7.

[60] D. V. Galtsov, V. I. Petukhov, "Black Hole in an External Magnetic Field", *Zh. Eksp. Teor. Fiz.* **1978**, *74*, 801–818.

[61] L. Barack, A. Pound, "Self-force and radiation reaction in general relativity", *Rept. Prog. Phys.* **2019**, *82*, 016904.

[62] C. M. DeWitt, B. S. DeWitt, "Falling charges", *Physics Physique Fizika* **1964**, *1*, [Erratum: Physics Physique Fizika 1, 145 (1964)], 3–20.

[63] M. J. Pfenning, E. Poisson, "Scalar, electromagnetic, and gravitational selfforces in weakly curved space-times", *Phys. Rev. D* **2002**, *65*, 084001.

[64] B. Wardell, C. R. Galley, A. Zenginoğlu, M. Casals, S. R. Dolan, A. C. Ottewill, "Self-force via Green functions and worldline integration", *Phys. Rev. D* **2014**, *89*, 084021.

[65] T. Regge, J. A. Wheeler, "Stability of a Schwarzschild singularity", *Phys. Rev.* **1957**, *108*, 1063–1069.

[66] F. J. Zerilli, "Effective potential for even parity Regge-Wheeler gravitational perturbation equations", *Phys. Rev. Lett.* **1970**, *24*, 737–738.

[67] S. A. Teukolsky, "Rotating black holes - separable wave equations for gravitational and electromagnetic perturbations", *Phys. Rev. Lett.* **1972**, *29*, 1114–1118.

[68] S. A. Teukolsky, "Perturbations of a rotating black hole. 1. Fundamental equations for gravitational electromagnetic and neutrino field perturbations", *Astrophys. J.* **1973**, *185*, 635–647.

[69] J. M. Bardeen, W. H. Press, "Radiation fields in the schwarzschild background", *J. Math. Phys.* **1973**, *14*, 7–19.

[70] S. Chandrasekhar, "On the equations governing the perturbations of the Schwarzschild black hole", *Proc. Roy. Soc. Lond. A* **1975**, *343*, 289–298.

[71] S. A. Teukolsky, W. H. Press, "Perturbations of a rotating black hole. III - Interaction of the hole with gravitational and electromagnet ic radiation", *Astrophys. J.* **1974**, *193*, 443–461.

[72] V. Cardoso, S. Chakrabarti, P. Pani, E. Berti, L. Gualtieri, "Floating and sinking: The Imprint of massive scalars around rotating black holes", *Phys. Rev. Lett.* **2011**, *107*, 241101.

[73] S. L. Detweiler, "Black Holes and Gravitational Waves. I. Circular Orbits About a Rotating Hole", *Astrophys. J.* **1978**, *225*, 687–693.

[74] M. Sasaki, T. Nakamura, "Gravitational Radiation From a Kerr Black Hole. 1. Formulation and a Method for Numerical Analysis", *Prog. Theor. Phys.* **1982**, *67*, 1788.

[75] N. Yunes, P. Pani, V. Cardoso, "Gravitational Waves from Quasicircular Extreme Mass-Ratio Inspirals as Probes of Scalar-Tensor Theories", *Phys. Rev. D* **2012**, *85*, 102003.

[76] T. Torres, S. R. Dolan, "Electromagnetic self-force on a charged particle on Kerr spacetime: Equatorial circular orbits", *Phys. Rev. D* **2022**, *106*, 024024.

[77] M. Davis, R. Ruffini, W. H. Press, R. H. Price, "Gravitational radiation from a particle falling radially into a schwarzschild black hole", *Phys. Rev. Lett.* **1971**, *27*, 1466–1469.

[78] M. Davis, R. Ruffini, J. Tiomno, F. Zerilli, "Can synchrotron gravitational radiation exist?", *Phys. Rev. Lett.* **1972**, *28*, 1352–1355.

[79] R. A. Breuer, P. L. Chrzanowksi, H. G. Hughes, C. W. Misner, "Geodesic synchrotron radiation", *Phys. Rev. D* **1973**, *8*, 4309–4319.

[80] C. Cutler, E. Poisson, G. J. Sussman, L. S. Finn, "Gravitational radiation from a particle in circular orbit around a black hole. 2: Numerical results for the nonrotating case", *Phys. Rev. D* **1993**, *47*, 1511–1518.

[81] E. Poisson, "Gravitational radiation from a particle in circular orbit around a black hole. 1: Analytical results for the nonrotating case", *Phys. Rev. D* **1993**, *47*, 1497–1510.

[82] E. Poisson, M. Sasaki, "Gravitational radiation from a particle in circular orbit around a black hole. 5: Black hole absorption and tail corrections", *Phys. Rev. D* **1995**, *51*, 5753–5767.

[83] V. Cardoso, A. del Rio, M. Kimura, "Distinguishing black holes from horizonless objects through the excitation of resonances during inspiral", *Phys. Rev. D* **2019**, *100*, [Erratum: Phys.Rev.D 101, 069902 (2020)], 084046.

[84] H. O. Silva, G. Tambalo, K. Glampedakis, K. Yagi, "Gravitational radiation from a particle plunging into a Schwarzschild black hole: frequency-domain and semi-relativistic analyses", **2023**.

[85] R. A. Breuer, R. Ruffini, J. Tiomno, C. V. Vishveshwara, "Vector and tensor radiation from schwarzschild relativistic circular geodesics", *Phys. Rev. D* **1973**, *7*, 1002–1007.

[86] R. Ruffini, J. Tiomno, C. V. Vishveshwara, "Electromagnetic field of a particle moving in a spherically symmetric black-hole background", *Lett. Nuovo Cim.* **1972**, *3S2*, 211–215.

[87] D. V. Gal'tsov, "Radiation reaction in the Kerr gravitational field", *J. Phys. A* **1982**, *15*, 3737–3749.

[88] A. A Sokolov, D. V. Galtsov, V. I. Petukhov, "Radiation Emitted by Relativistic Particles Moving in the Vicinity of the Schwarzschild Black Hole, Immersed in an External Magnetic Field", *Phys. Lett. A* **1978**, *68*, 1–2.

[89] A. N. Aliev, D. V. Galtsov, "Radiation from relativistic particle in nongeodesic motion in a strong gravitational field", *Gen. Rel. Grav.* **1981**, *13*, 899–912.

[90] A. N. Aliev, D. V. Galtsov, V. I. Petrukhov, "Negative absorption near a magnetized black hole: Black hole masers", *Astrophys. Space Sci.* **1986**, *124*, 137.

[91] R. P. Geroch, J. H. Traschen, "Strings and Other Distributional Sources in General Relativity", *Conf. Proc. C* **1986**, *861214*, (Ed.: M. P. Ulmer), 138–141.

[92] S. E. Gralla, A. I. Harte, R. M. Wald, "A Rigorous Derivation of Electromagnetic Self-force", *Phys. Rev. D* **2009**, *80*, 024031.

[93] C. J. Eliezer, R. E. Peierls, "On the classical theory of particles", *Proceedings of the Royal Society of London. Series A. Mathematical and Physical Sciences* **1948**, *194*, 543–555.

[94] L. D. Landau, E. M. Lifschits, *The Classical Theory of Fields*, Pergamon Press, Oxford, **1975**.

[95] H. Spohn, "The Critical manifold of the Lorentz-Dirac equation", *EPL* **2000**, *50*, 287–292.

[96] F. Rohrlich, "The correct equation of motion of a classical point charge", *Physics Letters A* **2001**, *283*, 276–278.

[97] G. D. Birkhoff, R. E. Langer, *Relativity and modern physics*, **1923**.

[98] S. W. Hawking, G. F. R. Ellis, *The Large Scale Structure of Space-Time*, Cambridge University Press, **2023**.

[99] R. M. Wald, *General Relativity*, Chicago Univ. Pr., Chicago, USA, **1984**.

[100] R. M. Wald, "Black hole in a uniform magnetic field", *Phys. Rev. D* **1974**, *10*, 1680–1685.

[101] J. R. Ipser, "Electromagnetic Test Fields Around a Kerr-Metric Black Hole", *Phys. Rev. Lett.* **1971**, *27*, 529–531.

[102] E. E. Flanagan, R. M. Wald, "Does back reaction enforce the averaged null energy condition in semiclassical gravity?", *Phys. Rev. D* **1996**, *54*, 6233–6283.

[103] C. V. Vishveshwara, PhD thesis, Maryland U., **1968**.

[104] F. J. Zerilli, "Gravitational field of a particle falling in a schwarzschild geometry analyzed in tensor harmonics", *Phys. Rev. D* **1970**, *2*, 2141–2160.

[105] J. Mathews, "Gravitational Multipole Radiation", *Journal of the Society for Industrial and Applied Mathematics* **1962**, *10*, 768–780.

[106] C. A. Clarkson, R. K. Barrett, "Covariant perturbations of Schwarzschild black holes", *Class. Quant. Grav.* **2003**, *20*, 3855–3884.

[107] K. Martel, E. Poisson, "Gravitational perturbations of the Schwarzschild spacetime: A Practical covariant and gauge-invariant formalism", *Phys. Rev. D* **2005**, *71*, 104003.

[108] L. Barack, C. O. Lousto, "Perturbations of Schwarzschild black holes in the Lorenz gauge: Formulation and numerical implementation", *Phys. Rev. D* **2005**, *72*, 104026.

[109] J. D. Bekenstein, "Extraction of energy and charge from a black hole", *Phys. Rev. D* **1973**, *7*, 949–953.

[110] E. Newman, R. Penrose, "An Approach to Gravitational Radiation by a Method of Spin Coefficients", *Journal of Mathematical Physics* **1962**, *3*, 566–578.

[111] A. Z. Petrov, "The Classification of spaces defining gravitational fields", *Gen. Rel. Grav.* **2000**, *32*, 1661–1663.

[112] V. Pravda, "On the algebraic classification of spacetimes", *J. Phys. Conf. Ser.* **2006**, *33*, (Eds.: M. Cadoni, M. Cavaglia, J. E. Nelson), 463–468.

[113] W. Kinnersley, "Type D Vacuum Metrics", *J. Math. Phys.* **1969**, *10*, 1195–1203.

[114] J. N. Goldberg, A. J. Macfarlane, E. T. Newman, F. Rohrlich, E. C. G. Sudarshan, "Spin-s Spherical Harmonics and "edth"", *Journal of Mathematical Physics* **1967**, *8*, 2155–2161.

[115] S. W. Hawking, J. B. Hartle, "Energy and angular momentum flow into a black hole", *Commun. Math. Phys.* **1972**, *27*, 283–290.

[116] V. Cardoso, M. Cavaglia, J.-Q. Guo, "Gravitational Larmor formula in higher dimensions", *Phys. Rev. D* **2007**, *75*, 084020.

[117] T. Apostolatos, D. Kennefick, E. Poisson, A. Ori, "Gravitational radiation from a particle in circular orbit around a black hole. 3: Stability of circular orbits under radiation reaction", *Phys. Rev. D* **1993**, *47*, 5376–5388.

[118] D. N. Page, "Particle Emission Rates from a Black Hole: Massless Particles from an Uncharged, Nonrotating Hole", *Phys. Rev. D* **1976**, *13*, 198–206.

[119] A. A. Starobinskil, S. M. Churilov, "Amplification of electromagnetic and gravitational waves scattered by a rotating "black hole"", *Sov. Phys. JETP* **1974**, *65*, 1–5.

[120] E. W. Leaver, "Solutions to a generalized spheroidal wave equation: Teukolsky's equations in general relativity, and the two-center problem in molecular quantum mechanics", *Journal of Mathematical Physics* **1986**, *27*, 1238–1265.

[121] S. Mano, H. Suzuki, E. Takasugi, "Analytic solutions of the Teukolsky equation and their low frequency expansions", *Prog. Theor. Phys.* **1996**, *95*, 1079–1096.

# Appendix A

# Killing vector fields, conserved quantities and electromagnetic fields

Consider a charged particle with charge $q$, mass $m$, and 4-velocity $u^\mu$, moving in a generic spacetime with metric tensor $g_{\mu\nu}$. We can define a Killing vector field as a generator of a continuous symmetry (isometry) of the manifold, that is: $\xi^\mu$ is a Killing vector field if and only if

$$\mathcal{L}_\xi g_{\mu\nu} = 0 \iff \nabla_\mu \xi_\nu + \nabla_\nu \xi_\mu = 0\,, \tag{A.1}$$

where $\mathcal{L}_\xi$ is the Lie derivative along $\xi$, and $\nabla_\mu$ is the Levi-Civita connection; Eq. (A.1) is called the Killing equation.

The Minkowski solution is a very symmetric solution and it possesses 10 linearly independent Killing vectors, corresponding to the generators of the Poincaré algebra. The Schwarzschild solution is still stationary and spherically symmetric, so it contains only 4 linearly independent Killing vectors. Killing vectors are particularly important as a result of Noether's theorem, which ties the existence of continuous symmetry in a system with the existence of a conserved quantity.

Take a particle of mass $m$ free falling under the action of the gravitational field of a Schwarzschild BH. The particle's equation of motion is just the geodesic equation

$$\frac{Du^\mu}{d\tau} = 0\,, \tag{A.2}$$

where $\tau$ is the proper time and $D/d\tau \equiv u^\mu \nabla_\mu$ is the covariant derivative along the velocity of the particle. It is easy to show, using Eqs. (A.1) and (A.2), that

$$\frac{D}{d\tau}\left(u_\alpha \xi^\alpha\right) = 0\,, \tag{A.3}$$

meaning that each Killing vector is associated with a conserved quantity, $u_\alpha \xi^\alpha$, along the motion of the particle. For example, in Minkowski spacetime, time translations are associated with energy, spatial translations with linear momentum, rotations with angular momentum, and boosts with the position at

$t = 0$.

Now we want to consider the case where the charged particle is under the action of an EM field $F_{\mu\nu}$, associated with a 4-vector potential $A_\mu$ such that

$$F_{\mu\nu} = \nabla_\mu A_\nu - \nabla_\nu A_\mu \,. \tag{A.4}$$

In this case, the particle no longer follows a geodesic; instead, the equation of motion becomes

$$\frac{Du^\mu}{d\tau} = \frac{q}{m} F^\mu_{\ \nu} u^\nu \,. \tag{A.5}$$

Consequently, the quantities defined in Eq. (A.3) are no longer conserved along the particle trajectory:

$$\begin{aligned} \frac{D}{d\tau}\left(u_\alpha \xi^\alpha\right) &= \xi_\alpha u^\beta \nabla_\beta u^\alpha + u^\beta u^\alpha \nabla_\beta \xi_\alpha \\ &= \frac{q}{m} F^{\alpha\beta} \xi_\alpha u_\beta \,. \end{aligned} \tag{A.6}$$

This is because the conserved quantities associated with a Killing vector are altered as a result of the minimal coupling between the charge and the EM field, according to which we should replace the previously defined $u_\alpha \xi^\alpha$ with

$$u_\alpha \xi^\alpha \to \left(u_\alpha + \frac{q}{m} A_\alpha\right) \xi^\alpha \,. \tag{A.7}$$

If we look at how these quantities vary along the particle's trajectory, we find

$$\begin{aligned} \frac{D}{d\tau}\left(\left(u_\alpha + \frac{q}{m} A_\alpha\right) \xi^\alpha\right) &= \frac{q}{m}\left(F^{\alpha\beta} \xi_\alpha u_\beta + \xi^\alpha u^\beta \nabla_\beta A_\alpha + A^\alpha u^\beta \nabla_\beta \xi_\alpha\right) \\ &= \frac{q}{m} u^\beta \left[A \,,\, \xi\right]_\beta \end{aligned} \tag{A.8}$$

where $[\cdot, \cdot]$ is the commutator of two vector fields. Thus, in the presence of EM fields, conserved quantities may still be defined by Killing vector fields as long as these commute with the EM 4-vector potential. This means, for example, that the energy measured by a stationary observer in flat space, as given by (A.7) with $\xi^\alpha = \delta^\alpha_t$, is conserved if the vector potential is stationary in that observer's reference frame, that is, if $[A \,,\, \xi] = 0$.

# Appendix B

# Radiation reaction in flat space

The radiation reaction force in flat space can be obtained directly from the expression for the Liénard-Wiechert potentials. We start with the wave equation with a source for the EM 4-potential $A_\mu$,

$$\Box A_\mu = \frac{1}{c} J_\mu, \tag{B.1}$$

where $\Box = \partial_\mu \partial^\mu$ and $J_\mu$ is the 4-current. The solution to this equation is the Liénard-Wiechert potential

$$A_\mu(x) = \frac{4\pi}{c} \int d^4x' D_{\text{ret}}\left(x - x'\right) J_\mu\left(x'\right), \tag{B.2}$$

$$D_{\text{ret}}\left(x - x'\right) = \frac{1}{2\pi} \theta(x_0 - x_0') \delta\left((x - x')^2\right), \tag{B.3}$$

where $D_{\text{ret}}\left(x - x'\right)$ is the retarded Green's function solution to (B.1). For a single charged particle of charge $q$, trajectory $z(\tau)$ and 4-velocity $u^\mu(\tau) = dz^\mu/d\tau$, where $\tau$ is the proper time, the 4-current may be written as

$$J^\mu(x) = qc \int d\tau\, u^\mu(\tau)\, \delta^4\left(x - z(\tau)\right). \tag{B.4}$$

Now once all this is replaced in (B.2), together with the expression for the retarded Green's function [42], we finally obtain the expression for the 4-potential generated by a moving charged particle:

$$A_\mu(x) = \frac{q\, u_\mu(\tau_0)}{|u_\alpha(\tau_0)(x - z(\tau_0))^\alpha|}, \tag{B.5}$$

where $\tau_0$ is the proper time for which the radiating charged particle lies in the past light cone of $x$. As for the EM fields, we get

$$F_{\mu\nu}(x) = \partial_\mu A_\nu - \partial_\nu A_\mu = \frac{q}{u_\alpha(x - z(\tau_0))^\alpha} \frac{d}{d\tau} \left[ \frac{(x - z(\tau))_\mu u_\nu - (x - z(\tau))_\nu u_\mu}{u_\beta(x - z(\tau))^\beta} \right]_{\tau=\tau_0}, \tag{B.6}$$

which yields electric and magnetic fields given by

$$\begin{aligned}\boldsymbol{E}(t,\boldsymbol{x}) &= q\left[\frac{\boldsymbol{n}-\boldsymbol{\beta}}{\gamma^2(1-\boldsymbol{\beta}\cdot\boldsymbol{n})^3 r^2}\right]_{\text{ret}} + \frac{q}{c}\left[\frac{\boldsymbol{n}\times\left((\boldsymbol{n}-\boldsymbol{\beta})\times\dot{\boldsymbol{\beta}}\right)}{(1-\boldsymbol{\beta}\cdot\boldsymbol{n})^3 r}\right]_{\text{ret}}, \\ \boldsymbol{B}(t,\boldsymbol{x}) &= \frac{1}{r}(\boldsymbol{r}\times\boldsymbol{E}),\end{aligned} \tag{B.7}$$

where $\boldsymbol{r} = \boldsymbol{x} - \boldsymbol{x}'$, for $\boldsymbol{x}'$ the position of the source charge, and the subscript serves to indicate that all quantities are to be calculated at a retarded time, which is, in the frame of reference of a static observer, $t' = t - r/c$. Moreover, $\boldsymbol{\beta}$ is the 3-velocity and $\gamma = (1-\beta^2)^{-1/2}$.

The first term on the RHS of Eq. (B.7) depends only on the particle's velocity and it is a static field, which reduces to Coulomb's law for stationary charges. Contrary to this, the second is an acceleration field which gives the radiation of EM waves.

## B.1 Larmor formula

We can find the power radiated away in EM waves from the radiation term. In a non-relativistic scenario, $\beta \ll 1$, we simply get the Larmor formula

$$\frac{dE}{dt} = \frac{2}{3}q^2\dot{\beta}^2. \tag{B.8}$$

We now seek to find a relativistic generalization of this formula. Since the energy transforms like the first component of a 4-vector, the radiated power must be a Lorentz invariant quantity. Furthermore, since $\boldsymbol{E}$ and $\boldsymbol{B}$ depend only on $\boldsymbol{\beta}$ and $\dot{\boldsymbol{\beta}}$, the most obvious way to obtain a relativistic power formula is

$$\begin{aligned}\frac{dE}{dt} &= \frac{2}{3}q^2\frac{du_\alpha}{d\tau}\frac{du^\alpha}{d\tau} \\ &= \frac{2}{3}q^2\gamma^6\left(\dot{\beta}^2 - \left(\boldsymbol{\beta}\times\dot{\boldsymbol{\beta}}\right)^2\right),\end{aligned} \tag{B.9}$$

which naturally reduces to the Larmor formula if we take the nonrelativistic limit $\beta \ll 1$.

## B.2 Radiation reaction force

To obtain the radiation reaction force, we must perform the calculation of how much energy is lost through radiation by a moving charged particle. This energy will then be associated with the work $W$ done by a

new force, the radiation reaction force $\boldsymbol{F}_{\text{rad}}$. In the non-relativistic limit, we get

$$\begin{aligned}
&\frac{dW}{dt} = -P(t) \iff \\
&\int_{t_1}^{t_2} \boldsymbol{F}_{\text{rad}} \cdot \boldsymbol{\beta}\, dt = -\int_{t_1}^{t_2} P(t)\, dt \iff \\
&\int_{t_1}^{t_2} \boldsymbol{F}_{\text{rad}} \cdot \boldsymbol{\beta}\, dt = -\int_{t_1}^{t_2} \frac{2q^2}{3} \dot{\boldsymbol{\beta}} \cdot \dot{\boldsymbol{\beta}}\, dt \iff \\
&\int_{t_1}^{t_2} \boldsymbol{F}_{\text{rad}} \cdot \boldsymbol{\beta}\, dt = \int_{t_1}^{t_2} \frac{2q^2}{3} \ddot{\boldsymbol{\beta}} \cdot \boldsymbol{\beta}\, dt - \left[\frac{2q^2}{3} \dot{\boldsymbol{\beta}} \cdot \boldsymbol{\beta}\right]_{t_1}^{t_2} \iff \\
&\int_{t_1}^{t_2} \left(\boldsymbol{F}_{\text{rad}} - \frac{2q^2}{3} \ddot{\boldsymbol{\beta}}\right) \cdot \boldsymbol{\beta}\, dt = 0,
\end{aligned} \tag{B.10}$$

where we have used integration by parts and assumed the motion is such that, on average, $\dot{\boldsymbol{\beta}} \cdot \boldsymbol{\beta} \approx 0$. Since $t_1$ and $t_2$ are arbitrary, we conclude

$$\boldsymbol{F}_{\text{rad}} = \frac{2q^2}{3} \ddot{\boldsymbol{\beta}}. \tag{B.11}$$

Once again we face the problem of obtaining a relativistic generalization of the previous formula, one that would give $f_R^\mu$ in the general equation of motion of a relativistic charged particle under the influence of an EM field:

$$\frac{Du^\mu}{d\tau} = f_L^\mu + f_R^\mu, \qquad f_L^\mu = F^{\mu\nu} u_\nu \,. \tag{B.12}$$

The obvious choice for this generalization is simply

$$f_R^\mu = \frac{2q^2}{3m} \frac{D^2 u^\mu}{d\tau^2} \,; \tag{B.13}$$

however, in relativistic scenarios, we must ensure that $f_\alpha u^\alpha = 0$, so that $\frac{d}{d\tau}(u_\alpha u^\alpha) = 0$. This forces us to include a nonlinear term in the formula, which now becomes

$$f_R^\mu = \frac{2q^2}{3m} \left[\frac{D^2 u^\mu}{d\tau^2} + u^\mu u_\alpha \frac{D^2 u^\alpha}{d\tau}\right]. \tag{B.14}$$

If we replace this in Eq. (B.12) we get a third order differential equation, which is famously plagued with runaway solutions. We go over this issue in more detail in the body of the text, but the idea for solving this problem is to perform an order reduction by taking $\frac{D^2 u^\mu}{d\tau^2} = \frac{D f_L^\mu}{d\tau}$ in the RHS of Eq. (B.14), yielding

$$f_R^\mu = \frac{2q^3}{3m^2} \left(\nabla_\alpha F^{\mu\nu} u^\alpha u_\nu\right) + \frac{2q^3}{3m^2} \left(\frac{q}{m} \left(F^{\mu\nu} F_{\nu\rho} + F^{\nu\alpha} F_{\alpha\rho} u_\nu u^\mu\right) u^\rho\right) . \tag{B.15}$$

# Appendix C

# Replacing the black hole by a static electric charge

Here we give a brief demonstration of how the particle ceases to gain energy spontaneously when we replace the BH with a static electric charge at the origin (in the Newtonian limit). Note that, besides the static electric charge and the electric field it produces, we also consider a uniform magnetic field in the $\hat{z}$ direction, as we did in the BH case.

The equation of motion of a nonrelativistic radiating charged particle of mass $m$ and charge $q$, in the presence of an arbitrary electric field $\boldsymbol{E}$ and an arbitrary magnetic field $\boldsymbol{B}$ is, in Gaussian units [42],

$$\boldsymbol{a} = \frac{q}{m}(\boldsymbol{E} + \boldsymbol{v} \times \boldsymbol{B}) + \frac{2q^2}{3m}\,\dot{\boldsymbol{a}}, \tag{C.1}$$

where the last term corresponds to the radiation reaction force. By performing the same order reduction procedure as we did to obtain Eq. (2.15), we get

$$\boldsymbol{a} = \frac{q}{m}(\boldsymbol{E} + \boldsymbol{v} \times \boldsymbol{B}) + \frac{2q^3}{3m^2}\left(\dot{\boldsymbol{E}} + \boldsymbol{v} \times \dot{\boldsymbol{B}}\right) + \frac{2q^4}{3m^3}(\boldsymbol{E} + \boldsymbol{v} \times \boldsymbol{B}) \times \boldsymbol{B}\,. \tag{C.2}$$

Now consider the case where we take the electric field to be generated by an electric charge $-Q$ at the origin, with $Q > 0$ and $q > 0$, and where the magnetic field is $\boldsymbol{B} = B_0\hat{z}$. We want to look for circular orbits of radius $r_0$ and frequency $\Omega_0$ in this system. In this context, the two timescales in the problem are given by the Keplerian orbital frequency $\omega_{\mathsf{K}}$ and the cyclotron frequency $\omega_{\mathsf{c}}$, which in this case are given by

$$\omega_{\mathsf{K}} = \sqrt{\frac{qQ}{mr_0^3}}, \qquad \omega_{\mathsf{c}} = \frac{qB_0}{m}. \tag{C.3}$$

To find the circular orbits for this system, we start by writing

$$\boldsymbol{r} = r_0(\cos(\Omega_0 t), \sin(\Omega_0 t), 0), \tag{C.4}$$

$$\boldsymbol{v} = r_0\Omega_0(-\sin(\Omega_0 t), \cos(\Omega_0 t), 0), \tag{C.5}$$

$$\boldsymbol{a} = -\Omega_0^2 \boldsymbol{r}, \tag{C.6}$$

$$\frac{q}{m}\boldsymbol{E} = -\omega_{\mathsf{K}}^2 \boldsymbol{r}, \tag{C.7}$$

$$\frac{q}{m}\boldsymbol{v} \times \boldsymbol{B} = \Omega_0 \omega_{\mathsf{c}} \boldsymbol{r}. \tag{C.8}$$

Replacing this in (C.2) without the radiative terms we obtain the dispersion relation

$$\omega_0^2 + \omega_0\omega_{\mathsf{c}} - \omega_{\mathsf{K}}^2 = 0. \tag{C.9}$$

We are now in the position to evaluate the rate of energy loss for a radiating particle in a circular orbit:

$$\begin{aligned}
\frac{1}{m}\frac{dE}{dt} &= \frac{d}{dt}\left(\frac{1}{2}v^2 + \tilde{q}\frac{Q}{r}\right) \\
&= \frac{2q^2}{3m}\left(\tilde{q}\dot{\boldsymbol{E}} + \tilde{q}^2\left(\boldsymbol{E} + \boldsymbol{v} \times \boldsymbol{B}\right) \times \boldsymbol{B}\right) \cdot \boldsymbol{v} \\
&= \frac{2q^2}{3m}\left(-\omega_{\mathsf{K}}^2 \boldsymbol{v} + \frac{\omega_{\mathsf{K}}^2\omega_{\mathsf{c}}}{\Omega_0}\boldsymbol{v} - \omega_{\mathsf{c}}^2 \boldsymbol{v}\right) \cdot \boldsymbol{v} \\
&= -\frac{2q^2}{3m} r_0^2 \Omega_0^2 \left(\left(\Omega_0^2 + \Omega_0\omega_{\mathsf{c}}\right)\left(1 - \frac{\omega_{\mathsf{c}}}{\Omega_0}\right) + \omega_{\mathsf{c}}^2\right) \\
&= -\frac{2q^2}{3m} r_0^2 \Omega_0^4 < 0\,.
\end{aligned} \tag{C.10}$$

Thus we conclude that: *a radiating charged particle in a circular orbit around a static electric charge of opposite sign and under the influence of a magnetic field, perpendicular to the plane of motion, always loses energy*.

# Appendix D

# Radiation reaction in the Newtonian limit

Here we will use a simple calculation to establish that a charged particle in a circular orbit on a curved spacetime must radiate according to Larmor's power formula in the Newtonian limit. Let us consider the metric

$$g = e^{2\Phi}\eta = e^{2\Phi}\left(-dt^2 + dx^2 + dy^2 + dz^2\right), \tag{D.1}$$

$$\Phi = -\frac{M}{r}, \tag{D.2}$$

which has the correct Newtonian limit, since the action for timelike geodesics is

$$S = \int e^{\Phi}\sqrt{1 - \left(\frac{dx}{dt}\right)^2 - \left(\frac{dy}{dt}\right)^2 - \left(\frac{dz}{dt}\right)^2}\,dt \simeq \int \left(1 - \frac{1}{2}v^2 - \frac{M}{r}\right)dt\,. \tag{D.3}$$

We now consider a free-falling test particle of mass $m$ and charge $q$ in this metric and allow the particle to radiate, so the equation of motion is Eq. (2.75). Since the metric is conformal to the Minkowski metric, and the Maxwell equations are conformally invariant in $(3+1)$ dimensions, there will be no tail; since there is no external force, there will also be no Abraham-Lorentz Dirac term. However, as it is not a solution of the vacuum EFE, the Ricci tensor will not vanish. In fact, it is given by (see [99], appendix D)

$$R_{\mu\nu} = -2\partial_\mu\partial_\nu\Phi - \Box\Phi\,\eta_{\mu\nu} + 2\partial_\mu\Phi\partial_\nu\Phi - 2(\partial_\alpha\Phi\,\partial^\alpha\Phi)\eta_{\mu\nu}\,. \tag{D.4}$$

The radiation reaction force term corresponding to the Ricci tensor is

$$F^\alpha = \frac{q^2}{3}(g^{\alpha\mu} + u^\alpha u^\mu)R_{\mu\nu}u^\nu\,. \tag{D.5}$$

Because of the projector in the plane orthogonal to $u^\alpha$, we can drop all terms in $R_{\mu\nu}$ proportional to $\eta_{\mu\nu} = e^{-2\Phi}g_{\mu\nu}$. If we consider circular orbits, we will have $u^\nu\partial_\nu\Phi = 0$, and so the third term in $R_{\mu\nu}$ can

also be dropped. Therefore we obtain

$$F^\alpha = -\frac{2e^2}{3}(g^{\alpha\mu} + u^\alpha u^\mu)(\partial_\mu \partial_\nu \Phi) u^\nu \,, \tag{D.6}$$

and so, since $\Phi$ is time-independent,

$$F^0 = -\frac{2e^2}{3} u^0 u^\mu u^\nu (\partial_\mu \partial_\nu \Phi) \,. \tag{D.7}$$

Assuming that the circular orbit is on the plane $z = 0$, and also that the particle is momentarily at $(x, y) = (r_0, 0)$ in this plane, we have, for large $r_0$,

$$u \simeq \frac{\partial}{\partial t} + v \frac{\partial}{\partial y} \,, \qquad v = \sqrt{\frac{M}{r_0}} \,. \tag{D.8}$$

We then obtain

$$F^0 \simeq -\frac{2q^2}{3} v^2 \frac{\partial^2 \Phi}{\partial y^2} = -\frac{2q^2}{3} v^2 \frac{\partial}{\partial y}\left(\frac{My}{r_0^3}\right) = -\frac{2q^2}{3} v^2 \left(\frac{M}{r_0^3}\right) \tag{D.9}$$

(as $y = 0$). In other words,

$$F^0 = \frac{dE}{dt} \simeq -\frac{2q^2}{3}\frac{M^2}{r_0^4} = -\frac{2}{3} q^2 a^2 \,, \tag{D.10}$$

where $a$ is the Newtonian acceleration of the orbit, in accordance with Larmor's formula (in Gaussian units).

Thus even in curved spacetime, we find that a particle under the action of a gravitational field will radiate according to Larmor's formula when the Newtonian limit applies.

# Appendix E

# General solution to radial equation with a source

In this appendix, we present a general solution to the ODE obtained for the radial component of the Teukolsky equation, for Kerr spacetimes and fields with arbitrary spin. The solution reduces to the solution presented in [73] for the gravitational case. The equation in question is of the form

$$\Delta^{-s}\frac{d}{dr}\left(\Delta^{s+1}\frac{dR(r)}{dr}\right) - V(r)R(r) = -T(r)\,, \tag{E.1}$$

and we want to find solutions in the outer domain of communications $r \in (r_+, \infty)$. We assume that boundary conditions are to be applied at the EH and at infinity, which is generally the case. Thus, we take $R^{\infty}$ and $R^{H}$ to be independent solutions to the homogeneous equation ($T = 0$), corresponding to the boundary conditions we want to impose at infinity and at the horizon, respectively. We may define a rescaled Wronskian

$$\mathcal{W} = \Delta^{s+1}\left(R^{\infty}\frac{dR^{H}}{dr} - R^{H}\frac{dR^{\infty}}{dr}\right)\,, \tag{E.2}$$

which is a constant as a result of the main equation (E.1). By using it, we can construct a general solution to the equation with a source, which is simply

$$R(r) = \frac{1}{\mathcal{W}}\left(R^{\infty}\int_{r_+}^{r} TR^{H}\Delta^{s}dr' + R^{H}\int_{r}^{\infty} TR^{\infty}\Delta^{s}dr'\right)\,. \tag{E.3}$$

This is the main result of this appendix.

# Appendix F

# Matched asymptotic expansions

To obtain the analytical results presented in Sec. 5, the main challenge is to solve the homogeneous Teukolsky equation (Eq. (4.20)) with physical boundary conditions. Even if we are looking at other values of $s$, be it scalar ($s=0$), gravitational ($s=-2$), or other types of radiation, the flux formulas do change, but the main challenge remains the same: solving the homogeneous Teukolsky equation (Eq. (4.20)) with physical boundary conditions. These boundary conditions are different for the two solutions $R^{H}_{\omega\ell m}(r)$ (purely ingoing waves at the horizon) and $R^{\infty}_{\omega\ell m}(r)$ (purely outgoing waves at infinity), which have the following asymptotic behavior (see Eqs. (4.27) and (4.29)):

$$R^{H}_{\omega\ell m}(r\to\infty) = A_{\rm in}\frac{e^{-i\omega r_\star}}{r} + A_{\rm out}\frac{e^{i\omega r_\star}}{r^{2s+1}}\,; \tag{F.1}$$

$$R^{\infty}_{\omega\ell m}(r\to\infty) = \frac{e^{i\omega r_\star}}{r^{2s+1}}\,; \tag{F.2}$$

$$R^{H}_{\omega\ell m}(r\to 2M) = \frac{e^{-i\omega r_\star}}{(r^2 f)^s}\,; \tag{F.3}$$

$$R^{\infty}_{\omega\ell m}(r\to 2M) = B_{\rm in}\frac{e^{-i\omega r_\star}}{(r^2 f)^s} + B_{\rm out}e^{i\omega r_\star}\,. \tag{F.4}$$

If we take $s=-1$ in the equations above, we recover Eqs. (4.33) and (4.34). The problem of finding analytical solutions to Teukolsky's equation is as old as the equation itself, starting with the work of Starobinsky and Churilov in 1974 [119], but with developments in the forthcoming years [118, 120, 121]. Here we will focus mainly on the procedure outlined in [118, 119], where the homogeneous Teukolsky equation is solved in the small frequency limit, $M|\omega| \ll 1$, where $\omega$ is the mode frequency and $M$ is the BH mass. We will calculate everything for generic $\ell$ and $s$, and then use these results in the main text to study the EM case ($s=-1$), as well and to briefly comment on the scalar ($s=0$) and gravitational ($s=-2$) cases.

## F.1 The low-frequency limit of the homogeneous Teukolsky equation

Proceeding to the actual calculation, the first thing to do is solve the homogeneous Teukolsky equation, given in Eqs. (4.20) and (4.21), in the relevant limit. To do so, we start by defining

$$x \equiv \frac{r}{2M} - 1 \quad \text{and} \qquad \varpi \equiv 2M\omega \,. \tag{F.5}$$

In the $|\varpi| \ll 1$ regime the radial homogeneous equation can be approximated by

$$\begin{aligned} &x^2(x+1)^2 \frac{d^2 R_{\omega\ell m}}{dx^2} + (s+1)x(x+1)(2x+1)\frac{dR_{\omega\ell m}}{dx} \\ &+ \left[\varpi^2 x^4 + 2is\varpi x^3 - (\ell - s)(\ell + s + 1)x(x+1) - is\varpi\right] R_{\omega\ell m} = 0 \,. \end{aligned} \tag{F.6}$$

The idea now is that we solve this equation for small and large $x$ and then match the two solutions. Starobinsky [119] discovered that there is a similar equation, which differs from ours only by subdominant terms, and which is much easier to solve near the BH horizon [1]. Therefore, the equation we will be using from now on is (dropping the subscripts in $R_{\omega\ell m}$ but keeping them in mind):

$$\begin{aligned} &x^2(x+1)^2 \frac{d^2 R}{dx^2} + (s+1)x(x+1)(2x+1)\frac{dR}{dx} \\ &+ \left[\varpi^2 x^4 + 2is\varpi x^3 - (\ell - s)(\ell + s + 1)x(x+1) - is\varpi(2x+1) + \varpi^2\right] R = 0 \,. \end{aligned} \tag{F.7}$$

### F.1.1 Near region

To look at the region closer to the BH we consider the limit $|\varpi| x \ll \ell(\ell+1)$. That means we can neglect the first two terms inside the square brackets in (F.7), yielding

$$\begin{aligned} &x^2(x+1)^2 \frac{d^2 R}{dx^2} + (s+1)x(x+1)(2x+1)\frac{dR}{dx} \\ &+ \left[ -(\ell - s)(\ell + s + 1)x(x+1) - is\varpi(2x+1) + \varpi^2\right] R = 0 \,. \end{aligned} \tag{F.8}$$

To find solutions to this we consider the ansatz

$$R(x) = x^{-s-i\varpi}(1+x)^{-s+i\varpi} F(x) \,, \tag{F.9}$$

and get the solution

$$\begin{aligned} R(x) =& C_1 \frac{x^{-i\varpi}(1+x)^{i\varpi}}{[x(1+x)]^s} \, {}_2F_1(-\ell - s, 1 + \ell - s; 1 - 2i\varpi - s; -x) \\ &+ C_2 \frac{x^{i\varpi}(1+x)^{i\varpi}}{(1+x)^s} \, {}_2F_1(-\ell + 2i\varpi, 1 + \ell + 2i\varpi; 1 + 2i\varpi + s; -x) \,, \end{aligned} \tag{F.10}$$

[1] We looked at both solutions and found that their behavior is indeed very similar.

where ${}_2F_1(a,b;c;z)$ is the standard hypergeometric function. Now we want to associate these functions with the asymptotic behavior of $R(r)$ at the horizon given in (4.29). It turns out that the ingoing mode is obtained with $C_1 = 4^{-s}$ and $C_2 = 0$, while the outgoing mode comes from taking $C_1 = 0$ and $C_2 = 1$. This motivates us to perform a rescaling, yielding

$$\begin{aligned} R_{\text{near}}(x) = C_{\text{in}} \frac{x^{-i\varpi}(1+x)^{i\varpi}}{4^s\,[x(1+x)]^s}\, {}_2F_1(-\ell-s, 1+\ell-s; 1-2i\varpi-s; -x) \\ + C_{\text{out}} \frac{x^{i\varpi}(x+1)^{i\varpi}}{(x+1)^s}\, {}_2F_1(-\ell+2i\varpi, 1+\ell+2i\varpi; 1+2i\varpi+s; -x)\,. \end{aligned} \tag{F.11}$$

In this form, taking $C_{\text{in}} = 1$ and $C_{\text{out}} = 0$ yields the asymptotic behavior of $R^H$ at the horizon, and for $R^\infty$ we can identify $C_{\text{in}}$ and $C_{\text{out}}$ with $B_{\text{in}}$ and $B_{\text{out}}$, respectively.

### F.1.2 Far region

To look now at the region far away from the BH we must take $x \gg \ell(\ell+1)$. That means we can take $(x+1) \to x$ and neglect the last two terms inside the square brackets in (F.7) altogether, yielding

$$x^4 \frac{d^2R}{dx^2} + 2(s+1)x^3 \frac{dR}{dx} + \left[\varpi^2 x^4 + 2is\varpi x^3 - (\ell-s)(\ell+s+1)x^2\right] R = 0\,. \tag{F.12}$$

The solution to this equation can be obtained directly, and when written in terms of special functions it takes the following form:

$$R_{\text{far}}(x) = C_3\, x^{\ell-s} e^{-i\varpi x}\, U(\ell-s+1, 2\ell+2, 2i\varpi x) + C_4\, x^{\ell-s} e^{-i\varpi x}\, L^{2\ell+1}_{s-\ell-1}(2i\varpi x)\,, \tag{F.13}$$

where $U(a,b,z)$ is the confluent hypergeometric function of the second kind and $L^\alpha_n(z)$ is a generalized Laguerre polynomial. As it turns out, however, this is not the most useful way of writing this solution; instead, we should employ the formula 22.5.54 from "Handbook of Mathematical Functions: With Formulas, Graphs, and Mathematical Tables" by M. Abramowitz and I. A. Stegun (which from here on out is referred to as AS), which states that

$$L^\alpha_n(z) = \binom{n+\alpha}{n}\, {}_1F_1(-n, \alpha+1, z)\,, \tag{F.14}$$

where ${}_1F_1(a,b;z)$ is the confluent hypergeometric function of the first kind. We can then use this to rewrite (F.13), which, after rescaling $C_4$, becomes

$$R_{\text{far}}(x) = C_3\, x^{\ell-s} e^{-i\varpi x}\, U(\ell-s+1, 2\ell+2, 2i\varpi x) + C_4\, x^{\ell-s} e^{-i\varpi x}\, {}_1F_1(\ell-s+1; 2\ell+2; 2i\varpi x)\,. \tag{F.15}$$

Next we focus on matching the solutions of (F.11) and (F.15) in the region where $\ell(\ell+1) \ll x \ll \ell(\ell+1)/|\varpi|$. We will do this separately for the two relevant boundary conditions, purely ingoing waves at the horizon and purely outgoing waves at infinity.

Before doing so, however, we want to clarify what it is we want to solve for, for which we must look back at Eqs. (4.52) and (4.58). What we don't know in those expressions is $A_{\text{in}}$ and $R^{H,\infty}(x_0)$, where $x_0 = r_0/2M - 1$ . Finding $A_{\text{in}}$ is straightforward and is done in the following subsection, but the problem with finding $R^{H,\infty}(x_0)$ is that we must say which branch of the analytical solution is valid at $x_0$. Since we are interested in studying circular orbits and we are working in the $|\varpi| \ll 1$ limit, we choose to use the near region branch, which is valid for studying slow

orbits, as $\omega = m\Omega_0$, and thus

$$|v_0| \ll 1 < \frac{\ell(\ell+1)}{|m|} \implies |\varpi| x_0 \ll \ell(\ell+1)\,, \tag{F.16}$$

where $\Omega_0$ and $v_0 = r_0\Omega_0$ are the angular and linear velocities seen by a stationary observer at infinity, respectively.

## F.2 Matching: purely ingoing waves at the horizon

The solution with purely ingoing boundary conditions at the horizon is $R^H$, and we want it to exhibit the asymptotic behavior given in Eqs. (F.3) and (F.1). Solving for $R^H$ will allow us to get two of the quantities we are looking for: $A_{\text{in}}$ and $R^H(x_0) = R^H_{\text{near}}(x_0)$. The first step to do so is imposing the behavior at the horizon, which is done by setting $C_{\text{in}} = 1$ and $C_{\text{out}} = 0$ in (F.11), so that

$$R^H_{\text{near}} = \frac{x^{-i\varpi}(1+x)^{i\varpi}}{4^s\,[x(1+x)]^s}\;{}_2F_1(-\ell-s, 1+\ell-s; 1-2i\varpi-s; -x)\,. \tag{F.17}$$

Proceeding to larger values of $r$, the matching of the two solutions is done in the region where $\ell(\ell+1) \ll x \ll \ell(\ell+1)/|\varpi|$. With that in mind, we start by looking at the $x \gg \ell(\ell+1)$ limit of (F.17). Using the formula AS 15.3.7,

$$\begin{aligned} {}_2F_1(a,b,c;z) =& \frac{\Gamma(c)\Gamma(b-a)}{\Gamma(b)\Gamma(c-a)}(-z)^{-a}\;{}_2F_1(a, 1-c+a, 1-b+a; 1/z) \\ &+ \frac{\Gamma(c)\Gamma(a-b)}{\Gamma(a)\Gamma(c-b)}(-z)^{-b}\;{}_2F_1(b, 1-c+b, 1-a+b; 1/z)\,, \end{aligned} \tag{F.18}$$

to rewritte (F.17), and then taking the limit $x \gg \ell(\ell+1)$, yields

$$R^H_{\text{near}} \approx \frac{4^{-s}\Gamma(1+2l)\Gamma(1-2i\varpi-s)}{\Gamma(1+\ell-2i\varpi)\Gamma(1+\ell-s)}x^{\ell-s} + \frac{4^{-s}\Gamma(-1-2l)\Gamma(1-2i\varpi-s)}{\Gamma(-\ell-2i\varpi)\Gamma(-\ell-s)}x^{-\ell-s-1} \quad (x \gg \ell(\ell+1))\,. \tag{F.19}$$

It is a well-known fact that the gamma function $\Gamma(z)$ has poles when $z$ is a non-positive integer. Since $\ell > |s| \geq 0$, this is the case in some of the gamma function values above. However, the poles of the gamma function are all simple, and can thus cancel out with each other. Indeed, using

$$\Gamma(-n+\varepsilon) \approx \frac{\text{Res}(\Gamma, -n)}{\varepsilon} = \frac{(-1)^n}{n!}\frac{1}{\varepsilon}\,, \tag{F.20}$$

where $n \in \mathbb{Z}^+$ and $\varepsilon \ll 1$, we will treat all potentially ill-behaved gamma function values from here on. Starting with Eq. (F.19), after we resolve the divergences in the gamma functions, we find

$$\begin{aligned} R^H_{\text{near}} \approx\; & i\,\varpi(-1)^s 2^{1-2s}\Gamma(-2i\varpi-s+1)\frac{\ell!\,(\ell+s)!}{(2\ell+1)!}x^{-1-\ell-s} \\ &+ \frac{4^{-s}\Gamma(2\ell+1)\Gamma(-2i\varpi-s+1)}{\Gamma(\ell-2i\varpi+1)\Gamma(\ell-s+1)}x^{\ell-s} \quad (x \gg \ell(\ell+1))\,. \end{aligned} \tag{F.21}$$

Now, turning to the behavior of (F.15) in the matching region where $x \ll \ell(\ell+1)/|\varpi|$, we must simply take the $\varpi x \to 0$ limit of said equation:

$$R^H_{\text{far}} \approx \left(\frac{\Gamma(-1-2l)}{\Gamma(-\ell-s)}C_3 + C_4\right)x^{\ell-s} - \left(\frac{i\,\ell\,e^{-i\pi l}}{4^\ell\varpi^{2\ell+1}}\frac{\Gamma(2l)}{\Gamma(\ell-s+1)}C_3\right)x^{-\ell-s-1} \quad (|\varpi|x \ll \ell(\ell+1))\,. \tag{F.22}$$

To get the behavior corresponding to (F.21), we must have

$$C_3 = \frac{e^{i\pi l}(-1)^{s+1}\varpi^{2\ell+2}2^{2l-2s+1}\Gamma(\ell-s+1)\Gamma(-2i\varpi-s+1)\,\ell!\,(\ell+s)!}{\ell\,\Gamma(2l)\,(2\ell+1)!} \tag{F.23}$$

and

$$C_4 = \frac{(-1)^{-\ell}2^{-2s}\Gamma(-2i\varpi - s + 1)}{\ell((2\ell+1)!)^2\Gamma(2l)\Gamma(\ell - 2i\varpi + 1)\Gamma(\ell - s + 1)} \times \left((-1)^l\Gamma(2l)\Gamma(2\ell+1)\,\ell\,((2\ell+1)!)^2 + 2^{2\ell+1}e^{i\pi l}(-1)^{2s+1}\varpi^{2\ell+2}\Gamma(\ell - 2i\varpi + 1)\Gamma(\ell - s + 1)^2\,\ell!\,((\ell+s)!)^2\right). \tag{F.24}$$

Now, the only thing missing is finding the value of $A_{\text{in}}$ (see Eq. (F.1)), as it will be needed to get the solution of the Teukolsky equation with a source. Thus, we must simply use the asymptotic form for (F.15) for $x \to \infty$. Using A.S 13.5.1,

$${}_1F_1(a,b;z) \xrightarrow{z\to\infty} \Gamma(b)\left(\frac{e^z z^{a-b}}{\Gamma(a)} + \frac{e^{i\pi a}z^{-a}}{\Gamma(b-a)}\right), \tag{F.25}$$

and AS 13.5.2,

$$U(a,b,z) \xrightarrow{z\to\infty} z^{-a}, \tag{F.26}$$

we obtain for $A_{\text{in}}$ and $A_{\text{out}}$

$$A_{\text{in}} = -\frac{2^{-l-s}e^{i\pi(l-s)}\Gamma(2l+1)\Gamma(2l+2)(i\varpi)^{-l+s-1}\Gamma(-2i\varpi - s + 1)}{\Gamma(l - 2i\varpi + 1)\Gamma(l - s + 1)\Gamma(l + s + 1)} \tag{F.27}$$

and

$$A_{\text{out}} = -\frac{2^{-l-s}(i\varpi)^{-l-s-1}\Gamma(-2i\varpi - s + 1)}{\Gamma(2l+1)\Gamma(2l+2)\Gamma(l - 2i\varpi + 1)\Gamma(l - s + 1)^2} \times \left(-\Gamma(2l+1)^2\Gamma(2l+2)^2 + 4^{l+1}e^{2i\pi s}l!\varpi^{2l+2}((l+s)!)^2\Gamma(l - 2i\varpi + 1)\Gamma(l - s + 1)^2\right) \tag{F.28}$$

Thus, to study energy flux to infinity, we already have everything we need in $A_{\text{in}}$ and $R^H_{\text{near}}(x)$; however, to get the energy flux into the horizon, we still need to find $R^\infty_{\text{near}}(x)$.

## F.3 Matching: purely outgoing waves at infinity

The procedure to perform the matching and find $R^\infty(x)$ is the opposite to that of the previous subsection, as now the boundary conditions are first applied at infinity (Eqs. (F.4) and (F.2)). That sets $C_3$ and $C_4$, and once we have the far region solution we can match it to the near region one to obtain $R^\infty_{\text{near}}(x)$, which is precisely what we need for Eq. (4.58), as $R^\infty(r_0) = R^\infty_{\text{near}}(x_0)$.

With that in mind, we need to start by looking at the asymptotic behavior of the solution in the far region (F.15) for $x \to \infty$, as that is where we will enforce the boundary conditions. We do this by employing Eqs. (F.25) and (F.26), which yields the following values for the coefficients:

$$C_3 = \frac{2^{l-s}e^{i\pi(l-s)}(i\varpi)^{l+s+1}\Gamma(l-s+1)}{\Gamma(l+s+1)} \quad \text{and} \quad C_4 = \frac{2^{l-s}(i\varpi)^{l+s+1}\Gamma(l-s+1)}{\Gamma(2l+2)}. \tag{F.29}$$

Once that has been done, we need to look at the solution $R_{\text{far}}$ in the matching region, which we do by taking the limit $|\varpi|x \ll \ell(\ell+1)$. The resulting expression is to be compared with the solution $R_{\text{near}}$ in the same region, which in that case reduces to taking the limit $x \gg \ell(\ell+1)$ of (F.11) and using the relation in Eq. (F.18). Altogether, the final

result for the coefficients is

$$C_{\text{in}} = -\frac{2^{-l+s-2}\varpi^{-2(l+1)}(i\varpi)^{l+s+1}\Gamma(l-2i\varpi+1)\Gamma(l-s+1)}{\Gamma(2l+1)\Gamma(2l+2)|l|!|2l+1|!\Gamma(l+s+1)\Gamma(-2i\varpi-s+1)} \tag{F.30}$$
$$\times \frac{1}{(-1)^{2s}\Gamma(l-2i\varpi+1)\Gamma(l-s+1)|l+s|!+\Gamma(l+2i\varpi+1)\Gamma(l+s+1)|l-s|!}$$
$$\times \Big(\Gamma(2l+1)^2\Gamma(2l+2)(|2l+1|!)^2+4^{l+1}\varpi^{2l+2}|l|!\Gamma(l+2i\varpi+1)\Gamma(l-s+1)\Gamma(l+s+1)|l$$
$$-s|!(\Gamma(2l+2)|l+s|!-|2l+1|!\Gamma(l+s+1))\Big),$$

$$C_{\text{out}} = \frac{\varpi^{-2(l+1)}2^{-l-s-2}(i\varpi)^{l+s+1}\Gamma(l+2i\varpi+1)}{\Gamma(2l+1)\Gamma(2l+2)|l|!|2l+1|!\Gamma(2i\varpi+s+1)} \tag{F.31}$$
$$\times \frac{1}{e^{2i\pi s}\Gamma(l-2i\varpi+1)\Gamma(l-s+1)|l+s|!+\Gamma(l+2i\varpi+1)\Gamma(l+s+1)|l-s|!}$$
$$\times \Big(\Gamma(2l+1)^2\Gamma(2l+2)(|2l+1|!)^2-|2l+1|!\Gamma(l+s+1))$$
$$-4^{l+1}e^{2i\pi s}\varpi^{2l+2}|l|!\Gamma(l-2i\varpi+1)\Gamma(l-s+1)^2|l+s|!(\Gamma(2l+2)|l+s|!\Big).$$

We now know $R^{\infty}_{\text{near}}(x)$, and so we have completed the task we set ourselves. To obtain an analytic expression for the solution to the homogeneous Teukolsky equation with the boundary conditions discussed in the beginning of this Appendix, we just have to replace the desired values of $s$, $\ell$ and $m$, provided, of course, that the orbit in question has $M|\omega| \ll 1$ as well as $|v_0| \ll 1$.

# Appendix G

# Explicit expressions for some analytical results

In this Appendix, we give the full explicit expressions for the quantities $\alpha_\ell$, $\zeta_\ell$, $\beta_\ell$, $\xi_\ell$ and $\sigma_\ell$ defined in Ch. 5:

$$\alpha_\ell = \frac{2}{\ell}\Bigg[\left(\frac{\ell-1}{\ell}\right)^{\ell-1}\frac{1}{(\ell+1)(r_0-2)\,{}_2F_1\left(1-\ell,\ell+2;2;1-\frac{r_0}{2}\right)} \\ \left(((l-2)r_0+4)\,{}_2F_1\left(1-\ell,\ell+2;2;1-\frac{r_0}{2}\right)-(l-1)r_0\,{}_2F_1\left(2-\ell,\ell+2;2;1-\frac{r_0}{2}\right)\right)\Bigg]^2; \tag{G.1}$$

$$\zeta_\ell = r_0^{-2}\left(\frac{\ell+1}{\ell}\right)^{2\ell+1}\frac{(\ell+2)^3\,{}_2F_1\left(-\ell,\ell+3;2;1-\frac{r_0}{2}\right)^2}{2(2\ell+1)^2(2\ell+3)\,{}_2F_1\left(1-\ell,\ell+2;2;1-\frac{r_0}{2}\right)^2}; \tag{G.2}$$

$$\beta_\ell = \frac{2}{\ell}\Bigg[\frac{(\ell-1)}{\ell(\ell+1)(r_0-2)^2\,{}_2F_1\left(\ell+1,\ell+2;2(\ell+1);-\frac{2}{r_0-2}\right)} \\ \times\Bigg((r_0-2)((\ell+3)r_0-4)\,{}_2F_1\Big(\ell+1,\ell+2;2\ell+2;-\frac{2}{r_0-2}\Big) \\ -(\ell+2)r_0\,{}_2F_1\Big(\ell+2,\ell+3;2\ell+3;-\frac{2}{r_0-2}\Big)\Bigg)\Bigg]^2; \tag{G.3}$$

$$\xi_\ell(r_0) = (r_0-2)^{-2}\frac{(\ell+1)^2(\ell+2)(2\ell+2)!((2\ell)!!)^2}{\ell(2\ell+1)(2\ell+3)(2\ell)!((2\ell+2)!!)^2}\frac{{}_2F_1\left(\ell+2,\ell+3;2(\ell+2);-\frac{2}{r_0-2}\right)^2}{{}_2F_1\left(\ell+1,\ell+2;2(\ell+1);-\frac{2}{r_0-2}\right)^2}; \tag{G.4}$$

$$\Sigma_\ell(r_0) = 3\,4^{\ell+1}r_0^2(r_0-2)^{-2(\ell+2)}\frac{l(2\ell+1)(2\ell)!\Gamma(\ell+1)^2\Gamma(\ell+2)^2\,{}_2F_1\left(\ell+1,\ell+2;2(\ell+1);-\frac{2}{r_0-2}\right)^2}{(\ell+1)((2\ell)!!)^2\Gamma(2\ell+2)^2}. \tag{G.5}$$

# Appendix H

# Numerical methods

In this Appendix, we discuss the methods employed to get the numerical results for the energy flux to infinity and into the BH horizon, which are thoroughly discussed in Sec. 6. As mentioned before, the problem of finding these energy fluxes boils down to solving for three quantities :

- $R^{H}_{\omega lm}(r_0)$: the solution of the homogeneous Teukolsky equation (Eq. (4.20)) with boundary conditions corresponding to purely ingoing waves at the horizon (see Eqs. (4.33) and (4.34)), evaluated at the orbital radius $r_0$;
- $R^{\infty}_{\omega lm}(r_0)$: the solution of the homogeneous Teukolsky equation (Eq. (4.20)), with boundary conditions corresponding to purely outgoing waves at infinity (see Eqs. (4.33) and (4.34)), evaluated at the orbital radius $r_0$;
- $A_{\text{in}}$: the coefficient for the ingoing mode at infinity for the solution $R^{H}_{\omega lm}(r)$ (see first item and Eq. (4.33)).

These are then replaced in Eqs. (4.52), (4.53), (4.58) and (4.59) to yield the desired result. Thus, once again, the only difficult task is solving the homogeneous Teukolsky equation, Eq. (4.20), with physical boundary conditions. From here on, in this Appendix, we drop the subscripts in the mode amplitudes $R_{\omega lm}$ to unclutter the notation.

The astrophysical reference values for the parameters in the simulations are those given in Table H.1. It is important to note that of the three parameters $B_0$ (magnetic field strength), $q$ (particle charge), and $m$ (particle mass), only two independent quantities end up being relevant for the simulations, namely $q$ and $\omega_c = qB_0/m$. This is because we work in the adiabatic approximation, meaning that the particle is always assumed to be in a circular orbit; hence, as a result of the equivalence principle, $m$ and $B_0$ can be eliminated in favor of $\omega_c$. We cannot eliminate $q$ from the simulation because the flux formulas are $\propto q^2$; however, we eliminated it from our analysis by always expressing the results in terms of ratios of fluxes. Thus, in the end, the only parameter controlling the results is the cyclotron frequency $\omega_c$. Still, for each simulation, we must give a value for $q$, for which we use the one in the table below; but we consider only variations of the magnetic parameter, which could happen through a variation in either $B_0$ or $m$. For reference, the values in the table correspond to $M\omega_c \approx 3.5 \times 10^{-5}$.

We perform all our calculations using a Mathematica notebook and solve the homogeneous equation using the function `NDSolve`. This method requires as inputs the equation, the boundary conditions, and the domain of interest. In our particular case, setting $M = 1$, the domain of interest is the outer domain of communications, $r \in (2, \infty)$. The boundary conditions are what changes between the two solutions: for $R^{\infty}$, we give the function and its derivative at infinity, which we get from Eq. (4.33); for $R^{H}$, we give the function and its derivative at the EH, which we get from (4.34).

| Qty | Value | Simulation |
|---|---|---|
| $M$ | $10\,M_\odot$ | $1$ |
| $B_0$ | $10^8\,G$ | $1.20\times10^{-11}$ |
| $q$ | $7\times10^{15}\,C$ | $1.44\times10^{-5}$ |
| $m$ | $10^{20}\,kg$ | $5\times10^{-12}$ |

Table H.1: Reference parameters used in our simulations: $M$ is the BH mass, $B_0$ is the value of the magnetic field strength, $q$ is the charge of the particle and $m$ is its mass. The second column gives values in SI units and solar masses ($M_\odot$) while the third gives the values used in the actual simulation (after normalizing to the BH mass).

This may seem simple, but, in fact, we have issues at both ends of our domain, as the computer is neither able to deal with $r=2$ (because the equation has a singularity) nor with $r=\infty$ (simply because infinity is not a number). The problem at the horizon is solved by bringing the lower bound of the domain to a radius

$$r_1 \equiv 2+\varepsilon\,, \quad 0<\varepsilon\ll 1\,, \tag{H.1}$$

where we can vary $\varepsilon$. Similarly, we approximate $\infty$ by the finite radius

$$r_2 \equiv \frac{N}{\omega}\,, \quad \mathbb{N}\ni N\gg 1, \tag{H.2}$$

where $\omega$ is the wave frequency and $N$ is a large integer we can vary. The idea is that, for large enough $N$, at $r_2$ the wave is propagating in a flat background with well-defined wave parameters, since we allowed for a large number of wavelengths to pass; that being the case, we expect its properties to remain roughly the same all the way out to infinity.

If by varying $\varepsilon$ and $N$ we find values for which decreasing the former or increasing the latter does not change the results, that means that we can use $r_1$ and $r_2$ as the boundaries of the domain with confidence. For the horizon, it was quite easy to establish a stable value of $\varepsilon$ and we settled for

$$\varepsilon = 10^{-6}\,M. \tag{H.3}$$

Doing the same for $N$ proved a lot more complicated, as increasing $N$ seemed to always lead to changes in the results. This is because $r_2$ is generally not far enough away from the BH for the asymptotic behavior of the solutions to be accurate. To solve the problem, we must consider extra terms in the behavior of the solutions at $r_2$, namely terms that will eventually die off but that may still be relevant at $r_2<\infty$. We choose to keep all terms up to $\mathcal{O}(r^{-4})$, so the actual asymptotic behaviour of the solutions becomes

$$\begin{aligned} R^H_{\omega lm}(r\to r_2) \to & \frac{A_{\text{in}}}{r}\,e^{-i\omega r_\star}\left(1+\frac{a_{\text{in}}}{r}+\frac{b_{\text{in}}}{r^2}+\frac{c_{\text{in}}}{r^3}\right) \\ & + A_{\text{out}}\,r\,e^{i\omega r_\star}\left(1+\frac{a_{\text{out}}}{r}+\frac{b_{\text{out}}}{r^2}+\frac{c_{\text{out}}}{r^3}+\frac{d_{\text{out}}}{r^4}+\frac{e_{\text{out}}}{r^5}\right)+\mathcal{O}(r^{-5}) \end{aligned} \tag{H.4}$$

and

$$R^\infty_{\omega lm}(r\to r_2) \to r\,e^{i\omega r_\star}\left(1+\frac{a_{\text{out}}}{r}+\frac{b_{\text{out}}}{r^2}+\frac{c_{\text{out}}}{r^3}+\frac{d_{\text{out}}}{r^4}+\frac{e_{\text{out}}}{r^5}\right)+\mathcal{O}(r^{-5})\,. \tag{H.5}$$

The eight coefficients in these expressions are determined by replacing the ansatz for $R^H_{\omega lm}$ from Eq. (H.4) in the homogeneous Teukolsky equation and solving order by order in $r$. This yields

$$a_{\text{in}} = \frac{i}{2\omega}\left(2 - \lambda + 4i\omega\right) , \tag{H.6}$$

$$b_{\text{in}} = \frac{i}{4\omega}\left(2(\lambda - 4) + a_{\text{in}}(6 - \lambda)\right) , \tag{H.7}$$

$$c_{\text{in}} = \frac{i}{6\omega}\left(8 + 2a_{\text{in}}(\lambda - 12) + b_{\text{in}}(12 - \lambda - 4i\omega)\right) , \tag{H.8}$$

$$a_{\text{out}} = \frac{i}{2\omega}\lambda , \tag{H.9}$$

$$b_{\text{out}} = -\frac{i}{4\omega}\lambda\, a_{\text{out}} , \tag{H.10}$$

$$c_{\text{out}} = \frac{i}{6\omega} b_{\text{out}}\left(\lambda - 2\right) , \tag{H.11}$$

$$d_{\text{out}} = \frac{i}{8\omega}\left(4\, b_{\text{out}} + c_{\text{out}}(\lambda - 6)\right) , \tag{H.12}$$

$$e_{\text{out}} = \frac{i}{10\omega}\left(12\, c_{\text{out}} + d_{\text{out}}(\lambda - 12)\right) , \tag{H.13}$$

where $\lambda = (l - s)(l + s + 1)$. After this expansion is included, it is indeed possible to find a stable value for $N$, and we settled for

$$N = 15,000. \tag{H.14}$$

Having sorted the problems with the horizon and infinity, everything is set and now we just let the computer do the work for us.

It is important to mention that the main reason we inferred for the code not converging was having an orbital velocity $v_0 \ll 1$ too small. Luckily, in that limit, we can resort to our analytical results.